

# UC San Diego

## UC San Diego Electronic Theses and Dissertations

**Title**

Designing nanosensors based on ion channel-forming derivatives of Gramicidin A

**Permalink**

<https://escholarship.org/uc/item/2bz4z20v>

**Author**

Blake, Steven

**Publication Date**

2008

Peer reviewed|Thesis/dissertation

UNIVERSITY OF CALIFORNIA, SAN DIEGO

Designing nanosensors based on ion channel-forming derivatives of  
Gramicidin A

A Dissertation submitted in partial satisfaction of the Requirements for the degree  
Doctor of Philosophy

in

Chemistry

by

Steven Blake

Committee in charge:

Professor Jerry Yang, Chair  
Professor Senyon Choe  
Professor Yoshihisa Kobayashi  
Professor Charles Perrin  
Professor Amy Sung

2008

Copyright  
Steven Blake, 2008  
All rights reserved.

The Dissertation of Steven Blake is approved, and it is acceptable in quality and form for publication on microfilm and electronically:

---

---

---

---

---

Chair

University of California, San Diego

2008

## TABLE OF CONTENTS

Signature Page.....	iii
Table of Contents.....	iv
List of Figures.....	vi
List of Schemes.....	viii
List of Tables.....	ix
Acknowledgements.....	x
Vita.....	xii
Abstract of the Dissertation.....	xiii
Chapter 1 Introduction.....	1
1.1 Why do we need sensors?.....	1
1.2 Ion channels in nature and their potential as a sensor.....	2
1.3 How the conductance of ion channels is measured.....	4
1.4 Examples of ion channel-based platforms.....	6
1.5 Properties of Gramicidin.....	9
1.6 Gramicidin A as a platform for ion channel sensors.....	12
Chapter 2 Principles behind charge-based sensing.....	15
2.1 Inspiration behind charge-based sensing.....	15
2.2 Influence of the distance of charge from the pore on the conductance of derivatives of gA.....	18
2.3 Influence of the ionic strength of the recording buffer on the conductance of negatively-charged derivatives of gA.....	22
2.4 Importance of a well-defined charge on the derivative of gA in the pH range of analysis.....	24
2.5 Dependence of the I-V characteristics of gA channels on the applied transmembrane voltage and on the molecular heterogeneity of the gA dimers.....	26
2.6 Influence of charge on the lipid headgroups on the single channel conductance of gA and its derivatives.....	30
2.7 Conclusion.....	33
2.8 Protocol for ion channel measurements.....	33
Chapter 3 Applications of charge-based sensing.....	38
3.1 Introduction.....	38
3.2 Demonstration of charge-based sensing.....	39

3.3	Conclusion.....	45
3.4	Protocol for monitoring chemical reactions.....	46
Chapter 4	Developing new building blocks for gA-based nanosensors.....	49
4.1	Introduction.....	49
4.2	Synthesis of chemically reactive derivatives gramicidamine and gramicidazide from native gA.....	52
4.3	Chemical reactivity of gramicidamine and gramicidazide.....	54
4.4	Monitoring a “click” reaction <i>in situ</i> using single ion channel recordings.....	60
4.5	Design and synthesis of an ion channel-based sensor for detection of protein-ligand interactions.....	63
4.6	Conclusion.....	66
4.7	Protocol for ion channel measurements.....	67
Chapter 5	Using an ion channel platform to detect enzyme activity.....	72
5.1	Introduction.....	72
5.2	Detection of the catalytic activity of Alkaline Phosphatase.....	74
5.3	Protocol for ion channel measurements.....	81
Chapter 6	Using hydrogen-bonding to tune the conductance of Gramicidin A.....	85
6.1	Introduction.....	85
6.2	Effect of H-bonding on the conductance of gA.....	86
6.3	Conclusions.....	90
6.4	Protocol for ion channel measurements.....	91
Chapter 7	Experimentals for the synthesis of derivatives of Gramicidin A.....	94
References.....		111

## LIST OF FIGURES

Figure 1.1.	Illustration of a voltage-gated potassium channel in a lipid membrane.....	2
Figure 1.2.	Cartoon depicting a ligand-gated ion channel in the closed and open conformation.....	3
Figure 1.3.	A picture and schematic of an electrophysiological setup and a single ion channel trace .....	5
Figure 1.4.	Demonstration of stochastic sensing using $\alpha$ -hemolysin ion channels .....	7
Figure 1.5.	An illustration depicting a light-gated K <sup>+</sup> ion channel and its current versus time trace below .....	8
Figure 1.6.	Cartoon showing the sequence and structure of a monomer of gramicidin A and the reversible dimeric assembly of a gA pore in a lipid bilayer.....	10
Figure 2.1.	Cartoon depicting Woolley's gA derivative as a pH sensor.....	15
Figure 2.2.	Illustration showing a generic example of charge-based sensing.....	17
Figure 2.3.	Sequence and calculated structure of two negatively-charged derivatives of gramicidin A.....	19
Figure 2.4.	Cartoon of gA pores in planar lipid bilayers and current versus time traces of the respective dimeric pores.....	21
Figure 2.5.	Current-voltage characteristic of a homodimeric pore of gA-gA, <b>2-2</b> , and a heterodimeric, asymmetric pore of gA and <b>2</b> .....	27
Figure 2.6.	Effect of a negatively-charged head group on the lipids in planar bilayers .....	31
Figure 3.1.	Monitoring chemical reactions on molecules attached to gA by analysis of single ion-channel currents.....	41

Figure 3.2.	Conductance measurements of derivatives of gramicidin A carrying a tert-butoxycarbonyl protected glycine <b>4</b> , glycine <b>5</b> , and glycolic acid <b>6</b> in aqueous buffered solution.....	42
Figure 3.3.	Monitoring of the single ion-channel currents during the conversion of gA derivative <b>5</b> to gA derivative <b>6</b> .....	43
Figure 4.1.	Cartoon illustrating the reversible dimerization of six different derivatives of gA ( <b>3</b> , <b>13</b> , <b>17</b> , <b>19-21</b> ) and original single channel traces of current versus time of all six derivatives.....	59
Figure 4.2.	Conversion of gramicidazide <b>13</b> to a negatively charged triazole sulfonate <b>20</b> .....	61
Figure 4.3.	Detection of carbonic anhydrase (CA) with gA derivative <b>21</b> .....	64
Figure 5.1.	Cartoon of the detection of Alkaline Phosphatase (AP) using an ion channel platform.....	76
Figure 5.2.	Single channel current versus voltage (I-V) curves of <b>25</b> and <b>26</b> .....	77
Figure 5.3.	Time dependent enzymatic hydrolysis of the phosphate group in <b>25</b> to <b>26</b> in the presence of 600 nM AP as determined using single ion channel conductance measurements.....	78
Figure 5.4.	Monitoring the formation of <b>26</b> from hydrolysis of <b>25</b> over time as a function of the concentration of AP using single ion channel conductance measurements.....	79
Figure 6.1.	Illustration depicting the chemical structure and energy minimized structure of <b>17</b> and <b>5</b> .....	87
Figure 6.2.	Single channel traces of <b>5</b> and <b>17</b> at 75 mV in low ionic strength and high ionic strength buffer.....	89

## LIST OF SCHEMES

Scheme 2.1.	Synthesis of gA carrying a sulfonate via long and short linker and an amine.....	20
Scheme 3.1.	Synthesis of <b>5-7</b> for the demonstration of charge-based sensing.....	40
Scheme 4.1.	Synthesis of gramicidamine and gramicidazide.....	53
Scheme 4.2.	The synthesis of gA derivatives from gA-based building blocks <b>3</b> and <b>13</b> and the structures of two ester derivatives of gA ( <b>5</b> and <b>6</b> ) derived from native gA.....	57
Scheme 5.1.	Synthesis of Alkaline Phosphatase substrates <b>24</b> and <b>25</b> and their respective hydrolysis products <b>8</b> and <b>26</b> .....	75

## LIST OF TABLES

Table 2.1.	Single-channel conductances, $\gamma$ , of homodimers of gA-SO <sub>3</sub> <sup>-</sup> with a long spacer arm ( <b>1</b> ) and of gA-SO <sub>3</sub> <sup>-</sup> with short spacer arm ( <b>2</b> ) compared to native gA at different concentrations of KCl in the recording buffer.....	23
Table 2.2.	Single-channel conductances of homodimers of gA, <b>2</b> , and <b>3</b> at pH 7.4 and pH 12.....	25
Table 4.1.	Summary of reactions of native gA, gramicidamine ( <b>3</b> ), and gramicidazide ( <b>13</b> ) with molecules that represent typical substrates for conjugation to amines and azides.....	55

## ACKNOWLEDGEMENTS

I would like to start off by thanking everyone who directly contributed to the collection of data that is presented in this thesis. My gratitude goes out to Professor Michael Mayer for providing me with an ion channel setup in his lab at the University of Michigan and for providing me with his house temporarily, so that I don't freeze to death in the cold, harsh winters of Michigan. Dr. Ricardo Capone was a big help in training me to use the ion channel setup. I thank him for acquiring much of the electrophysiological measurements that are presented in this work.

Next, I would like to thank the members of my lab. Dr. Petra Herguth was extremely instrumental in getting me started with the basics of organic chemistry. I know I ended up chewing her head off with many questions, but because of her infinite patience, she was a great instructor. Lani was really great to talk to in times of trouble and despair. Mark was cool to have around in lab as the lab clown. Keep those PAB grade materials coming. Alice is a very fashionable girl with a really big heart. It was nice to have her around to talk to and I especially appreciate all the food she would bring in. I hope she one day discovers the cure for cancer. Mike (aka "The Great Nubinski") worked with me on the project and he is one of the closest friends I'll ever have. Thanks for all the advice. His presence in the lab definitely made the lab into a better and livelier place. Christina was a terrific person to interact with in the lab. I had a lot of fun doing the ice lounge with her (I'm pretty sure she swallowed more than I did). Whenever

I speak to Linnie, she seems like she's always in a good mood. Don't let grad school wear you out and stay happy. I didn't get a chance to know Yuchen and Lila really well, but I'm glad they showed up to my interview practice talk and they were really supportive. I also want to thank Katie Li for her hard work in trying to purify Gramicidin D by column chromatography. I had a lot of fun hanging out with her in and out of the lab. Michelle Lee was a very nice person to have around. She was really supportive and helpful in times of great ordeal. I'm sure she'll make her future boyfriends/husbands really happy. Finally I would like to thank my advisor Jerry Yang. He provided with me with an endless supply of chemicals and a bench space to make all the magic in this thesis come to life. I appreciate all the hard-work and dedication he put into running the lab and helping me to be a better scientist. Now that I'm leaving, I'm sure his blood pressure will drop down to normal.

**Notes about the Chapter 2, 3, and 5:** Parts of these chapters are reprints from the published reference: Steven Blake, Ricardo Capone, Michael Mayer, and Jerry Yang. Chemically Reactive Derivatives of Gramicidin A for Developing Ion Channel-Based Nanoprobes. *Bioconjugate Chem.*, 19 (8), 1614–1624, **2008**. I would like to thank Ricardo Capone, Jerry Yang and Michael Mayer for helping me get this paper published and ACS Publications for publishing our work.

## VITA

2003	B.S. in Chemistry, University of California, Irvine
2003	B.S. in Biological Sciences, University of California, Irvine
2005	M.S. in Chemistry, University of California, San Diego
2008	Ph.D. in Chemistry, University of California, San Diego

# ABSTRACT OF THE DISSERTATION

Designing nanosensors based on ion channel-forming derivatives of Gramicidin  
A

by

Steven Blake

Doctor of Philosophy in Chemistry

University of California, San Diego, 2008

Professor Jerry Yang, Chair

This dissertation will focus on detecting analytes in aqueous solution that chemically react with or bind to functional groups near the opening of synthetic ion channels derived from gramicidin A (gA). Detection is achieved when a measurable change in the conductance of ions across the ion channel is produced after the analyte interacts with the channel. Ion channel sensors have great potential for achieving ultrasensitive detection since a single chemical modification near the lumen of the channel can lead to detectable changes in channel conductance. The dissertation will specifically focus on: (1) the development of design parameters to improve sensing with gA-based nanosensors; (2) the demonstration of sensing analytes in aqueous solution by manipulating the charge of a chemical group near the pore of gA (charge-based

sensing); (3) the chemistry for producing reactive building blocks of gA for developing robust and diverse gA-based nanosensors; (4) the detection of enzyme activity using our charge-based sensing approach to achieve picomolar limits of detection; and (5) the small structural changes that can be introduced to the peptide near the lumen of the channel to control conductance.

# Chapter 1

## Introduction

### 1.1 Why do we need sensors?

Society is under constant exposure to harmful agents in the environment such as disease-causing microorganisms or toxic, industrial chemicals. These agents, in general, are undetectable to the naked eye, leaving unaware individuals victim to their deleterious effects. To solve the problem, chemical and biological sensors have been employed that give people the ability to “see” harmful agents. In general, sensors are devices that work by converting the information about the state of the environment (e.g. concentration of an analyte, presence of an antigen) into a measurable signal. Specifically, these sensors range from chromogenic / immunogenic assays for the detection of harmful biological agents to electrochemical methods for the detection of industrial

contaminants. The ultimate goal for the development of any effective sensor is to achieve the lowest limit of detection possible. Having the capacity to detect low concentrations of industrial contaminants in the ecosystem or infectious agents in the human body will allow for their expeditious removal before their detrimental effects negatively impact society.

## 1.2 Ion channels in nature and their potential as a sensor

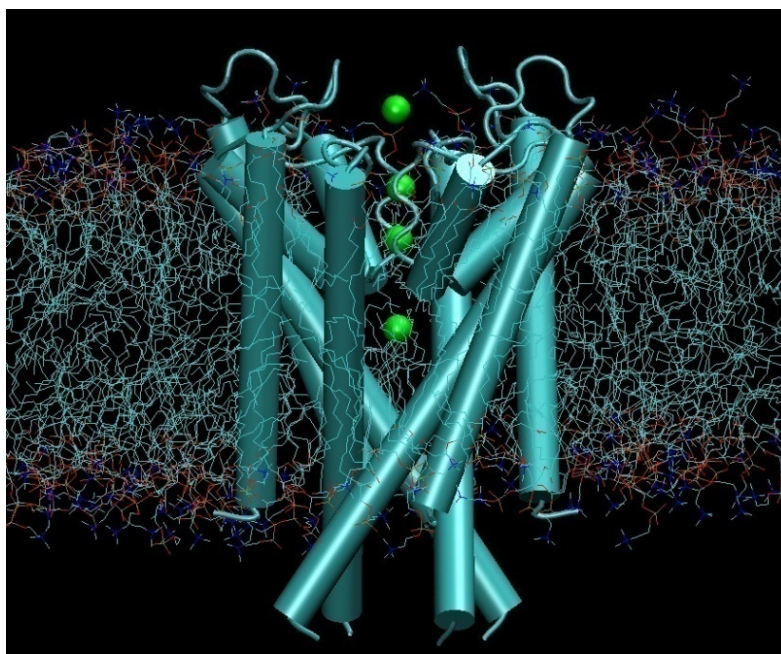


**Figure 1.1.** Illustration of a voltage-gated potassium channel in a lipid membrane. When a threshold electric potential across the lipid membrane is reached, a 3D conformational change is induced in the ion channel, causing the channel to open to the influx of ions.

In nature, ion channels are pore-forming proteins that incorporate into the lipid bilayer membranes of cells. An ion channel regulates the passive transport

of ions ( $10^6 - 10^9$  ions per second) across the bilayer, which is important for major biological processes such as intra- and intercellular signaling, propagation of impulses across neurons and maintenance of cellular osmotic potential.<sup>8</sup> The flow of ions is regulated when an external stimulus induces a conformational change in the channel causing it to be opened or closed to the flow of ions. There are three major categories of ion channels depending on how the flow of ions is regulated: ligand-gated, voltage-gated (Figure 1.1) and mechanically-gated. Ligand-gated ion channels open or close when a small ligand binds the channel; voltage-gated channels open or close when there is a change in the electric potential across the lipid membrane of the cell; and mechanically-gated channels open or close in the presence of mechanical stress such as touch.

One of the major properties of ion channels is their ability to amplify a signal. For example with a ligand-gated ion channel, a single molecule binds an ion channel, which then leads to the flow of millions of ions per second (Figure

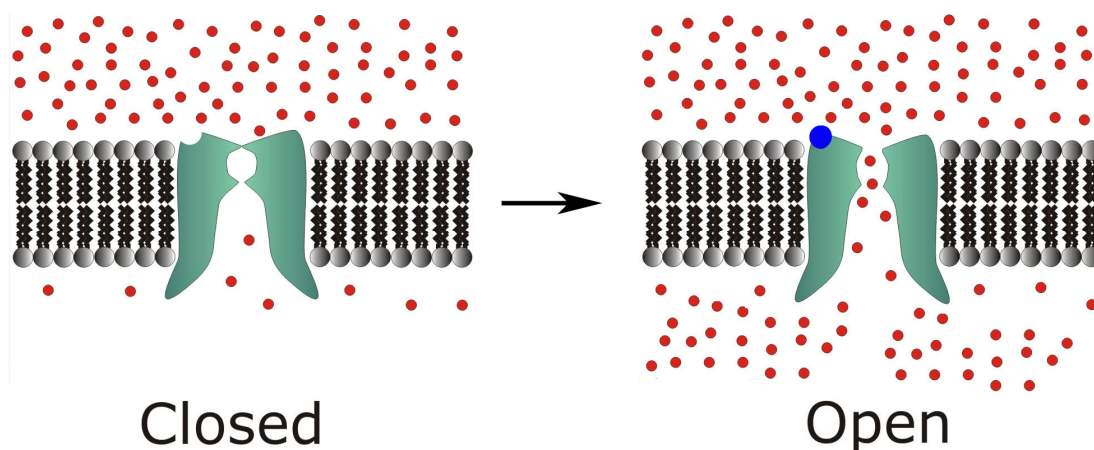


**Figure 1.2.** Cartoon depicting a ligand-gated ion channel in the closed and open conformation. Upon the binding of a small molecule, ions can passively diffuse across the channel down their electrochemical gradient. The movement of ions produces current across the channel.

1.2). In short, a binding event from only a single molecule (signal) is amplified in the form of a measurable change in the current across the channel. Scientists have borrowed this idea of signal amplification from nature to create synthetic ion channels that can produce a measurable change in current upon the interaction of any single molecule of interest with the ion channel. Consequently, synthetic ion channels are widely used to develop a platform for selectively sensing an analyte of choice with high sensitivity.

### **1.3 How the conductance of ion channels is measured**

The conductance of ions across the ion channel is measured using an electrophysiological setup (Figure 1.3A). The lipid bilayer membrane is formed over the pore (100  $\mu\text{m}$ ) of the teflon membrane that separates two compartments containing electrolytic solutions. When the lipid membrane is present, there is an impenetrable barrier between the aqueous solutions in the two compartments. Once the ion channel is incorporated into the lipid membrane, the solutions in both compartments are now in contact via the nanoscale holes produced by the ion channels in the lipid membrane. When an electric potential (applied voltage) is generated from the head stage, one electrode becomes positively charged (anode) while the other is negatively-charged (cathode), resulting in a driving force for the movement of ions across the channel. If we assume for this example that the ion channel in the lipid membrane is cation-selective, then only cations will cross the channel to go toward the compartment containing the negatively-

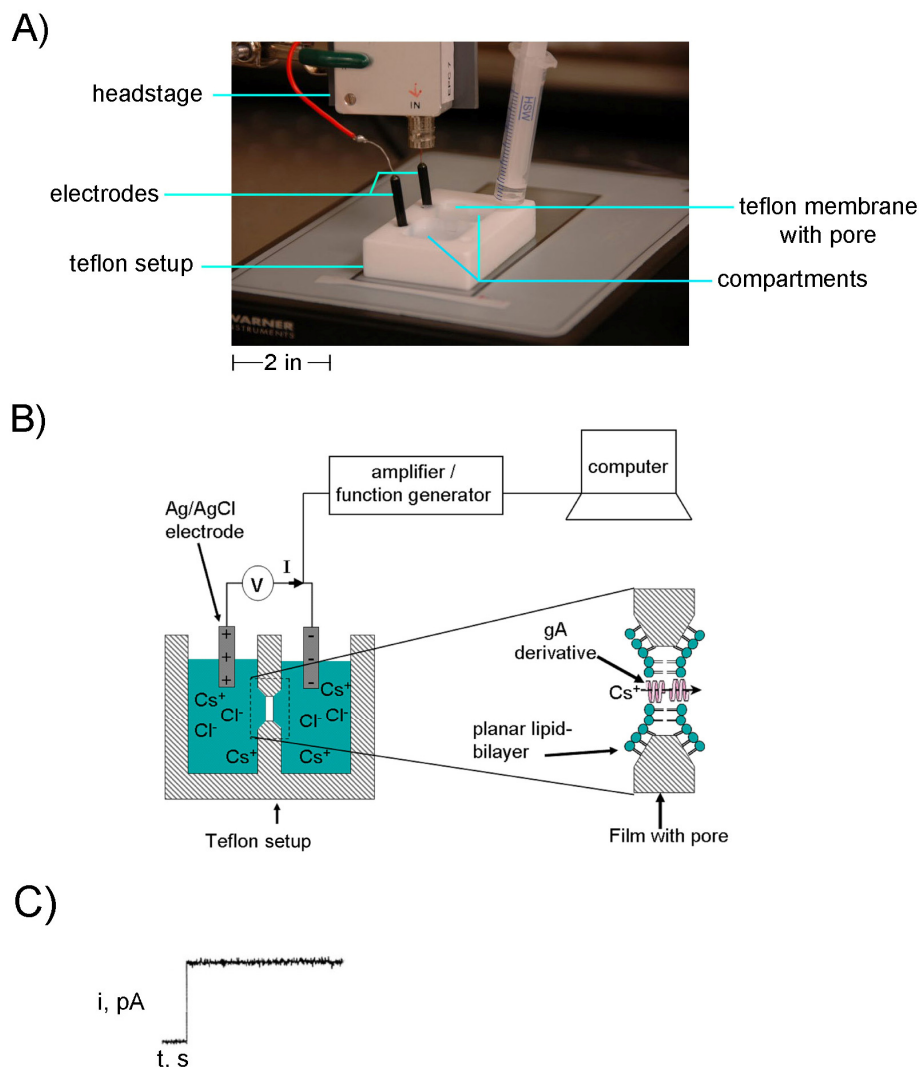


**Figure 1.3.** A picture and schematic of an electrophysiological setup and a single ion channel trace (current vs. time). A) The electrophysiological setup consists of: a Teflon setup, with two compartments that contain electrolytic solutions; Ag / AgCl electrodes that are submerged in the solutions of each compartment; a teflon membrane with a tiny pore (100  $\mu\text{m}$ ) that separates the two compartments when a lipid bilayer is placed over the pore; and a headstage which applies the electric potential and measures the current at the electrodes. B) A schematic representation of A) detailing a function generator that applies a potential allowing  $\text{Cs}^+$  cations to conduct across the lipid bilayer through the gA derivative while the amplifier enhances the current across the channel, so that a computer can process the data. C) When a single ion channel begins conducting ions across the lipid membrane, a current ( $i$ ) on the order of  $10^{-12}$  amps (pA) is typically generated across the channel over time ( $t$ ) and is graphed as a current-vs-time trace.

charged cathode. When cations leave the compartment containing the anode for the compartment containing the cathode, the compartment containing the anode develops a net negative charge in the solution. This resulting negative charge will cause the Ag / AgCl anode to undergo spontaneous oxidation according to the half-reaction:  $\text{Ag} \rightarrow \text{Ag}^+ + \text{e}^-$ . The silver cation that is produced from the half-reaction neutralizes the net negative charge in the compartment, while the electron will be measured as current by the amplifier (Figure 1.3B). In short, for each cation that crosses the channel, an electron is generated at the anode to yield the measured current.

## 1.4 Examples of ion-channel based platforms

Many researchers have explored ion channels derived from genetically engineered proteins,<sup>9-12</sup> peptides,<sup>13-18</sup> or oligomers of organic molecules<sup>19, 20</sup> to explore their potential utility as a sensor for chemical and biochemical agents or to explore their physical properties.

One example of these ion-channel platforms is based on  $\alpha$ -hemolysin (a transmembrane protein produced by *Staphylococcus aureus*) for the development of sensors for organic analytes. Bayley and coworkers<sup>11</sup> demonstrated that  $\alpha$ -hemolysin containing a molecule of  $\beta$ -cyclodextrin bound inside the protein's pore can sense and differentiate between two adamantane derivatives (2-adamantanamine hydrochloride and 1-adamantane carboxylic acid) in solution (Figure 1.4). When inside the pore of  $\alpha$ -hemolysin bound to  $\beta$ -

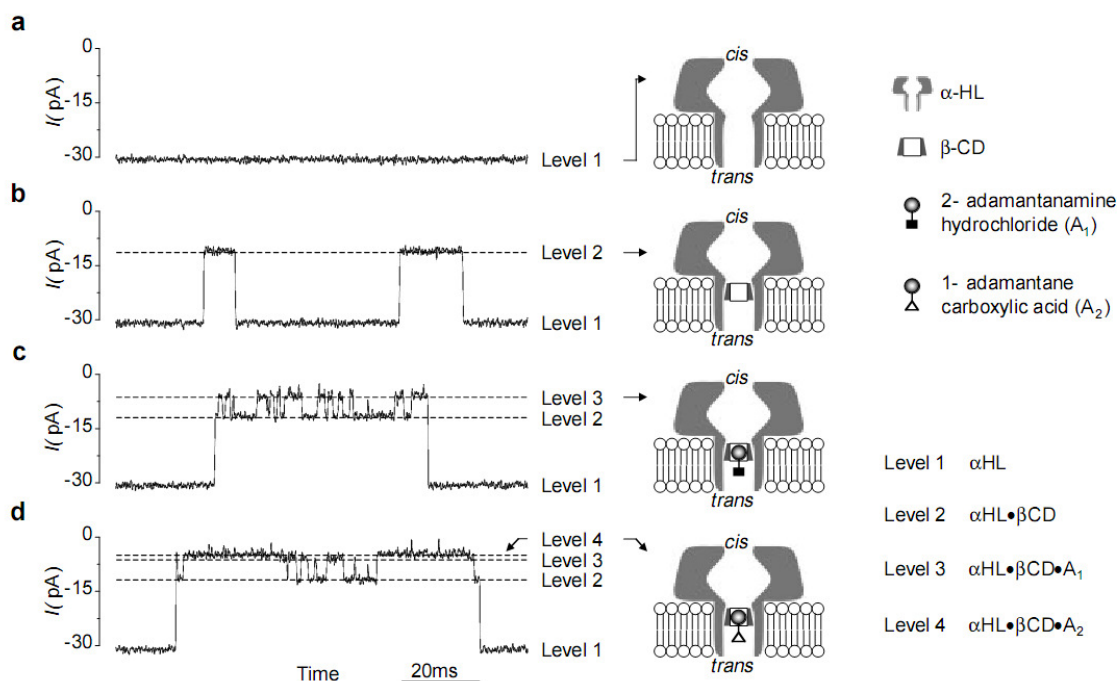


**Figure 1.4.** Demonstration of stochastic sensing using  $\alpha$ -hemolysin ion channels. Single channel traces depicting the effect of adamantane derivatives inside the pore of  $\alpha$ -hemolysin. A) The current is due to  $\alpha$ -hemolysin in the lipid membrane. B) The current is due to  $\alpha$ -hemolysin containing a bound  $\beta$ -cyclodextrin ( $\beta$ -CD, a known binder of adamantane) inside the hydrophobically-rich region in the channel. Depending on whether 2-adamantanamine hydrochloride or 1-adamantane carboxylic acid is bound inside the channel, a unique current versus time trace is produced, resulting in C) and D), respectively.

cyclodextrin, each derivative of adamantane created a particular steric environment in the pore which uniquely affected the rate of conducting ions. Hence, one can sense which particular derivative of adamantane was inside the channel from the signature current-vs-time trace that it produced.

In another example of an ion channel-based platform for sensing, Trauner, Kramer and coworkers<sup>21</sup> chemically derivatized Shaker K<sup>+</sup> ion channels to produce light-gated channels. These ion channels were derivatized with a photo-isomerizable azobenzene derivative through a combination of genetic

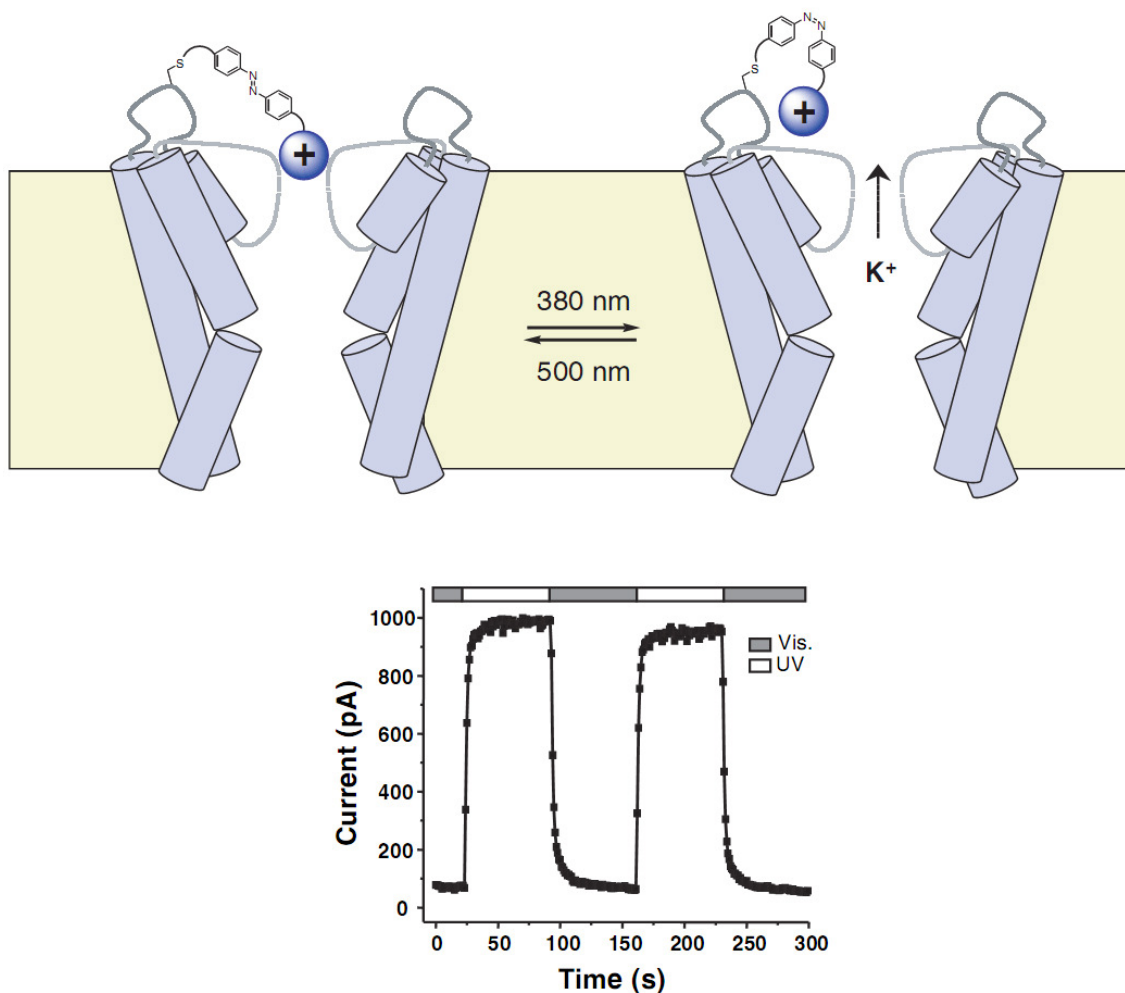


**Figure 1.5.** An illustration depicting a light-gated  $K^+$  ion channel and its current versus time trace below. In the presence of visible light (500 nm), the conformational change in the azobenzene derivative allows the positively-charged triethylammonium group to block the pore, resulting in a 90% reduction in the conductance of  $K^+$  ions compared to the open state when the ion channel is exposed to UV light (380 nm).

engineering and synthetic chemistry (Figure 1.5). In the presence of visible light, the azobenzene moiety adopts the extended *trans*-conformation, allowing the covalently-attached triethylammonium (TEA) functional group to block the pore and thus reducing conductance by 90%. On the other hand, in the presence of UV light, the azobenzene group adopts the contracted *cis*-conformation, causing

the TEA functional group to move away from the pore and hence, restoring ion channel activity.

## 1.5 Properties of Gramicidin

Gramicidin (isolated from *Bacillus brevis*) consists of six 15-amino acid peptides that have been used medicinally as antibiotics against gram-positive and some gram-negative bacterial infections. Gramicidin forms ion channels in the lipid membranes of bacteria and eventually causes cell death by disrupting the membrane potential of the cell.

The crude mixture of Gramicidin that is naturally isolated is called Gramicidin D (gD) and consists of six isoforms with the general peptide sequence, formyl-L-**X**-Gly-L-Ala-D-Leu-L-Ala-D-Val-L-Val-D-Val-L-Trp-D-Leu-L-**Y**-D-Leu-L-Trp-D-Leu-L-Trp-HNCH<sub>2</sub>CH<sub>2</sub>OH. **X** can be either Val (consisting of 95% of gD) or Ile (consisting of 5% of gD) and **Y** can be: Trp (this isoform called Gramicidin A, gA, makes up 80% of gD); Phe (this isoform called Gramicidin B, gB, makes up 14% of gD); or Tyr (this isoform called gramacidin C, gC, makes up 6% of gD).<sup>22</sup> Due to the higher abundance of the gA isoform, the biophysical properties of gA have been more extensively studied compared to the other isoforms. From this point on, this dissertation will focus only on gA.

The structural properties of gA make it possible for the conductance of ions across this ion-channel forming peptide. gA consists of alternating D and L amino acids. This alternating stereoconfiguration of amino acids allows for the

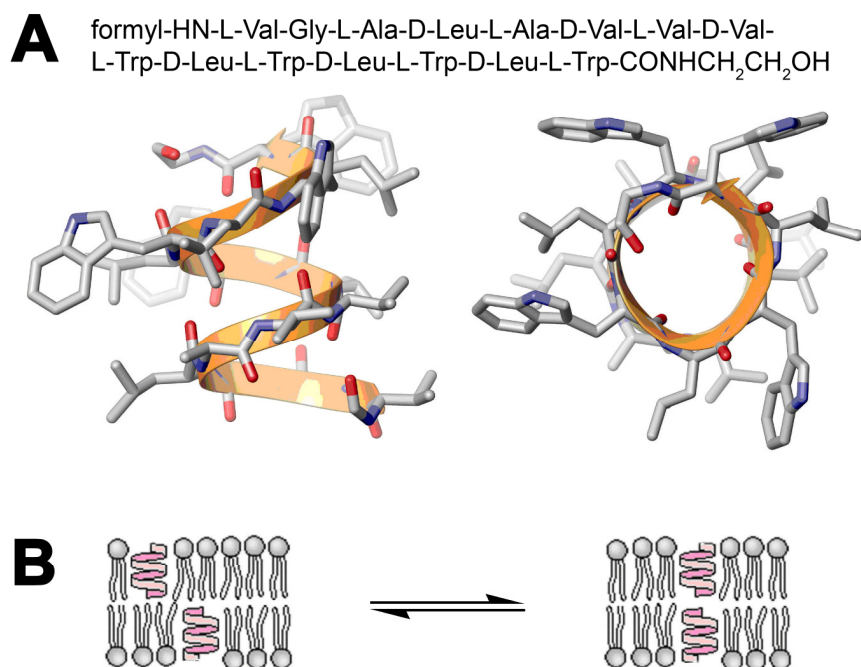


**Figure 1.6.** Cartoon showing the sequence and structure of a monomer of gramicidin A (gA) (adapted from the crystal structure of gA, 1GRM) and the reversible dimeric assembly of a gA pore in a lipid bilayer. A) Sequence and helical structure (side view on the right and top view on the left) of gA. B) Pore formation of gA: the reversible dimerization of two gA molecules at their N-termini via hydrogen bonding produces an open pore that spans the lipid bilayer and conducts monovalent cations. This ion flux results in distinct and measurable conductance levels that are characteristic for certain derivatives of gA.<sup>1-6</sup>

formation of a right-handed  $\beta$ -DL-helix structure in a lipid membrane that places all of the hydrophobic side chains extended radially away from the pore and internalizes the peptide backbone, forming the hydrophilic lumen of the channel (Figure 1.6A). This 3D configuration of gA permits the channel to incorporate into a lipid membrane and function as a membrane protein. The  $\beta$ -helix has 6.5 residues per turn, forms a pore of about 4 Å in diameter<sup>23</sup> and has a length of 26 Å.<sup>24</sup> Due to the length of  $\beta$ -helix, two monomers of gA must reversibly dimerize at the N-termini via hydrogen bonding (6 intermolecular hydrogen bonds) to

generate an ion channel that can span the width of the lipid membrane and conduct ions (Figure 1.6B).

Gramicidin A is selective with respect to the ions that can diffuse across the channel. gA is cation selective, allowing only the passage of monovalent cations, and their rates of conductance are the following from greatest to least:  $\text{H}^+$ ,  $\text{Cs}^+$ ,  $\text{Rb}^+$ ,  $\text{K}^+$ ,  $\text{Na}^+$ , and  $\text{Li}^+$ . For example,  $10^7$   $\text{K}^+$  ions per second traverse gA at an applied potential of 150 mV across the membrane.<sup>8</sup> The trend for the rates of conductance of these cations can be explained by taking into account the size of the hydration shell around the ion in solution. In order for an ion to conduct across the channel, the ion must first shed its hydration shell which is an energetically-costly process. The energetic cost is offset when the ion binds the channel (specifically, the partially negative-charged carbonyls).<sup>25</sup> Because smaller cations have a larger charge density on the surface, their hydration shells are larger compared to larger cations with a smaller charge density.<sup>8</sup> As a result, there is a larger enthalpic cost for smaller cations to shed their hydration shell, which raises the activation energy for conductance, thus slowing the rate of conductance.<sup>26</sup> The case with  $\text{H}^+$  is an exception to the rule as it conducts faster than the other cations even though it is the smallest ion. It is believed that because there is a continuous row of water molecules inside the pore,  $\text{H}^+$  can jump.<sup>26</sup> The diameter of the lumen restricts ion mobility across the channel to a single-file process. It is thought that water and ion transport through the channel are coupled during diffusion. For example, Levitt and coworkers<sup>27</sup> reported that nine water molecules are coupled to the diffusion of each  $\text{Na}^+$  ion across the

channel regardless of the  $\text{Na}^+$  concentration in the surrounding solution; however, seven water molecules are coupled with  $\text{K}^+$  transport at low concentrations of  $\text{K}^+$  in the surrounding solution while five are coupled to  $\text{K}^+$  at high concentrations. Most of these models for cation diffusion across the channel assume single occupancy (only one cation being present in the channel at any one time). Single occupancy more likely dominates in conditions where conductance rates are slow such as when  $\text{K}^+$ ,  $\text{Na}^+$ , and  $\text{Li}^+$  (slower conducting) are present<sup>28</sup> and the concentrations of the ions are millimolar or less in the surrounding solution (slower conductance due to smaller concentration of ions).<sup>29</sup> gA is unable to conduct divalent cations and when they are introduced (0.1 – 0.5 M) to a solution containing monovalent cations (~1 M), conductance is significantly reduced because divalent cations bind to the lumen of the channel and block it.<sup>30</sup>

## 1.6 Gramicidin A as a platform for ion channel sensors

There are several reasons that make Gramicidin A attractive as a practical, molecular platform for the development of ion channel-based nanosensors: 1) its ion conducting properties can measurably amplify a signal by monitoring a flux of ions through a single pore; 2) its current levels are distinct and quantized, which allows the measurement of changes in conductance on a single channel level; 3) its C-terminus can be derivatized without abolishing channeling activity;<sup>1, 13-15, 31-34</sup> 4) its availability in large quantities from

commercial sources makes it possible to generate derivatives on practical scales; 5) its self-incorporation into lipid bilayers makes its use straightforward as opposed to ion channel proteins that require incorporation into bilayers through proteoliposome fusion;<sup>35-38</sup> 6) its electrophysiological characteristics are well known, making it an excellent model for fundamental biophysical studies of pores in membranes; and 7) its size is on the order of nanometers, which allows for incorporation into miniaturized device designs and may enable parallel assays developed in a high density format.

In order to exploit the potentially useful advantages of gA for purposes of detection, several groups including the Yang group have used gA for a number of sensor applications. Derivatives of gA, for example, have been used to sense protein-ligand interactions,<sup>14, 15, 39</sup> redox potential of the electrolyte solution,<sup>40</sup> ammonium ions,<sup>41</sup> light,<sup>42, 43</sup> and pH at membrane interfaces.<sup>33, 44</sup> Lauger's group showed that charged derivatives of gA can have dramatically different conductance values based on the polarity and number of the attached charges.<sup>2, 3, 32</sup>

The rest of this dissertation will focus on the work that was carried out by our group on: (1) the development of design parameters to improve sensing with A-based nanosensors; (2) the demonstration of detecting analytes in aqueous solution by modifying the charge of a chemical group near the lumen of gA (charge-based sensing); (3) the chemistry for producing reactive building blocks of gA developing more robust and diverse gA-based nanosensors; (4) the detection of enzyme activity using charge-based sensing to achieve picomolar

limits of detection; and (5) the small structural changes that can be introduced to the peptide near the lumen of the channel to manipulate the conductance.

# Chapter 2

## Principles behind charge-based sensing

### 2.1 Inspiration behind charge-based sensing

In 2002, Woolley and co-workers developed a pH sensor from a derivative of gA that carried an amine functional group at the C-terminus.<sup>17</sup> Using an

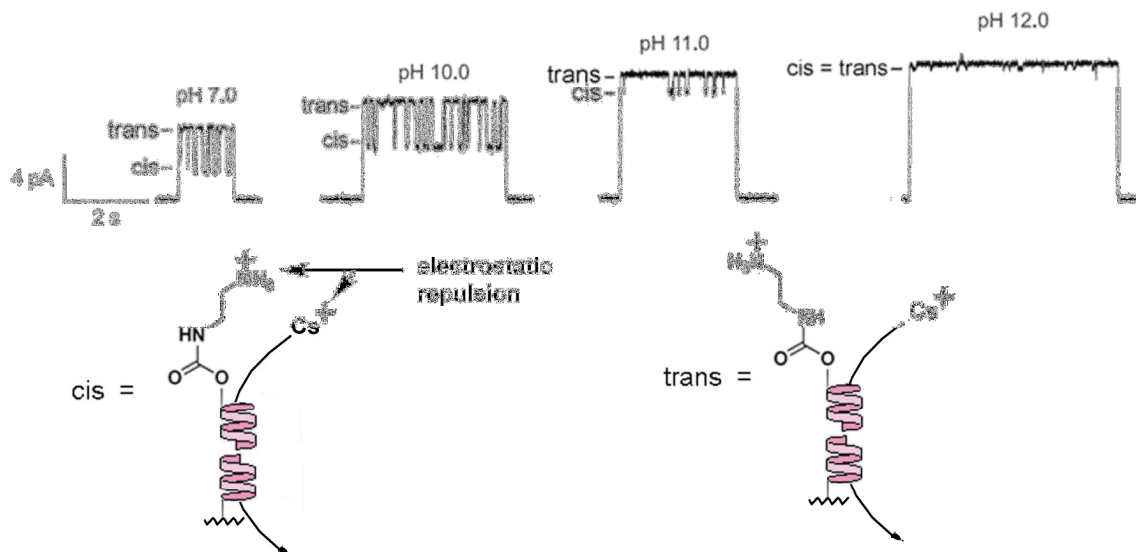


**Figure 2.1.** Cartoon depicting Woolley's gA derivative as a pH sensor. The current vs. time traces represent a single ion channel event. Two pH-dependent effects can be seen here. As the pH decreases, the difference between the cis and trans current levels increase. Furthermore, as the pH decreases, the conductance of cesium ions across the channel decreases.

electrophysiological setup, they incorporated the derivative of gA into a lipid membrane and observed two pH-dependent effects on the conductance of cations. First, as pH decreased, the overall conductance of ions decreased across a single channel and, second, as pH decreased, the difference between two current levels (they call cis and trans) became more distinct (Figure 2.1). Woolley explained that the decrease in conductance across a single channel occurs because of the electrostatic barrier that the positively-charged amino group poses for conducting cations at lower pH. To explain the development of distinguishable cis and trans currents at low pH, Woolley reasoned that the cis conformation of the carbamate bond places the positively charged amino group closer to the pore than the trans conformation; as a result the cis conformation had a larger electrostatic effect on cations (Figure 2.1).

Woolley concluded that the distance of a charged functional group from the lumen of the ion channel and the charged state of the functional group can affect the conductance of ions across the channel. Based on these findings, we envisioned a principle that we later called charge-based sensing (Figure 2.2). The principle involved using a chemical analyte to chemically react selectively with a functional group on a derivative of gA, so that a change in the charged state of the functional group occurs. We hypothesized that this change in the charge state of the functional group should produce a measurable change in conductance. Since this chemical reaction can occur only in the presence of the chemical analyte, selective detection of the analyte is achieved when the conductance of ions across the channel changes.

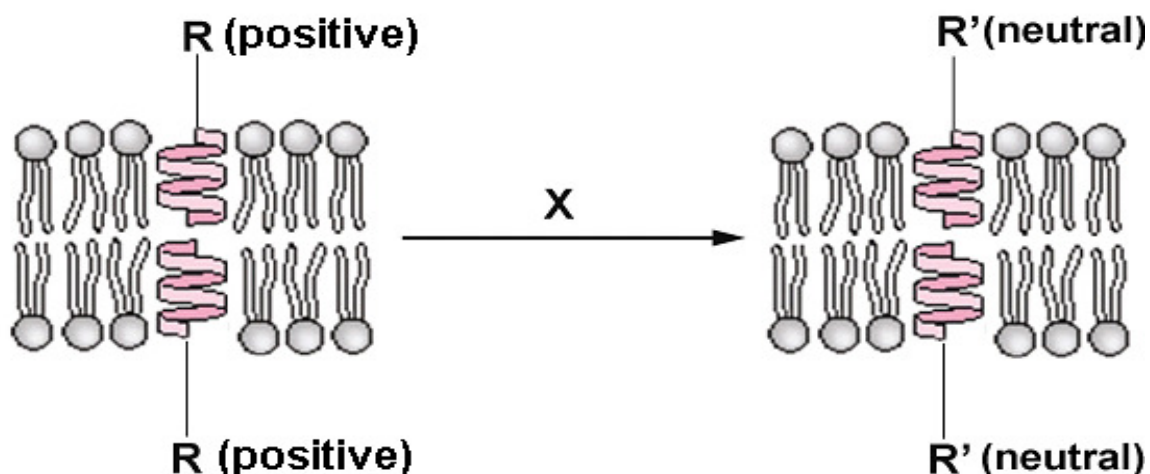


**Figure 2.2.** Illustration showing a generic example of charge-based sensing. gA is functionalized with a substrate (R) that carries a positive charge. Upon the addition of X to the solution, a chemical reaction is initiated between X and R, resulting in R' (which is uncharged). The change in charge will cause a measurable increase in the conductance of ions and X is selectively detected.

In order to effectively demonstrate the principle of charge-based sensing, we needed to optimize the environmental parameters which would maximize the change in conductance when going from R to R' on a derivative of gA. By maximizing the change in conductance, the conversion from R to R' can be easily monitored, facilitating the detection of X through electrophysiological measurements (Figure 2.2). There were 6 key parameters for charge-based sensing that we investigated for their influence on differently charged derivatives of gA: (1) the distance of the charge on the functional group from the entrance of the lumen of the channel; (2) the ionic strength of the recording buffer; (3) the importance of a well-defined charge on the derivative of gA in the pH range of analysis; (4) the applied transmembrane voltage; (5) the molecular asymmetry of

the gA dimer (homo- vs heterodimer); and (6) the charge on the headgroups of the lipid membrane.

## **2.2 Influence of the distance of charge from the pore on the conductance of derivatives of gA**

To study the effect of the distance of the charged functional group attached near the lumen of gA on the single channel conductance, we synthesized two sulfonate derivatives of gA (Figure 2.3): one with a long spacer arm, **1**, and one with a short spacer arm, **2**.<sup>45</sup> We chose the sulfonate functional group because it remains negatively charged over a wide pH range ( $pK_a = -3$ ). Figures 2.3B and 2.3C show the energy-minimized structures of **1** and **2**, respectively, as computed from a conformational search based on molecular mechanics calculations using Macromodel software. From the conformations shown in Figure 2.3B and 2.3C, we compared the location of the negative charge in **1** and **2** by measuring the distance of the sulfur atoms to a fixed point in space near the opening of the pore (located at half the distance between the  $\alpha$ -carbon of Leu14 and the  $\alpha$ -carbon of Trp11). From this comparison, the molecular mechanics calculations estimate that the sulfonate group of **1** is 0.75 nm and the sulfonate group of **2** is 0.68 nm from this fixed point at the opening of the pore. If we measure the distance of the sulfur atoms in **1** and **2** with the spacers in fully extended conformation, we estimate the charge of the sulfonate group in **1** to be located at a maximum distance of 1.81 nm and in **2** to be located at a maximum

A) formyl-HN-L-Val-Gly-L-Ala-D-Leu-L-Ala-D-Val-L-Val-D-Val-L-Trp-D-Leu-L-Trp-D-Leu-L-Trp-D-Leu-L-Trp-CO-**X**

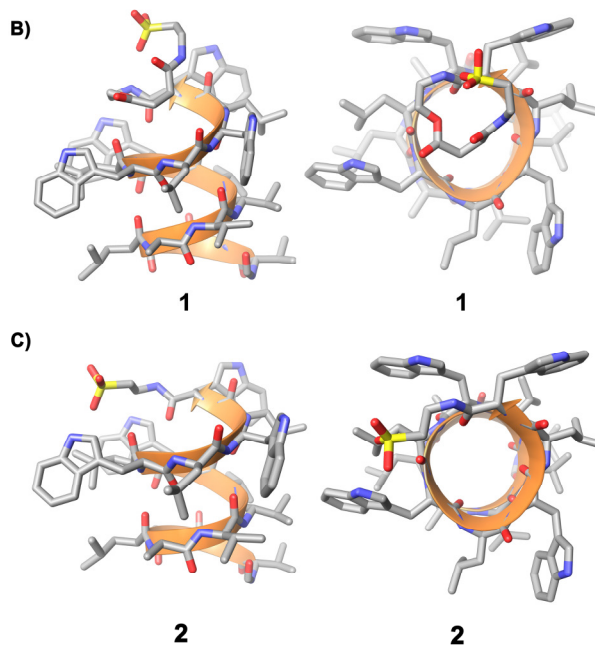
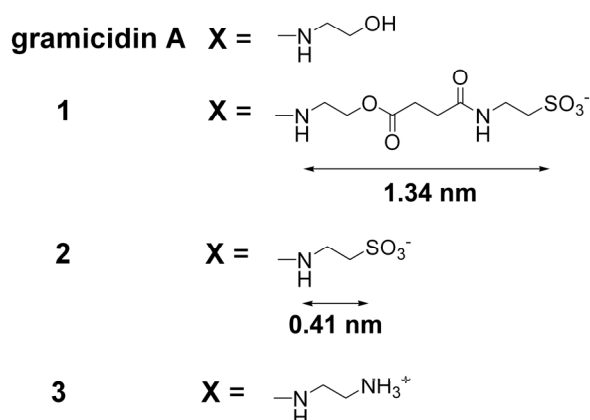
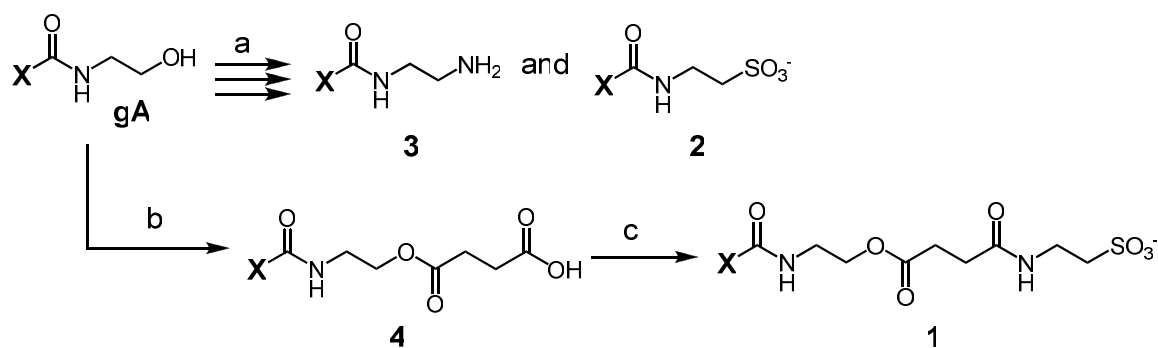


**Figure 2.3.** Sequence and calculated structure of two negatively-charged derivatives of gramicidin A (gA). A) Sequence of gA, of a negatively-charged sulfonate group covalently attached to gA via a long spacer (**1**), a negatively-charged sulfonate group covalently attached to gA via a short spacer (**2**), and a positively charged amine group covalently attached to gA via a short spacer (gramicidamine, **3**). The lengths shown for the spacers in **1** and **2** (from the nitrogen atom to the sulfur atom) were estimated by energy minimization in their fully extended conformation. B) Computer-generated side view (left) and top view model (right) of **1** based on molecular mechanics calculations. C) Computer-generated side view (left) and top view model (right) of **2** based on molecular mechanics calculations.

distance of 0.88 nm from this same fixed point near the opening of the pore. Although these charged derivatives of gA adopt many conformations with a range of distances of the charge from the pore when incorporated in a lipid membrane, these calculations are consistent with the prediction that the charge in **1** is located further away (0.75 - 1.81 nm) on average from the opening of the pore compared to the charge in **2** (0.68 - 0.88 nm).

We synthesized **1**, **2**, and **3** from commercially available native gA (Scheme 2.1). Details involving the synthesis of **2** and **3** will be discussed in Chapter 4. To lead to the synthesis of **1**, we reacted the C-terminal alcohol of gA with succinic anhydride to give the mono-succinic acid derivative of gA, **4**. Finally the free carboxylic acid of **4** was amidated with taurine to afford the long sulfonate derivative of gA, **1**.



$X = HCO-Va-Gy-Aa-Let-Aa-Va-Va-Va-Trp-Let-Trp-Let-Trp-$

**Scheme 2.1.** Synthesis of gA carrying a sulfonate via long (**1**) and short linker (**2**) and an amine (**3**). a) Discussed in Chapter 4; b) succinic anhydride, pyridine, dichloromethane (DCM); c)  $ClCO_2t-Bu$ , tetrahydrofuran (THF), diisopropylethylamine (DIEA), taurine (28% yield, 2 steps)

Figure 2.4 shows representative traces of the currents generated from different derivatives of gA at an applied potential of 150 mV in a recording buffer

containing 0.02 M KCl. The difference in conductance of ions through pores formed from gA-gA, **1-1**, or **2-2** homodimers resulted from the type of charge (negative vs. uncharged) near the pore and the distance of the charge attached from the pore.

Figure 2.4 demonstrates that the conductances of **1-1**, and **2-2** are measurably different from the conductance of gA-gA and illustrates that this difference is bigger when the negative charge is located close to the

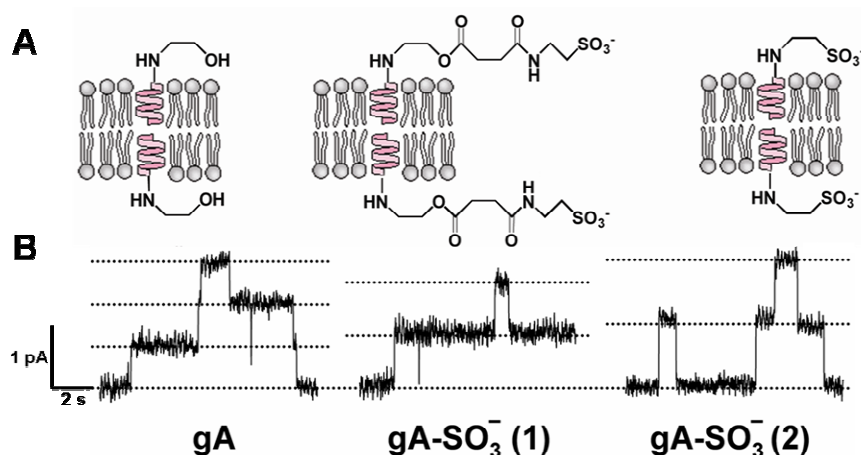


**Figure 2.4.** Cartoon of gA pores in planar lipid bilayers and current versus time traces of the respective dimeric pores. A) Cartoon representation of homodimeric pores of gA-gA, **1-1**, and **2-2** in a bilayer and B) corresponding representative ion channel traces of pores of gA-gA, **1-1**, and **2-2**. All three traces were obtained at an applied potential of +150 mV from lipid bilayers made with 1,2-diphytanoyl-sn-glycero-3-phosphocholine (DiPhyPC) in an electrolyte containing 0.02 M KCl buffered with 0.2 mM HEPES at pH 7.4. Note the increased single channel conductance of pores of **1-1** compared to gA-gA and of **2-2** compared to **1-1** and gA-gA. All current traces are shown with the same scaling of y- and x- axis.

entrance of the pore (**2**) compared to a charge that is located further away (**1**).

According to the Debye-Hückel theory,<sup>46</sup> there is a pre-concentration of cations around the negative sulfonate group of **1** and **2**; and this pre-concentration near

the pore increases the rate of conductance of cations in **1-1** and **2-2** compared to gA-gA. The pre-concentration of cations will decrease as a function of distance from the negative charge, explaining the lower conductance of the longer-spaced derivative **1** compared to **2**. From this experiment, we concluded that it is important to design charge-based sensors where the charge on the functional group is as close as possible to the pore, so that the change in conductance is maximized when going from one charged state on R to another on R' (Figure 2.2).

### **2.3 Influence of the ionic strength of the recording buffer on the conductance of negatively-charged derivatives of gA.**

The Debye-Hückel theory also predicts that the electrostatic attraction of cations in solution by the negative sulfonate group in **1** and **2** decreases with increasing ionic strength of the electrolyte solution because of the enhanced shielding of the negative charge by the increased concentration of cations in the solution. We tested this hypothesis by comparing the ion channel conductance of gA, **1**, and **2** in recording buffers with different ionic strengths. Table 2.1 shows the single-channel conductance of homodimers of gA and of negatively charged gA derivatives, **1** and **2**. The effect of the negative charge on the gA derivatives with respect to their single-channel conductance decreased with increasing ionic strength of the solution, as predicted by the Debye-Hückel theory. We found the

**Table 2.1.** Single-channel conductances,  $\gamma$ , of homodimers of gA-SO<sub>3</sub><sup>-</sup> with a long spacer arm (**1**) and of gA-SO<sub>3</sub><sup>-</sup> with short spacer arm (**2**) compared to native gA at different concentrations of KCl in the recording buffer.<sup>a</sup>

Conc. of KCl (M)	$\gamma$ gA-gA (pS)	$\gamma$ 1-1 (pS)	$\gamma$ 2-2 (pS)	$\gamma$ -ratio 1-1/gA- gA	$\gamma$ -ratio 2-2/gA-gA
0.01	2.7 ± 0.5	3.5 ± 0.3	4.3 ± 0.3	1.3	1.6
0.10	10.3 ± 0.1	11.0 ± 0.4	12.6 ± 0.4	1.1	1.2
1.00	20.0 ± 0.2	19.5 ± 0.4	21.5 ± 0.3	1.0	1.1

<sup>a</sup>Bilayers were made from DiPhyPC lipids. Conductances were obtained from the slope of current versus voltage curves (I-V curves) in the linear range between -100 mV and +100 mV of the I-V curves. Errors represent the standard deviation calculated from at least two (typically three) independent experiments. 1 pS =  $1 \cdot 10^{-12} \Omega^{-1}$ . A two sample t-Test and a one-way ANOVA test both confirmed that the mean conductance values of gA-gA, **1-1**, and **2-2** were with a significance level of 0.05.

biggest relative difference in conductance between homodimers of **2** and homodimers of gA when we used a buffer with a concentration of 0.01 M KCl. At this concentration, the conductance of **2-2** was larger by a factor of 1.6 than that of gA-gA. Even at a concentration of 0.10 M KCl, the single-channel conductance of **2-2** was larger by a factor of 1.2 than the conductance of gA-gA. On the other hand, at a concentration of 1.00 M KCl, the difference in single channel conductance between gA-gA and **2-2** was less than 10% (Table 2.1). At low ionic strength (0.01 M KCl), the difference in conductance of **1-1** compared to gA-gA was greater by a factor of 1.3, at 0.1 M KCl and 1 M KCl the difference was 7% and 3%, respectively. Based on the results from Table 2.1, KCl concentrations lower than 0.01 M could be expected to enhance further the difference in conductance between the charged gA derivatives and the original, uncharged

gA. We found, however, that the formation of stable lipid bilayers from lipids was difficult at these low KCl concentrations. Consequently, in order to obtain reliable and reproducible recording conditions, we found that KCl concentrations of at least 0.01 M worked best for charge-based sensing applications.

## **2.4 Importance of a well-defined charge on the derivative of gA in the pH range of analysis**

Since the charge on functional groups attached to gA may depend on the protonation state of the molecule, it is important to consider the  $pK_a$  of functional groups in the design of a charge-based gA sensor. To show the importance of a well-defined charge on the gA derivative at the pH range of analysis, we compared the conductance of pores from **2-2** with the conductance of pores from gA-gA at pH 7.4 and pH 12 (Table 2.2). As expected, we found that the conductance of pores from **2-2** was significantly larger than the conductance from gA-gA at both pH values (because of the presence of the sulfonate group on **2**, which was charged negatively at both pH values since its  $pK_a$  in water is  $\sim -3$ ). To provide an example of a functional group whose charge is not well-defined over the same pH range, we synthesized an amine-terminated derivative of gA (gramicidamine, **3**, see Figure 2.3). The derivative, **3**, is expected to be predominantly protonated (and hence positively charged) at pH 7.4 and predominantly uncharged at pH 12 (since the  $pK_a$  of a primary amine in water is  $\sim 10$ ). When we compared the conductance of pores from **3-3** with the

conductance of pores from gA-gA at pH 7.4 (Table 2.2), we found, as expected, that the conductance of **3-3** was significantly smaller than the conductance of gA-gA (presumably because of the positively-charged amine group on **3**). In contrast at pH 12, the predominant conductance of **3-3** was indistinguishable from the conductance of gA-gA (presumably because of the uncharged state of the unprotonated amine group being similar to uncharged state of native gA at pH 12). These results demonstrate that it is important to design charge-based sensors such that at the operational pH, there is a difference in the charge state between R and R' on gA (Figure 2.2), resulting in a measurable difference in the conductance between the two derivatives.

**Table 2.2.** Single-channel conductances,  $\gamma$ , of homodimers of gA, **2**, and **3** at pH 7.4 and pH 12. Bilayers were made from DiPhyPC lipids in 20 mM KCl buffered with HEPES (pH 7.4). For the measurements at pH 12, 10 mM KOH was added to this electrolyte to give the desired pH. As a result, the conductances at pH 12 increase due to the increase in the concentration of  $K^+$ . Conductances were obtained from the slope of current versus voltage curves (I-V curves) in the linear range between -100 mV and +100 mV.

Composition of pore	$\gamma$ at pH 7.4 (pS)	$\gamma$ at pH 12 (pS)
gA-gA	$4.5 \pm 0.1$	$7.8 \pm 0.2$
<b>2-2</b>	$5.8 \pm 0.1$	$9.8 \pm 0.2$
<b>3-3</b>	$3.8 \pm 0.2$	$7.7 \pm 0.9$

## **2.5 Dependence of the I-V characteristic of gA channels on the applied transmembrane voltage and on the molecular heterogeneity of the gA dimers**

Figure 2.5 demonstrates that the absolute difference in conductance between gA and its negatively charged derivative **2** increased with increasing transmembrane voltage in a recording buffer containing 0.02 M KCl. Figure 2.5 also shows, however, that the current through all gA pores did not increase linearly with applied voltages above 100 mV. We observed this nonlinear behavior only at low concentrations of KCl ( $\leq 0.10$  M KCl). At a concentration of 1.00 M KCl, the I-V curve of gA, as expected, was linear (data not shown). One possible explanation for the non-linear behavior of the I-V curve of gA and of negatively-charged derivatives of gA at low KCl concentrations is that the flux of ions through the pore was so fast that the effective molarity of potassium ions near the pore started to decrease at high applied potentials ( $> 100$  mV).<sup>47</sup> We, therefore, expected that a negatively charged group that is able to increase the effective molarity of potassium ions close to the entrance of the pore should result in an increase in conductance compared to native gA under the same applied potential. This increase should be most pronounced at low ionic strength of the bulk solution (due to the lack of shielding from cations surrounding the negative charge as discussed in section 2.3) and at high transmembrane voltages when the movement of the ions through the pore is fast. The results in Figure 2.5 are consistent with these predictions. The relative difference in

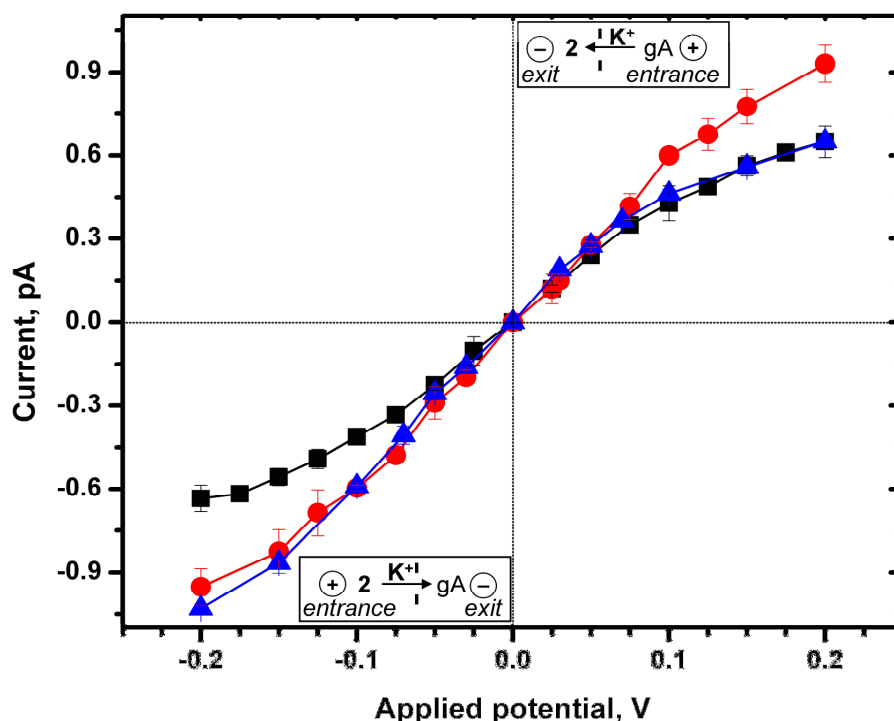


**Figure 2.5.** Current-voltage characteristic of a homodimeric pore of gA-gA (■), 2-2 (●), and a heterodimeric, asymmetric pore of gA and 2 (▲). The hybrid, asymmetric pore was assembled by adding native gA to the cis compartment and 2 to the trans compartment of the bilayer setup<sup>7</sup> (the cis compartment refers to the compartment that defined the polarity of the applied voltage, the trans compartment was connected to ground). The concentration of KCl was 0.02 M for these experiments and bilayers were formed with DiPhyPC lipids using the folding method. Each data point represents the average of at least three measurements of current. The annotations of gA and 2 in the boxes of the graph indicate the direction of the flux of K<sup>+</sup> ions (arrows) and thus illustrate whether gA or 2 was at the entrance or at the exit of the pore at a given polarity of the applied voltage.

conductance between the negatively-charged gA derivatives compared to gA increased with increasing transmembrane voltage; the ratio between the conductance of 2-2 and gA-gA (at a KCl concentration of 0.02 M), for instance, increased from 1.4 at 100 mV to 1.5 at 200 mV applied potentials.

Due to our interest in developing sensors based on changing the charge of functional groups attached to the entrance of a gA pore, we attempted to determine whether it was important for the derivatives of gA used here to change the charge of both gA monomers in a dimeric pore in order to observe a measurable change in conductance. We, therefore, investigated the conductance behavior of an asymmetric gA pore (Figure 2.5). These asymmetric hybrid pores were composed of gA in one leaflet of the bilayer (here, the leaflet facing the aqueous compartment that defined the polarity of the applied voltage, denoted as the cis compartment) and of **2** in the opposite leaflet of the bilayer (denoted as the trans compartment). The question was would the I-V curve of these asymmetric pores be the same as the I-V curve of symmetric pores of gA, or would it be similar to the I-V curve of symmetric pores of **2**, or would it be different than the I-V curve of either symmetric pores, resulting in a hybrid of gA and **2**? We found (Figure 2.5) that at transmembrane potentials above 100 mV, the I-V characteristics of asymmetric pores were dominated by the charge on the derivative of gA that was located at the entrance of the pore; it was not affected by the charge on the derivative of gA at the exit of the pore. In other words, if the polarity of the applied potential was such that the negatively charged gA derivative **2** was located at the entrance of the pore for K<sup>+</sup> ions (i.e., **2** added to the positively-polarized compartment) while native gA was located at the exit of the pore (i.e., gA added to the negatively-polarized compartment), then the overall conductance was approximately the same as that of symmetric pores from **2**. Switching the polarity and thus placing **2** at the exit of the pore and gA at

the entrance of the pore resulted in a single-channel conductance that was similar to symmetric pores of gA.

To provide an explanation for the observed conductance behavior of asymmetric pores, we considered once again the local ion concentrations near the pore due to the presence of the negative charge on molecule, **2**. Derivative, **2**, in an asymmetric pore, will, according to Debye-Hückel theory, increase the local concentration of  $K^+$  ions close to the side of the pore that is made up by **2**. The gA molecule in the asymmetric pore on the opposite leaflet of the bilayer, will not, however, influence significantly the local concentration of  $K^+$  ions near the membrane (since gA is not charged). Hence, if the polarity of the applied voltage is such that **2** is located at the entrance of the asymmetric pore, the local increase in  $K^+$  ions will result in an increased conductance and the resulting conductance will be similar to homodimeric pores of **2-2**. On the other hand, if the polarity of the applied voltage is such that gA is located at the entrance of the asymmetric pore, the concentration of  $K^+$  ions at the entrance is not increased because **2**, being at the exit of the pore, will not have a significant effect on the concentration of  $K^+$  ions at the entrance and the conductance of such a pore will be similar to homodimeric pores of gA-gA. The data in Figure 2.5 is in excellent agreement with the predictions from this simple model.

## 2.6 Influence of charge on the lipid headgroups on the single channel conductance of gA and its derivatives

In order to explore the single channel conductance of the different gA derivatives in neutral, negatively-charged, and positively-charged planar bilayers in the lowest possible KCl concentration for maintaining stability of the bilayer, we formed bilayers in 0.01 M or 0.02 M KCl. As shown in Figure 2.6, the negative charges on the headgroups of lipids in bilayers neutralized the difference observed in Figure 2.4 in single channel conductance between gA-gA, **1-1**, and **2-2** almost completely.

Figure 2.6 shows that negative charges on the lipid membrane can override the effect of the negative charge on the sulfonate group of derivatives **1** or **2** even at concentrations of low ionic strength (here, 0.01 M). On the other hand, as illustrated in Figure 2.4, in bilayers that were made with neutral (zwitterionic) DiPhyPC lipids, the single channel conductance of **2-2** was significantly different from the conductance of gA-gA pores at low ionic strength (Table 2.1). Only at high ionic strength (1.00 M KCl) were the conductances of pores of **2-2** in zwitterionic lipid membranes approximately the same as pores of gA-gA (Table 2.1).

An interesting aspect of the conductance in negatively charged membranes (50% DOPS, 50% POPE) is that the conductance of symmetric dimers of gA and its derivatives are increased compared to zwitterionic

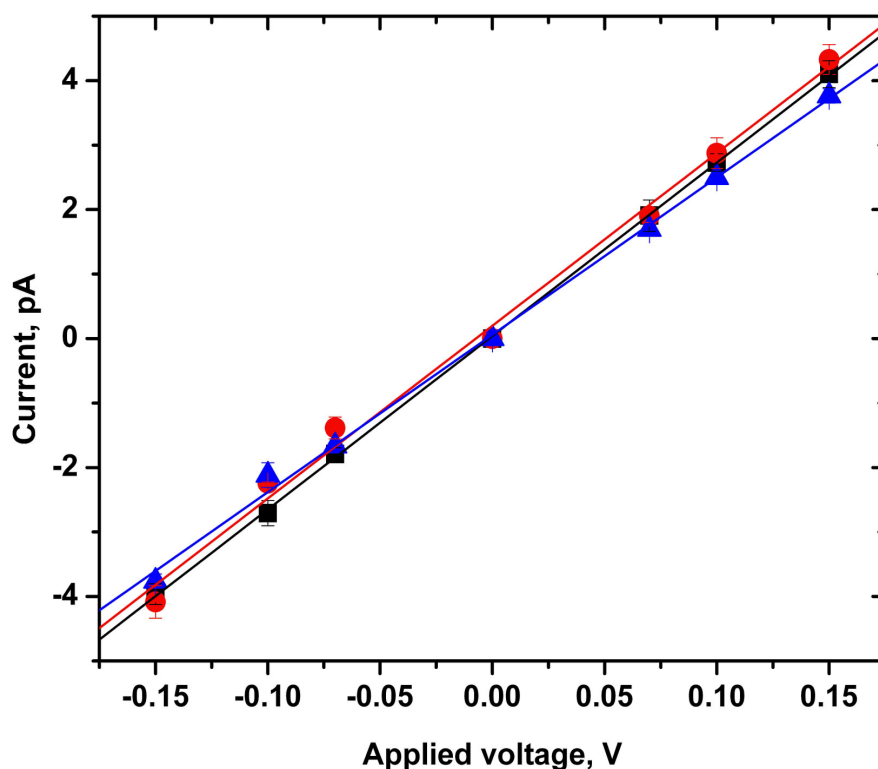


**Figure 2.6.** Effect of a negatively-charged head group on the lipids in planar bilayers. Current-voltage characteristics of homodimeric pores of gA (■), **1** (●) and **2** (▲) in negatively charged bilayers at low ionic strength. Planar bilayers were made with 50% zwitterionic POPE (1-palmitoyl-2-oleoyl-sn-glycero-3-phosphoethanolamine) and 50% negatively charged DOPS (1,2-dioleoyl-sn-glycero-3-phospho-L-serine). All experiments were performed in 0.01 M KCl with 0.1 mM HEPES (pH = 7.4) as electrolyte. Each data point represents the average of at least three mean current values calculated from fitting a Gaussian distribution to histograms of the current from original current versus time traces.

membranes. This observation supports the prediction that permanent negative charges near the entrance of the pore increase the local concentration of cations. This increase in concentration results in increased flux of  $K^+$  ions through the pores and this effect can be caused by charges at the entrance of the pore such as in **2** or by charges on the surrounding membrane lipids close to the entrance of the pore.

Figure 2.6 shows that, at a concentration of 0.01 M KCl, the effect of electrostatic attraction of ions to the bilayer predicted by the Debye-Hückel theory is very strong to the point that the conductance of gA-gA pores (27 pS) in 50% DOPS bilayers is higher than the conductance of gA-gA (20 pS) in zwitterionic bilayers made with DiPhyPC in a electrolyte containing 1.00 M KCl. Similar results have been reported previously for gA in charged lipids,<sup>2, 48</sup> and these observations emphasize the need for using appropriately charged lipid headgroups in the bilayers for development of charge-based sensors from gA.

Interestingly, when we measured the conductance of gA-gA and **2-2** in lipid bilayers that contained 10% of a lipid with positively-charged headgroups (here, 1,2-dioleoyl-3-(dimethylamino)propane, DODAP and 90% DiPhyPC), we found that the relative ratio of conductance of **2-2** to gA-gA was 10% larger than the relative ratio of conductance of these two homodimeric ion channels in purely zwitterionic lipids (in 20 mM KCl). These results show that using membranes that are oppositely charged than the gA derivatives makes it possible to enhance the relative difference in conductance between the charged and uncharged pores compared to measurements in zwitterionic lipids.

Thus, to maximize the effect of the change in charge of gA derivatives for charged-based sensing applications, the lipid headgroups in the bilayers should be zwitterionic or oppositely charged than the gA derivatives used for sensing.

## 2.7 Conclusion

Implementing the key design parameters and experimental conditions outlined in this paper in order to sense changes in the single-channel conductance of gA-based ion channels makes these semi-synthetic nanopores an excellent platform for development of sensors. Although the conditions outlined in this chapter are focused on the development of charge-based sensors, chemical or physical properties other than charge (i.e., steric hindrance discussed in Chapter 6) may also be useful for designing gA-based sensors. The sensitivity of single ion channel recordings (typical concentrations for gA used in single channel recordings in commercial bilayer chambers with 1 mL volume are 1-100 pM) makes it possible to perform more than one million assays from 1 mg of gA-based nanosensors. Current challenges for successful implementation of ion channel-based sensors are limited mechanical stability and requirement for manual preparation of planar lipid bilayers.<sup>49</sup> Recent advances in microfabrication techniques, however, make it possible to form bilayers in an automated fashion<sup>50-60</sup> as well as to prepare bilayers with improved mechanical stability by forming bilayers over pores with diameters below 15  $\mu\text{m}$ <sup>10, 61, 62</sup> or by embedding bilayers in hydrogels.<sup>63, 64</sup>

## 2.8 Protocol for Ion channel measurements

**Molecular modeling.** The molecular mechanics calculations shown in Figure 2.3 were performed using MacroModel (version 7.5, Schroedinger, Inc.) with energy

minimizations (using MM2 force field parameters) in water. We constructed **1** and **2** *in silico* by modification of the C-termini of the crystal structure of gA (1GRM) in MacroModel. The first 14 residues of the peptide were fixed during the conformational analyses since they represent residues most likely embedded in the bilayer. After performing 5000 iterations of conformational analyses each for **1** and **2**, we examined the structures of the 20 lowest energy conformations calculated for **1** and **2** and found they were all very similar to the structures shown in Figure 2.3. We estimated the distance from the pore of the negative charge in **1** and **2** by measuring the distance of the sulfur atoms to a fixed point in space near the opening of the pore (located at half the distance between the  $\alpha$ -proton of Leu14 and the  $\alpha$ -proton of Trp11). To determine the maximum distance that the charge can exist from the pore in **1** and **2**, we created a hypothetical structure *in silico* for **1** and **2** with spacers (Figure 2.3A) in their fully extended conformation and measured the distance between the sulfur atoms and this same fixed point in space near the opening of the pore.

**Formation of planar lipid bilayers.** We formed most planar lipid bilayers with the “folding technique.” A Teflon film (Eastern Scientific Inc, pore diameter 0.18-0.25 mm) was pretreated on each side with 2.5  $\mu$ L of 5% hexadecane in pentane and air dried. The film was mounted using vacuum grease (Dow Corning, High vacuum grease) to a custom made Teflon chamber separating two buffer compartments each with a volume capacity of 4 mL.<sup>61</sup> After adding 1 mL of electrolyte (0.01 M to 1.00 M KCl buffered with HEPES pH 7.4) to each

compartment, lipids were spread from a solution in pentane onto the surface of the electrolyte solutions (specifically, 4-6  $\mu\text{L}$  from 25  $\text{mg mL}^{-1}$  solution DiPhyPC or from 6.25  $\text{mg mL}^{-1}$  each of 50% DOPS and 50% POPE or from 25  $\text{mg mL}^{-1}$  DODAP mixed with 25  $\text{mg mL}^{-1}$  DiPhyPC in a 1:9 ratio. Three additional milliliters of electrolyte solution were added to each side of the chamber to raise the liquid levels above the aperture. We formed the bilayers from apposition of two monolayers of lipids using the method described by Montal et al.<sup>65</sup> Briefly, bilayers were obtained by consecutively raising the liquid level in each compartment until the pore was completely covered by electrolyte. If at this point the pore was not closed by a lipid bilayer, then the liquid level in one or both compartments was lowered below the pore level by aspirating electrolyte into a 3 mL syringe, followed by raising the electrolyte solution again. This cycle was repeated until a bilayer was obtained that had a minimum capacitance of 70 pF, and until the resulting membrane was stable (i.e., no significant current fluctuations above the baseline noise level) in the range of  $\pm 200$  mV applied potential for several minutes.

Planar lipid bilayers were also made with the “painting technique.” We pretreated each side of a pore in a bilayer cup (Warner Instruments, Delrin perfusion cup, volume 1 mL, pore diameter 250  $\mu\text{m}$ ) with  $\sim 2$   $\mu\text{L}$  of a 25  $\text{mg mL}^{-1}$  solution of DiPhyPC in hexane. After adding recording buffer (0.01 M KCl to 1.0 M KCl buffered with HEPES, pH = 7.4) to both compartments of the bilayer setup, we “painted” a solution of 20  $\text{mg mL}^{-1}$  DiPhyPC in n-decane over the pore by using a paint brush with a fine tip. We followed the thinning of the decane

droplet to form a planar bilayer by monitoring the capacitance of the bilayer. In case the decane droplet did not thin out spontaneously, we bubbled air in the chamber underneath the pore. The rise of these air bubbles in the vicinity of the pore usually helped to thin out the decane/lipid droplet.<sup>61</sup> After verifying that bilayers were stable for several minutes (in the range of  $\pm 200$  mV applied voltage) and that the capacitances were above 70 pF for folded and above 80-90 pF for painted bilayers, we added gA (4-8  $\mu$ L from 1 ng mL<sup>-1</sup> in ethanol), derivatives **1** or **2** (2-10  $\mu$ L from 100 ng mL<sup>-1</sup> in ethanol), or derivative **3** (4-10  $\mu$ L from 100 ng mL<sup>-1</sup> in ethanol) directly to the bilayer chambers.

**Ion channel measurements.** We performed single channel recordings in “voltage clamp mode” using Ag/AgCl electrodes (Warner Instruments) in each compartment of the bilayer chambers. Data acquisition and storage was carried out using custom software in combination with either an EPC-7 patch clamp amplifier from List Medical Electronic (set at a gain of 10 mV pA<sup>-1</sup> and a filter cutoff frequency of 3 kHz) or a Geneclamp 500 amplifier from Axon Instruments (with a CV-5B 100GU headstage, set at a gain of 100 mV pA<sup>-1</sup> and filter cutoff frequency of 1 kHz). We used the EPC-7 amplifier for most folded bilayers and the Geneclamp 500 amplifier for most painted bilayers. The data acquisition boards for both amplifiers were set to a sampling frequency of 15 kHz. All current traces shown in the figures were further filtered using a digital Gaussian low-pass filter with a cutoff frequency of 30 Hz. The current traces we used to generate all data recorded at applied potentials  $\leq 50$  mV were filtered at 10 Hz.

We performed the analysis of the single channel current traces by computing histograms of the currents from the original current-time traces with ClampFit 9.2 software from Axon Instruments. From these histograms we extracted the main current values by fitting a Gaussian function to the peaks in the histograms. All gramicidin molecules showed a predominant conductance and occasionally sub-conductance states (i.e. single channel currents that were smaller than the main current values). Single channel conductances reported in this paper always refer to the main conductance state (i.e. to the dominant peaks in the current histograms).

**Note about the chapter:** Parts of these chapters are reprints from the published reference: Steven Blake, Ricardo Capone, Michael Mayer, and Jerry Yang. Chemically Reactive Derivatives of Gramicidin A for Developing Ion Channel-Based Nanoprobes. *Bioconjugate Chem.*, 19 (8), 1614–1624, **2008**.

## Chapter 3

# Applications of charge-based sensing

### 3.1 Introduction

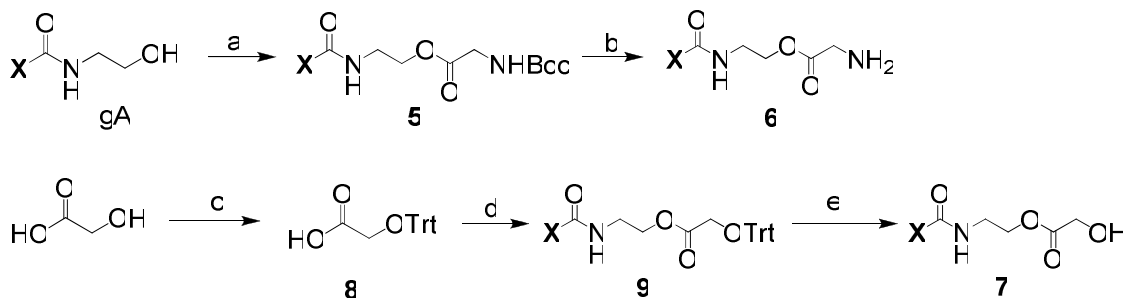
In this chapter, we applied the design parameters behind charge-based sensing that were developed in Chapter 2 to detect chemical agents in aqueous solution through their chemical reactivity with derivatives of gA. To achieve detection of chemical agents in solution, we followed the conversion of charged functional groups to uncharged functional groups attached near the gA pore or vice versa, which resulted in a measurable change in conductance.

Based on our observations in Chapter 2, we hypothesized that as the charge of the functional group is modified near the gA pore over the course of the reaction, a measurable change in conductance can be observed. The ideal reactions for charge-based sensing should have the following characteristics: (1) the conversion to product should be quantitative, so that a mixture of conductance states can be minimized upon completion of the reaction; (2) the

reactions should take place in water; (3) the reactions should result in a change of the charge on the functional group attached to the ion channel; and (4) the reaction should be relatively fast due to the limited stability of lipid membranes over a long period of time. Based on those characteristics, we decided that two reactions would be fit the criteria. One reaction would involve the conversion of a derivative of gA carrying an uncharged N-*tert*-butylcarbonyl protected (BOC) amine to a positively-charged ammonium functional group in the presence of HCl. Then, the ammonium functional group is converted to an uncharged alcohol in the presence of nitrite via the diazotization / hydrodediazonation reaction. As we learned in Chapter 2 that in order to maximize the change in conductance when chemically transforming one derivative of gA to the next, we needed to use high applied voltage of 100 mV, zwitterionic lipids (1,2-diphytanoyl-sn-glycero-3-phosphocholine), relatively low ionic strength buffer and a charged functional group that is close to the entrance of the gA derivative.

## 3.2 Demonstration of charge-based sensing

We synthesized three derivatives of gA, **5-7** by functionalizing the C-terminal alcohol of commercially-available native gA with BOC-protected glycine, glycine, and glycolic acid, respectively (Scheme 3.1). We produced derivative, **5**, through a coupling reaction between gA and BOC-protected glycine using the dicyclohexylcarbodiimide coupling agent. To remove the BOC group and obtain **6**, we used a solution of trifluoroacetic acid (TFA) and methylene chloride (DCM)



X = HCC-Va -G y-A α-Leu-A α-Va -Va -Va -Trp-Leu-Trp-Leu-Trp-Leu-Trp-

**Scheme 3.1.** Synthesis of **5-7** for the demonstration of charge-based sensing. a) BOC-Glycine, dicyclohexylcarbodiimide (DCC), 4-dimethylaminopyridine (DMAP), DCM (87% yield); b) TFA, EDT, Me<sub>2</sub>S, DCM (90% yield); c) trityl chloride, DIEA, DCM (22% yield); d) gA, DCC, DMAP, DCM (55% yield); e) TFA, EDT, Me<sub>2</sub>S, DCM (98% yield)

in the presence of ethanedithiol (EDT) and dimethyl sulfide (Me<sub>2</sub>S), which we will refer from this point on as a “TFA cocktail”. EDT was added to the reaction to prevent addition of *t*-butyl cations (generated from BOC-deprotection) to the indole groups on the tryptophans of gA<sup>66</sup> and Me<sub>2</sub>S was added to prevent oxidation of the indole groups which typically occurs under acidic conditions, respectively. In order to esterify gA with glycolic acid, we first protected the hydroxyl group of glycolic acid with a trityl group to obtain **8**. The protection of the hydroxyl group was necessary because in the following step where we couple gA to the carboxylic acid functionality of glycolic acid, the potential for polymerization through esterification of glycolic acid molecules was imminent. After **9** was obtained, the trityl group was deprotected with the TFA cocktail to afford the free alcohol, **7**.

Using an electrophysiological setup, we measured the single-channel current of **5-7** (Figure 3.1A). Figure 3.1B shows representative traces of current-

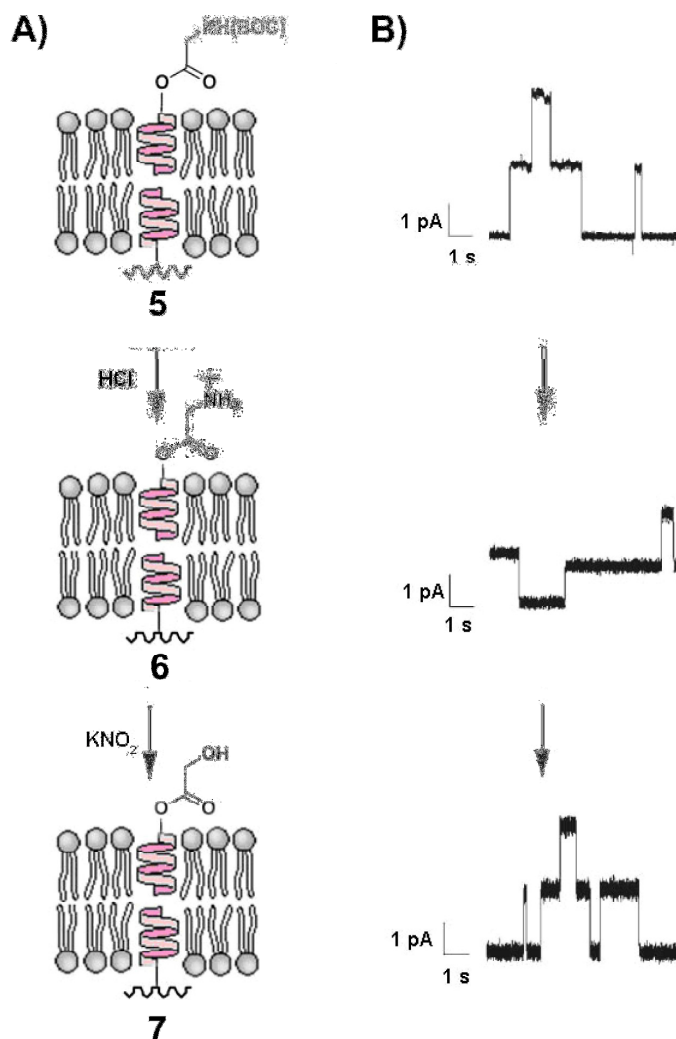


**Figure 3.1.** Monitoring chemical reactions on molecules attached to gA by analysis of single ion-channel currents. A) Illustration of the stepwise conversion of gA carrying a Boc-protected glycine group (top) to gA carrying a glycolic acid group (bottom) in the presence of external reagents. B) Representative single ion-channel recordings (in 1 M KCl, 0.01 M HEPES buffer, pH 7.4) of the corresponding derivatives of gA, **5–7**, shown in part (A).

versus-time for **5–7** under an applied potential of 100 mV in buffered solution (1 M KCl, 0.01 M HEPES buffer, pH 7.4). These traces show that the conductance of ions through derivatives **5–7** was dependent on the functional group present on the C-terminus. Analysis of the I-V curves (Figure 3.2) reveals a distinct

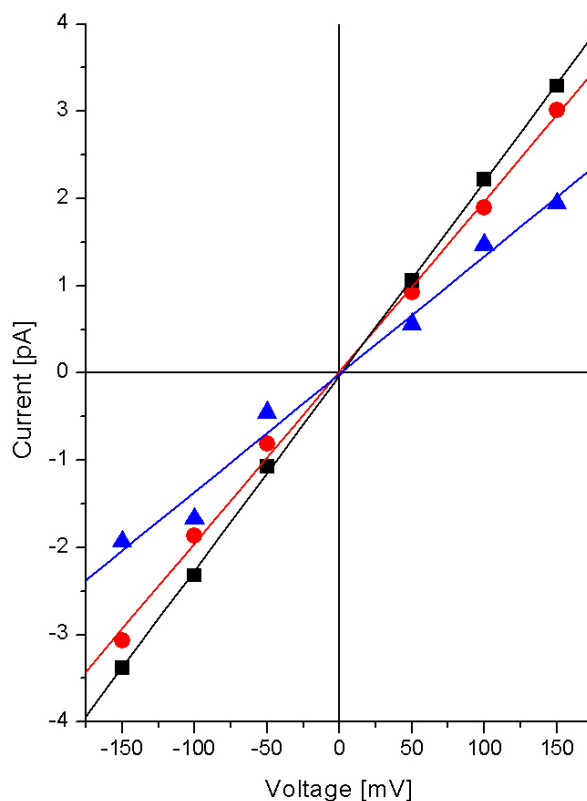


**Figure 3.2.** Conductance measurements of derivatives of gramicidin A carrying a tert-butoxycarbonyl protected glycine **4** (black), glycine **5** (blue), and glycolic acid **6** (red) in aqueous buffered solution (1 M KCl, 0.01 M HEPES, pH 7.4). The slopes of the linear fits were:  $22.3 \pm 0.2$  pS,  $13.5 \pm 0.8$  pS, and  $19.6 \pm 0.5$  pS, respectively.

single-channel conductance of  $22.3 \pm 0.2$ ,  $13.5 \pm 0.8$ , and  $19.6 \pm 0.5$  pS (S denotes siemens, current normalized over the voltage) for derivatives **5–7**, respectively. The measurably different conductance of these derivatives made it possible to monitor the conversion of **5–7** upon addition of external chemical reagents in an aqueous environment.

The deprotection of BOC groups on amines is typically done under acidic conditions.<sup>67</sup> We added **5** to a final concentration of 50 pM to both 1.0 mL chambers of a stirred planar lipid bilayer setup<sup>59, 61</sup> containing unbuffered

solutions of 0.5 M HCl and 0.5 M KCl and monitored the ion-channel activity after approximately 10 min. Initially, the main single-channel current at a potential of 100 mV was  $19.0 \pm 0.9$  pA (corresponding to a single-channel conductance of  $190 \pm 9$  pS) as indicated by the histogram in Figure 3.3B. After 30 min, the

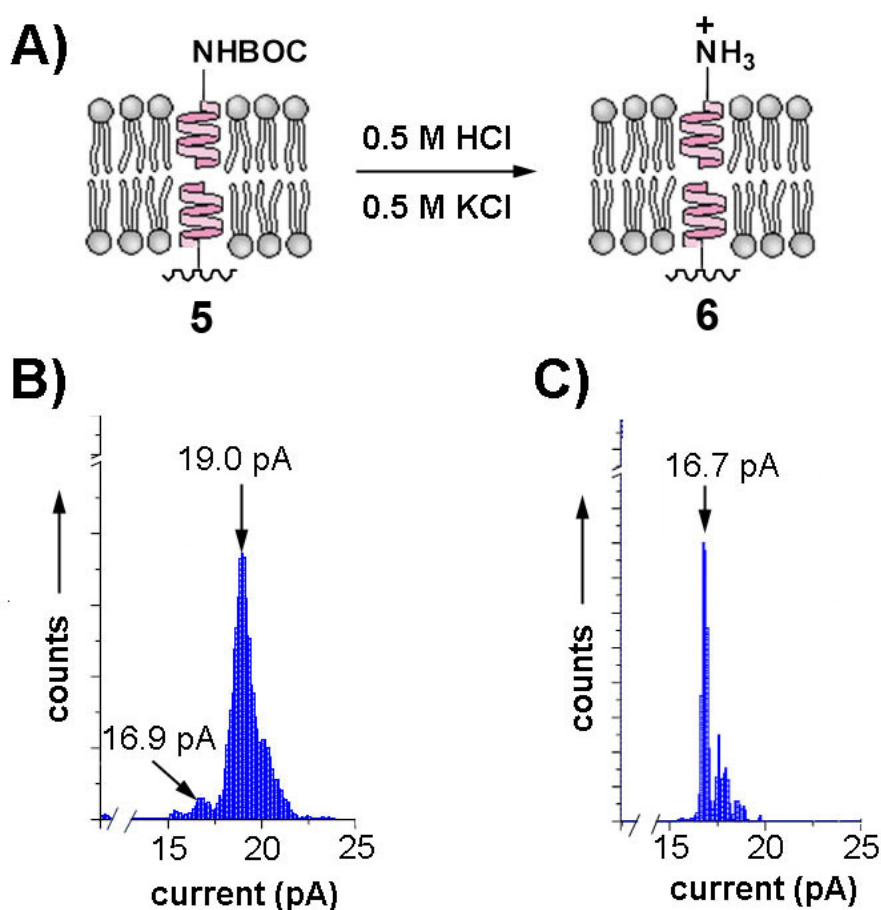


**Figure 3.3.** Monitoring of the single ion-channel currents during the conversion of gA derivative **5** to gA derivative **6**. A) Illustration of the removal of a *tert*-butyloxycarbonyl group from an amine under aqueous acidic conditions. Histograms of the observed single-channel current states of **5** recorded B) 10 min and C) 60 min after the initiation of the reaction shown in A).

occurrence of the single-channel current value of 19.0 pA was significantly reduced and after an additional 30 min (60 min total after the introduction of **5**), the main single-channel current observed was at  $16.7 \pm 0.3$  pA (Figure 3.3C). We

independently measured a current of  $17.1 \pm 0.3$  pA for **6** under the same conditions (i.e., 0.5 M KCl and 0.5 M HCl), which is consistent (within experimental error) with the final current value of  $16.7 \pm 0.3$  pA recorded for the deprotection of **5** in aqueous acidic solution. We believe the smaller single-channel conductance of **6** compared to **5** is due to the presence of a positive charge on the deprotected amine of **6** (as opposed to the uncharged character of **5**). A positive charge near the opening of the channel decreases the effective molarity of  $K^+$  ions thereby reducing the conductance across **6** compared to **5**. We confirmed by  $^1H$ -NMR spectroscopy that 1 mM Boc-protected glycine is deprotected within 80 min under analogous conditions in  $D_2O$ .

To demonstrate further the possibility of following the transformation of functional groups on molecules attached to gA, we monitored the conversion of the free amine on the C-terminally linked glycine moiety of **6** (i.e., the product of the reaction of **5** with HCl) to an uncharged alcohol group in the presence of potassium nitrite under aqueous acidic conditions.<sup>68</sup> We recorded a single ion-channel current of  $1.4 \pm 0.1$  pA for **6** (final concentration 20 pM) in a stirred planar lipid-bilayer setup containing 0.1 M KCl and 0.5 M potassium acetate buffer (pH 3.8) at a potential of 100 mV. We added  $KNO_2$  to both chambers of the planar lipid-bilayer setup (to give a final concentration of 0.03 M  $KNO_2$  in each chamber) and monitored the ion-channel activity. After approximately 45 min, we recorded a single-channel current value of  $1.8 \pm 0.1$  pA. Independent measurement of **7** under the same experimental conditions gave a single ion-channel current of  $1.8 \pm 0.1$  pA, which was consistent with the results from monitoring the conversion of **6**

to **7** by single ion-channel recordings. As expected, the conversion of the positively-charged amine in **6** to the uncharged alcohol in **7** resulted in a higher single-channel conductance of **7** compared to **6**. For comparison, we observed by  $^1\text{H}$  NMR spectroscopy that 0.01 M glycine can be converted quantitatively to glycolic acid within 60 min in the presence of 0.3 M nitrite under similar buffered conditions in  $\text{D}_2\text{O}$ .

### 3.3 Conclusion

We have, thus, shown that it is possible to detect chemical agents in aqueous solution by following the conversion of chemically reactive functional groups on derivatives of gA through single ion channel currents. This approach to the use of ion channel-forming peptides as chemical sensors complements studies on fluorescent chemosensors<sup>69-75</sup> which monitor changes in local environment of a molecule (here, manipulating the charge of functional groups near the opening of an ion channel pore) to sense a chemical process. Further development of ion channel-forming molecules with synthetically tailored conductance properties may make it possible to detect a wide range of chemically and biochemically active agents in solution with high sensitivity and selectivity. Synthetically tailored ion channels may also be useful for fundamental studies on organic reactions on molecules embedded in bilayers for cell surface engineering applications.<sup>76</sup>

### 3.4 Protocol for monitoring chemical reactions

**Monitoring the reaction of glycine with  $\text{KNO}_2$  by NMR.** A 10-ml buffer of 0.4 M potassium acetate / acetic acid buffer was prepared in  $\text{D}_2\text{O}$  with glycine (7.5 mg, 0.01M) and KCl (7.4 mg, 0.01M) dissolved (pH 3.9). Sodium nitrite (20.7mg, 0.3mmol) was added to a 1 ml aliquot of the buffered solution and  $^1\text{H}$ -NMR's were taken at various time points to monitor the conversion of glycine to glycolic acid.  $^1\text{H}$ -NMR ( $\text{D}_2\text{O}$ , 400 MHz): Glycine methylene:  $\delta$  3.422 (s, 2H), Glycolic acid methylene:  $\delta$  3.898 (s, 2H). The chemical shift of glycolic acid was confirmed using an authentic sample. Upon completion of the reaction (80 min), the pH was 3.9.

**Ion channel measurements.** Planar lipid bilayers were formed with the "painting technique". We pretreated each side of a pore (diameter 0.25 mm) in a bilayer cup (Warner Instruments, Delrin perfusion cup, volume 1 mL) with  $\sim 3 \mu\text{L}$  of a  $20 \text{ mg mL}^{-1}$  solution of 1,2-Diphytanoyl-*sn*-Glycero-3-[Phospho-*rac*-(1-glycerol)] (DiPhyPC, Avanti Polar Lipids) in hexane. After adding recording buffer to both compartments of the bilayer setup, we "painted" a solution of  $20 \text{ mg mL}^{-1}$  DiPhyPC in *n*-decane over the pore by using a paint brush with a fine tip. Before addition of the gA derivatives, we followed the thinning of the decane droplet to a planar bilayer by monitoring the capacitance of the bilayer. In case the decane droplet did not thin out, we bubbled air in one chamber underneath the pore. The rise of these air bubbles in the vicinity of the pore usually helped to

thin out the decane/lipid droplet. After bilayer formation we stirred both chambers with a small stir bar (using a Spin-2 bilayer stirplate from Warner Instruments) at all times except during the 60 s recording intervals (to minimize electrical current noise). We performed single ion channel recordings in “voltage clamp mode” using a Ag/AgCl pellet electrode (Warner Instruments) in each compartment and a Geneclamp 500 amplifier (Axon Instruments) with a CV-5B 100GU PROBE headstage (Gain: 100mV pA<sup>-1</sup>). We selected a filter cutoff frequency of 1 kHz on the amplifier (sampling frequency 25 kHz). The current traces shown in Fig. 1 were filtered further using a digital Gaussian filter with a cutoff frequency of 0.2 kHz.

We performed the analysis of the single channel current traces by computing histograms of the current with ClampFit 9.2 software from Axon Instruments. From these histograms we extracted the main channel conductances for each of the derivatives **5–7**. All three derivatives typically showed a predominant single channel conductance but also sub-conductance states (i.e. a single-channel current that were somewhat smaller than the main conductance). These sub-conductance states were less frequent than the main conductance state but in some cases (e.g. with derivative **6**), we had to analyze several traces to establish the main conductance state since these molecules fluctuated between several single channel conductance states.

**Note about the chapter:** Parts of these chapters are reprints from the published reference: Steven Blake, Ricardo Capone, Michael Mayer, and Jerry Yang.

Chemically Reactive Derivatives of Gramicidin A for Developing Ion Channel-Based Nanoprobes. *Bioconjugate Chem.*, 19 (8), 1614–1624, **2008**.

## Chapter 4

# Developing new building blocks for gA-based nanosensors

### 4.1 Introduction

Among the most significant challenges for the development of ion channel-based sensors is the lack of widely accessible, reliable, and cost-effective methods to modify these sensors chemically with tailored functional groups.<sup>6</sup> Here, we present a method to formally convert the C-terminal alcohol on gramicidin A (gA, a natural ion channel forming peptide) to a reactive amine or azide functionality in order to make gA readily accessible for facile and selective synthesis of ion channel-based molecular probes. We demonstrate that these two gA-based building blocks, which we call gramicidamine (**3**) and gramicidazide (**13**), are readily amenable to conventional synthetic derivatization to produce robust and active ion channels carrying tailored chemical functionality. Starting from these two building blocks, we introduce four additional, novel derivatives of

gA and characterize them electrophysiologically on a single channel level. Additionally, we illustrate the usefulness of these reactive gA building blocks for the development of ion channels that can be used for monitoring a “click” reaction, in situ, or for detecting a specific protein-ligand interaction in solution.

To date, two major synthetic approaches to install modifications at the C-terminus of gA have been employed: solid-phase peptide synthesis or direct functionalization of the C-terminal alcohol of native gA. Although solid phase peptide synthesis can afford small quantities of tailored gA derivatives,<sup>15, 45, 77-81</sup> esterification or carbamoylation of the C-terminal alcohol of native gA has been the dominant reported synthetic approach for constructing gA-derivatives.<sup>13, 14, 17, 32, 44</sup> This choice for synthetic approach is presumably due to simplicity, available equipment and facilities, and cost. The poor chemical reactivity of the C-terminal alcohol on native gA, however, restricts the use of native gA for construction of gA derivatives carrying tailored functionality.<sup>81</sup>

In order to develop an improved method to generate C-terminally modified derivatives of gA, we developed a practical procedure to convert large quantities of native, commercial gA to gA-based building blocks carrying reactive C-terminal functional groups. We developed a protocol to generate these gA-based building blocks with the following five goals in mind: 1) the synthetic steps must afford desired products in good purity and yield, 2) the protocol must be amenable to conversion of commercial gA on a scale of at least 100 milligrams, 3) the protocol must not require any HPLC purification steps (to make these gA-based building blocks readily accessible to non-synthetic laboratories), 4) the new chemical

functionality introduced on the C-terminus of gA must be readily amenable to selective and chemically stable conjugation, and 5) the new chemical functionality on the C-terminus must be as close to the opening of the pore as possible (a characteristic that is important for, e.g., charge-based sensing applications<sup>82</sup>).

Within these design constraints, we describe here a practical synthetic procedure for preparing gramicidamine, **3**, and gramicidazide, **13**. We used these building blocks to synthesize four novel derivatives of gA and characterized them electrophysiologically using single channel recordings. We confirmed that **3** and **13** are more reactive than native gA towards desired chemical derivatization. We also demonstrated the expected increased stability under conventional ion channel recording conditions of the amide and triazole groups generated from derivatization of **3** and **13** compared to previously reported ester linkages on gA.<sup>14, 44</sup>

To highlight the selective reactivity of the azide group in **13**, we used single channel recordings to monitor, in situ, a “click” reaction between **13** and propargyl sulfonate (**16**) under typical conditions for 1,3-dipolar cycloaddition reactions.<sup>83</sup> In addition, we demonstrated an example of a biochemically-relevant sensing application of a molecule derived from **13** that reports the interaction between a sulfonamide moiety and carbonic anhydrase. Finally, we confirmed specificity of this protein-ligand interaction by competitive displacement of a gA derivative carrying a sulfonamide (**21**) with 4-carboxybenzene sulfonamide.

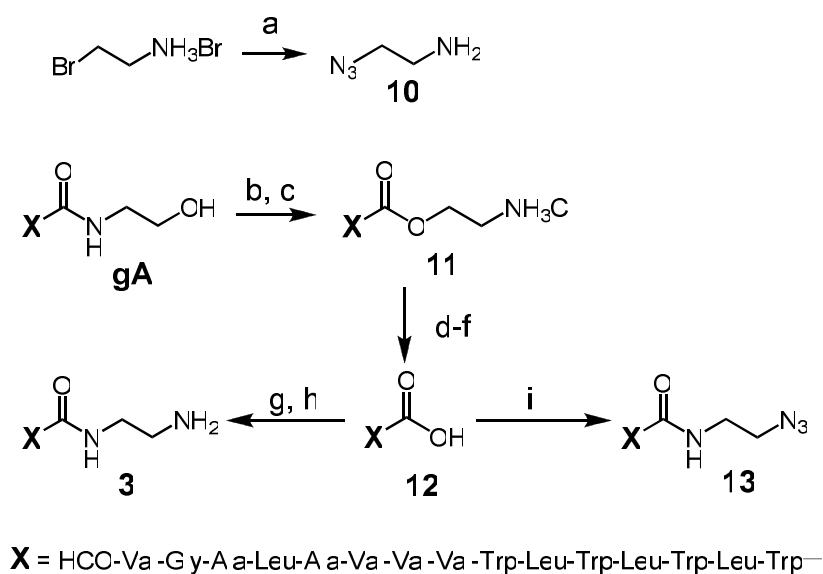
## 4.2 Synthesis of chemically reactive derivatives gramicidamine and gramicidazide from native gA

In order to develop a general route to prepare nanosensors based on gA, we synthesized two derivatives of gA carrying chemically reactive groups on the C-terminus of the peptide. We envisioned that these reactive gA derivatives could be used as common building blocks for the synthesis of ion channels with chemical functionality. One of these gA-based building blocks carried a reactive, primary amine functionality. Amines can be conjugated to readily synthesized or to commercially available substrates that bear an activated ester group to form stable amide linkages.<sup>84</sup> The other gA-based building block carried a C-terminal azide functionality on gA. Azides can be used as a reactive chemical group for bioconjugation due to the well-known reactivity of azides with terminal alkynes under mild conditions to furnish cycloaddition products in good yield.<sup>83</sup>

To formally convert the C-terminal alcohol of native gA to an amine or azide functionality, we began with a modified strategy<sup>85</sup> that removed the entire C-terminal ethanolamine residue of gA to afford desethanolamine gA (**12**, Scheme 4.1). We reacted native gA with excess POCl<sub>3</sub> to convert the C-terminal ethanolamine to a oxazoline intermediate, followed by treatment with H<sub>2</sub>O in acetonitrile to afford the 2-amino ethyl ester, **11** (Scheme 4.1). To hydrolyze the ester in **11**, we protected the primary amine in **11** with a formyl group (to prevent it from converting rapidly back to gA under alkaline conditions), and hydrolyzed the ester group of this N-formyl derivative of **11** with LiOH to give

desethanolamine gA (**12**). Finally, we reacted **12** with N-BOC-ethylenediamine (followed by acidic deprotection of the BOC group) to afford the desired gramicidamine, **3**, or with azidoethylammonium chloride, **10** (which was obtained from an S<sub>N</sub>2 reaction between sodium azide and 2-bromoethylammonium bromide) to afford the desired gramicidazide, **13**.

Although the overall yields of 48% for **3** and 45% for **13** from native gA are relatively modest, we were able to convert 150 mg of native gA to 38 mg of **3** or 28 mg of **13** in two days without the need for HPLC purification (the ability to



**Scheme 4.1.** Synthesis of gramicidamine (**3**) and gramicidazide (**13**). a) sodium azide, H<sub>2</sub>O (65% yield); b) POCl<sub>3</sub>, acetonitrile (ACN); c) H<sub>2</sub>O, ACN (96% yield, 2 steps); d) acetic anhydride, formic acid, tetrahydrofuran (THF) (72% yield) e) LiOH, H<sub>2</sub>O, THF; f) HCl, H<sub>2</sub>O (65% yield, 2 steps); g) ClCO<sub>2</sub>Et, NEt<sub>3</sub>, dichloromethane (DCM) followed by N-*tert*-butoxycarbonyl-ethylenediamine (N-BOC-ethylenediamine); h) trifluoroacetic acid (TFA), ethanedithiol (EDT), dimethyl sulfide (Me<sub>2</sub>S), DCM (74% yield, 2 steps); i) ClCO<sub>2</sub>Et, NEt<sub>3</sub>, THF followed by 2-azidoethylammonium chloride (**10**), H<sub>2</sub>O, NaOH (69% yield).

work with gA derivatives at scales above 20 mg significantly facilitates the purification of intermediates and final products by precipitation and flash column chromatography, and therefore circumvents the need for HPLC purification). Furthermore, the purities of **3** (85%) and **13** (95%) obtained from these comparably<sup>82</sup> large-scale preparations were sufficient to explore the synthetic utility of these gA-based building blocks for development of four additional, novel ion channel-based probes.

### 4.3 Chemical reactivity of gramicidamine and gramicidazide

In order to examine whether gramicidamine, **3**, and gramicidazide, **13**, can be readily derivatized using conventional chemical methods, we tested their chemical reactivity using a set of molecules that represent typical substrates for conjugation to amine or azide groups. For gramicidamine, **3**, we examined the reactivity of the amine functionality with molecules containing activated ester groups (BOC-glycine and 4-carboxybenzene sulfonamide). The N-hydroxysuccinimidyl (NHS) ester of 4-carboxybenzenesulfonamide (**15**) was prepared through the EDC coupling of NHS and the sulfonamide. Scheme 4.2 shows that **3** reacts in good yield with the NHS ester of BOC-glycine and with the NHS ester of 4-sulfonamidobenzoate in the presence of diisopropylethylamine (as a base catalyst) to produce **17** and **19**, respectively. We demonstrate in several organic solvents that these common amidation conditions afforded the

**Table 4.1.** Summary of reactions of native gA, gramicidine (**3**), and gramicidazide (**13**) with molecules that represent typical substrates for conjugation to amines and azides.

compound <sup>a</sup>	substrate <sup>b, c</sup>	solvent	product	% yield <sup>e</sup>
<b>3</b>	BOC-Gly-NHS	DCM	<b>17</b>	67
<b>3</b>	BOC-Gly-NHS	MeCN	<b>17</b>	67
<b>3</b>	BOC-Gly-NHS	DMF	<b>17</b>	67
<b>3</b>	BOC-Gly-NHS	MeOH	<b>17</b>	65
<b>3</b>	BOC-Gly-NHS	THF	<b>17</b>	64
<b>gA</b>	BOC-Gly-NHS	DCM	<b>5</b>	0
<b>gA</b>	BOC-Gly-NHS	MeCN	<b>5</b>	0
<b>gA</b>	BOC-Gly-NHS	DMF	<b>5</b>	0
<b>gA</b>	BOC-Gly-NHS	MeOH	<b>5</b>	0
<b>gA</b>	BOC-Gly-NHS	THF	<b>5</b>	0
<b>3</b>	NHS 4-sulfonamido- benzoate	THF	<b>19</b>	73
<b>13</b>	propargyl sulfonate	H <sub>2</sub> O + <i>t</i> -BuOH <sup>d</sup>	<b>20</b>	32
<b>13</b>	N-propargyl-4-sulfamoyl- benzamide	H <sub>2</sub> O + <i>t</i> -BuOH <sup>d</sup>	<b>21</b>	88

<sup>a</sup>The concentration of gA and **3** was 1.6 mM in all cases. The concentration of **13** was 1.7 mM when reacted with sodium propargyl sulfonate and 2.6 mM when reacted with N-propargyl-4-sulfamoylbenzamide.

<sup>b</sup>All reactions with gA and **3** contained 1.5 equivalents (eq) of diisopropylethylamine (DIEA) and 2 eq of the NHS ester. The reaction between **13** and sodium propargyl sulfonate contained 8 eq of sodium ascorbate, 3 eq of CuSO<sub>4</sub>·5H<sub>2</sub>O, and 1.6 eq of sodium propargyl sulfonate. The reaction between **13** and N-propargyl-4-sulfamoylbenzamide contained 7 eq of sodium ascorbate, 3.5 eq of CuSO<sub>4</sub>·5H<sub>2</sub>O, and 1.6 eq of N-propargyl-4-sulfamoylbenzamide.

<sup>c</sup>NHS = N-hydroxysuccinimidyl

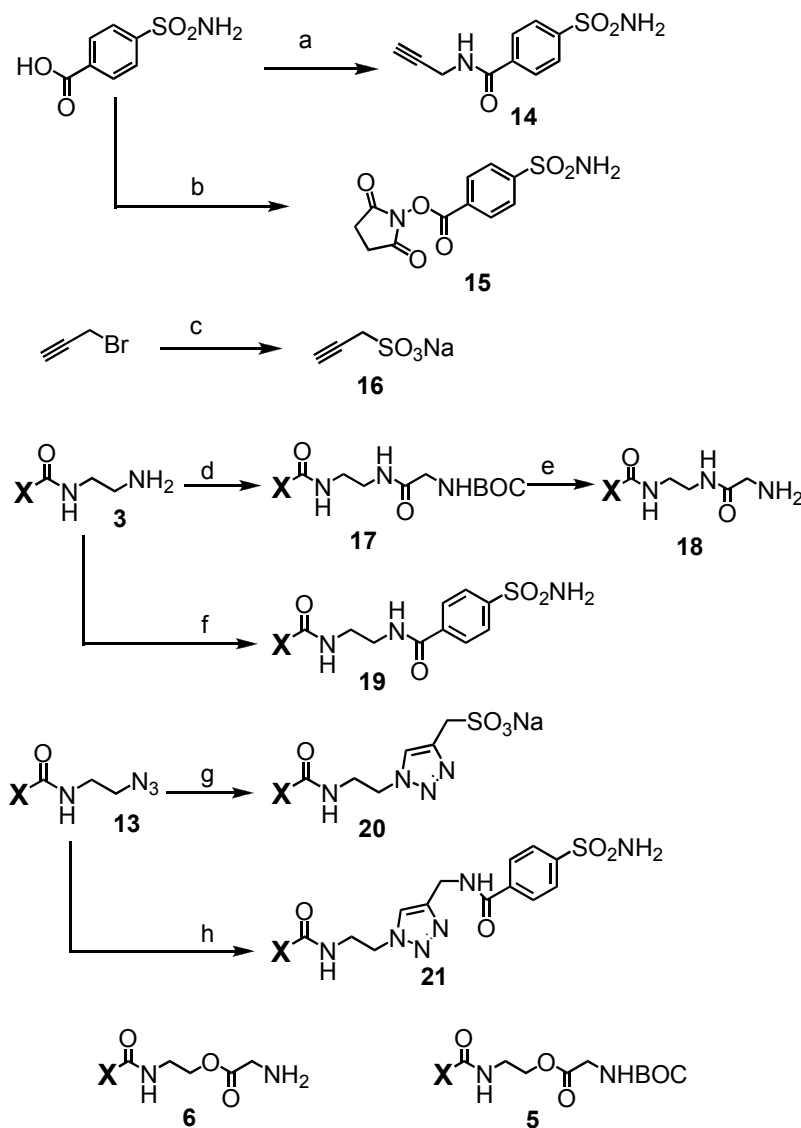
<sup>d</sup>The solvent was a 2:1 mixture of *t*-BuOH:H<sub>2</sub>O.

<sup>e</sup>Yields were determined by HPLC.

expected products in good yield (here, demonstrated in the case of the NHS ester of BOC-protected glycine) (Table 4.1), suggesting that issues of substrate

solubility, which are often problematic,<sup>86</sup> should not limit the ability to synthesize desired gA derivatives. For comparison, we demonstrated that native gA had little to no reactivity with the NHS ester of BOC-protected glycine in the presence of a base catalyst in a variety of organic solvents to give **4** (Table 4.1).

Although in a few examples we and others have succeeded in esterifying the C-terminal alcohol of native gA,<sup>14, 44</sup> these ester derivatives of gA can have limited stability under typical aqueous conditions for ion channel measurements (especially over a wide range of pH). To confirm the limited stability of ester derivatives of gA, we synthesized gramicidyl glycinate<sup>82</sup> (**6**, Scheme 4.2) and tested its stability in acidic (pH 3.5) and in basic solutions (pH 10.4). In acidic solutions, we did not observe hydrolysis of the ester moiety of **6** after 24 hours at 23 °C. We did, however, observe the expected complete hydrolysis of the ester of **6** after 3 hours at 23 °C in the basic solution (as determined by HPLC analysis). For comparison, **18**, which was prepared by the BOC deprotection of **17** using the same TFA cocktail discussed earlier in the chapter, contained an amide linkage between the gramicidamine and a glycine group (Scheme 4.2) as opposed to the ester in **6**. The ester, **6**, was stable toward hydrolysis under acidic (pH 3.4) and basic (pH 10.4) conditions over a period of 24 hours at 23 °C. These results highlight two important advantages of molecules derived from **3**: first, the synthetic route to molecules derived from **3** is simplified and proceeds in reasonable yield compared to molecules derived from native gA,<sup>13</sup> and second, the stability of molecules derived from **3** in aqueous solutions



**X** = HCO-Val-Gly-Ala-Leu-Ala-Val-Val-Val-Trp-Leu-Trp-Leu-Trp-

**Scheme 4.2.** The synthesis of gA derivatives from gA-based building blocks **3** and **13** and the structures of two ester derivatives of gA (**5** and **6**) derived from native gA. a) propargylamine, N-hydroxybenzotriazole, O-(benzotriazol-1-yl)-N,N,N',N'-tetramethyluronium hexafluorophosphate, DIEA (44% yield); b) N-hydroxysuccinimide (NHS), 1-Ethyl-3-[3-dimethylaminopropyl]carbodiimide Hydrochloride (EDC) (75% yield); c) Na<sub>2</sub>SO<sub>3</sub>, MeOH (81% yield); d) NHS ester of BOC-protected glycine, diisopropylethylamine (DIEA), THF; e) TFA, Me<sub>2</sub>S, EDT, DCM (62% yield over 2 steps); f) **15**, DIEA, THF (41% yield); g) **16**, CuSO<sub>4</sub>·5H<sub>2</sub>O, sodium ascorbate, H<sub>2</sub>O, *tert*-butanol (t-BuOH) (88% yield); h) **14**, CuSO<sub>4</sub>·5H<sub>2</sub>O, sodium ascorbate, H<sub>2</sub>O, t-BuOH (32%).

extends the range of applications of ion channel-based probes compared to ion channels generated through direct esterification of native gA.

In addition to synthesizing gramicidine (**3**) for direct comparison of reactivity and stability with gA, we synthesized gramicidazide (**13**) containing an azide group that is expected to have orthogonal reactivity to the C-terminal alcohol in native gA or the C-terminal amine in gramicidine (**3**). Since organic azides undergo 1,3-dipolar cycloaddition reactions with terminal alkynes under mild conditions in water,<sup>83</sup> we tested the reactivity of gramicidazide (**13**) with propargyl sulfonate, **16**, (obtained from the S<sub>N</sub>2 reaction between propargyl bromide and sodium sulfite)<sup>87</sup> and N-propargyl-4-sulfamoylbenzamide (obtained from HBTU and HOBT amide-coupling of propargyl amine and 4-carboxybenzene sulfonamide)<sup>88</sup> as representatives of typical, terminal alkyne substrates (Scheme 4.2). As expected, reaction of **13** with these two alkyne substrates (**14** and **16**) in the presence of Cu<sup>I</sup> as metal catalyst afforded triazole cycloaddition products **20** and **21** in modest to good yield (Table 4.1). These yields are in agreement with similar “click” reactions under comparable experimental conditions.<sup>83</sup> We confirmed analytically by HPLC, as expected, that the triazole linkage in **21** resulting from conjugation of the terminal alkyne to gramicidazide is stable to acidic (pH 3.4) and basic (pH 10.4) solutions over a period of 24 hours at 23 °C. In order to demonstrate that molecules derived from **3** and **13** retained their activity as functional ion channels, we measured the single channel conductance of **3**, **13**, **17**, **19-21** in planar lipid bilayers. Figure 4.1 shows representative single channel traces of current versus time of these gA

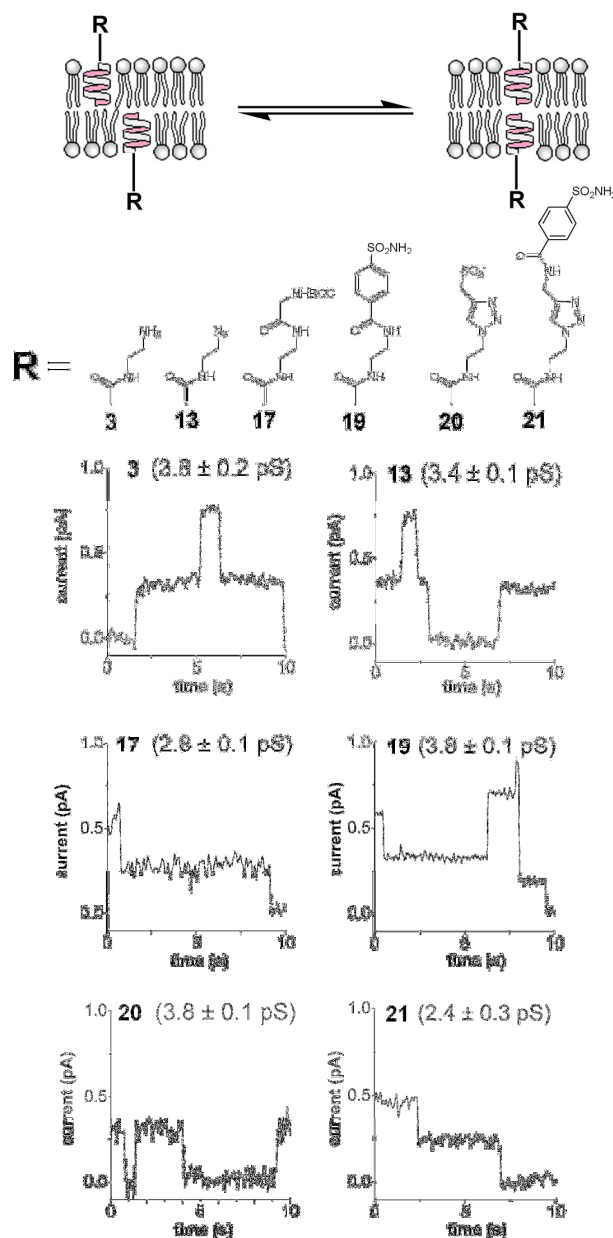


**Figure 4.1.** Cartoon illustrating the reversible dimerization of six different derivatives of gA (**3**, **13**, **17**, **19-21**) and original single channel traces of current versus time of all six derivatives. The applied potential was 100 mV and the electrolyte solution contained 20 mM KCl and 0.2 mM HEPES (pH 7.4) in all experiments. The conductance values (listed on top of every current trace) were determined from the slopes of current versus voltage (I-V) curves. The traces shown here were selected for clarity. Complete analysis of traces over long periods of time showed occasional subconductance states (shown here, for example, in the case of **19**). Conductance values are mean values determined from linear best fits of the I-V curves of the main conductance states in the linear range from -75 mV to +75 mV.

derivatives under an applied potential of 100 mV. These current recordings illustrate that **3** and **13**, as well as derivatives generated from **3** and **13**, all retained well-defined ion channel activity.

#### 4.4 Monitoring a "click" reaction *in situ* using single ion channel recordings

We recently reported that chemical analytes that react with and change the charge of functional groups attached to the opening of a gA pore can be detected using single ion channel recordings.<sup>82</sup> Here, we use conductance measurements to again highlight the reactivity of the azide group of **13** towards reaction with terminal alkynes in the presence of a Cu<sup>I</sup> catalyst and also to demonstrate the capability to follow the course of this chemical reaction on individual pores. We used single ion channel conductance measurements to monitor, *in situ*, the conversion of the azide group in **13** to a negatively-charged triazole cycloaddition product, **20** (Figure 4.2). Since we<sup>82</sup> and others<sup>44, 45</sup> have previously shown that derivatives of gA carrying a negative charge near the opening of the pore have higher conductance compared to neutrally charged derivatives of gA (under conditions of low ionic strength in the recording electrolyte<sup>82</sup>), we expected the product of cycloaddition **20** to have higher conductance than **13**. Measurement of the conductance of pure samples of **20** and **13** confirmed this prediction, indicating a single channel conductance ( $\gamma$ ) of

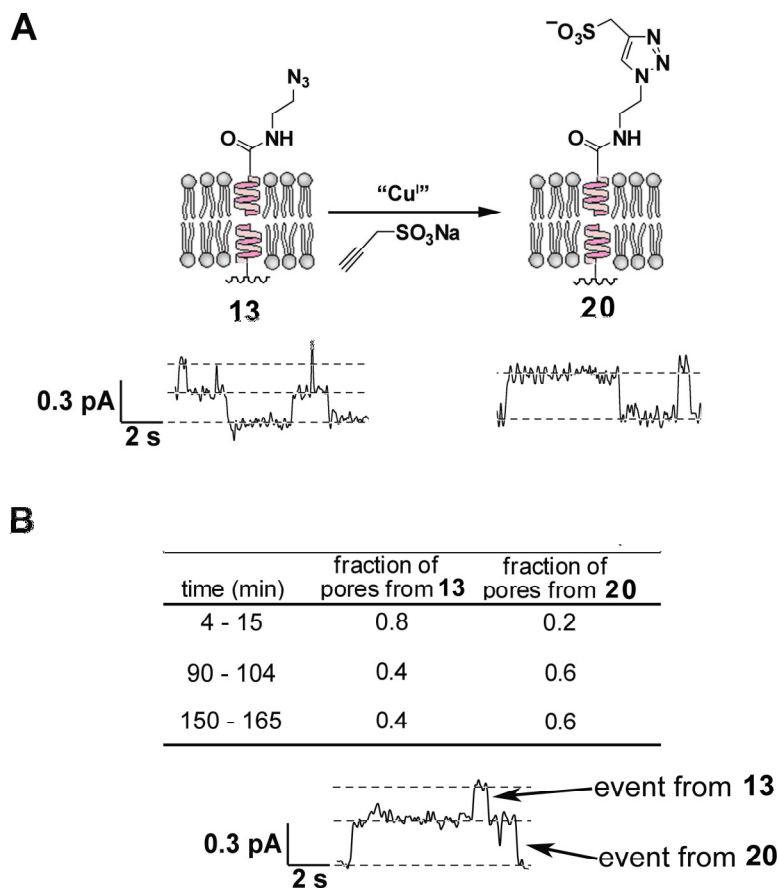


**Figure 4.2.** Conversion of gramicidazole **13** to a negatively charged triazole sulfonate **20**. A) Cartoon of ion channels comprised of **13** and **20** in a membrane and their corresponding single ion channel conductance traces. As expected, the single channel conductance of **20** ( $4.3 \pm 0.1$  pS) is larger than the single channel conductance of **13** ( $3.3 \pm 0.1$  pS) when measured in low ionic strength recording media. B) The table indicates the fraction of observed ion channel events that correspond to the starting material (gramicidazole **13**) and the product of the reaction (triazole sulfonate **20**) over time windows of 4-15, 90-104, and 150-165 minutes throughout the course of the reaction. The current versus time trace in B shows a time window during the course of the reaction where an ion channel event from **13** occurs at the same time as an ion channel event from **20**. All current versus time traces were generated at an applied voltage of +75 mV in recording media containing 20 mM KCl, 0.2 mM HEPES (pH 7.4), 2 mM sodium ascorbate, 2 mM propargyl sulfonate, and 0.5 mM  $\text{CuSO}_4$ . The pH of the solution was 6.9. The initial concentration of **13** was 40 pM. **Note:** the single channel conductances of **13** and **20** are different from conductances reported in Figure 4.1 due to the differences in the recording buffer.

$4.3 \pm 0.1$  pS for **10** and  $3.3 \pm 0.1$  pS for **13** under the recording conditions used to monitor the cycloaddition reaction shown in Figure 4.2. By making the rough assumption that **13** and **20** distribute equally between the bilayer and the aqueous media, we can use the difference in conductance between **13** and **20** to estimate the relative conversion of starting material **13** to product **20** throughout the course of the reaction (Figure 4.2).

We added **13** to a final concentration of 40 pM to both 4 mL chambers of a stirred lipid bilayer setup comprised of zwitterionic 1,2-diphytanoyl-sn-glycero-3-phosphatidylcholine (DiPhyPC) lipids that separated two compartments containing 20 mM KCl, 0.2 mM HEPES buffer, 2 mM sodium ascorbate (as a reducing agent for Cu<sup>II</sup>), and 2 mM propargyl sulfonate. The final pH of this solution was 6.9. We added CuSO<sub>4</sub> (to give a final concentration of Cu<sup>II</sup> of 0.5 mM) to both chambers of the bilayer setup and recorded the single ion channel activity over time. Although we added the substrate and catalyst to both chambers of the bilayer setup, we previously showed in section 2.5 that only changes in the chemical properties of molecules attached near the entrance of the pore (and not the exit of the pore) affect the conductance through gA-based ion channels.<sup>32</sup> Since we monitor this cycloaddition reaction at a constant applied potential of +75 mV, these experiments reveal the chemical reactions on **13** occurring only on the positively polarized side of the membrane (which represents the entrance of the pore). Figure 4.2B summarizes the results from ion channel conductance measurements throughout the course of this reaction. We observed that approximately 20% of the ion channel events recorded over a

time window of 4-15 minutes corresponded to an ion channel with conductance value significantly higher than **13**, which we attribute to the presence of product, **20**. Measurement of ion channel events over a window of time between 90-104 minutes of incubation revealed that the reaction between **13** and **20** had proceeded to give approximately 60% product. Analysis of the channel events from the reaction mixture between 150-165 minutes showed the same ratio of product **20** to starting material **13** as observed between the time window of 90-104 minutes, suggesting the reaction didn't proceed any further after ~90 minutes. Although these reaction conditions were not optimized for this 1,3-dipolar cycloaddition reaction,<sup>89, 90</sup> these results illustrate the utility of tailored gA derivatives for monitoring the progress of synthetic reactions using single ion channel conductance measurements.

## 4.5 Design and synthesis of an ion channel-based sensor for detection of protein-ligand interactions

In order to illustrate the synthetic utility of gA-based building blocks **3** and **13** for construction of ion channel-based sensors, we carried out a proof-of-principle study for the detection of a protein-ligand interaction using ion channel recordings. In Scheme 4.2, we show that molecules **3** and **13** can be used to synthesize gA derivatives **19** and **21**, which both carry benzenesulfonamide moieties. Benzenesulfonamides are well-known to serve as ligands for the binding of carbonic anhydrase II (CA, EC 4.2.1.1), a  $\text{Zn}^{2+}$ -containing protein<sup>7, 91-97</sup>

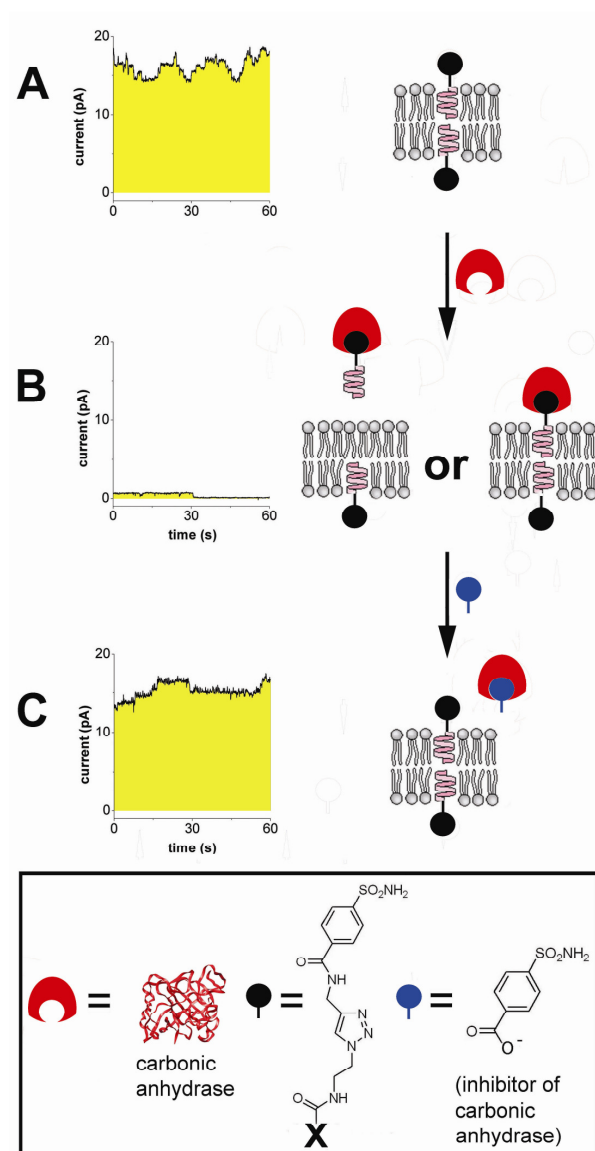


**Figure 4.3.** Detection of carbonic anhydrase (CA) with gA derivative **21**. A) Cartoon of two molecules of **21** that dimerize to form an open pore across a membrane. The accompanying current versus time trace shows the conductance of multiple, simultaneous opening events in the membrane. B) Binding of gA-sulfonamide **21** by CA almost completely abolished the observed transmembrane ion flux through **21**. This dramatic reduction in observed conductance could either be caused by extraction of the gA derivative from the bilayer upon binding to CA or by blockage of the pores by CA. C) Addition of a competitive inhibitor of CA (4-carboxybenzenesulfonamide) restored ion channel activity and hence demonstrates specificity of binding of **21** to CA. The recording electrolyte contained 140 mM KCl and 10 mM phosphate buffer (pH 8.0). The current traces were recorded at 100 mV. **X** = HCO-Val-Gly-Ala-Leu-Ala-Val-Val-Val-Trp-Leu-Trp-Leu-Trp-Leu-Trp-.

We, therefore, examined whether a derivative of gA carrying a benzenesulfonamide group could be used to detect the presence of CA in solution. In previous work, Cornell,<sup>14</sup> Antonenko,<sup>31, 98</sup> and Futaki<sup>15</sup> showed the use of biotinylated derivatives of gA to detect streptavidin or an anti-biotin antibody. Here, we demonstrate that gramicidazide, **13**, makes it possible to expand the scope of biological interactions that can be explored using ion channel measurements by focusing on a protein-ligand interaction with a binding constant that is typically found in biology ( $K_d = 10^{-6}$ - $10^{-9}$ ) such as the association of CA with a benzenesulfonamide ligand.<sup>99</sup>

Figure 4.3A shows the conductance of multiple, simultaneous openings of pores of **21** (at a concentration of 12 pM) in a bilayer made from DiPhyPC lipids. Upon addition of CA to one side of the bilayer to give a final concentration of CA of 50  $\mu$ M, we observed nearly complete suppression of ion channel activity (Figure 4.3B). Since the  $K_d$  for binding of benzenesulfonamides to CA can range from  $10^{-6} - 10^{-9}$  M,<sup>99</sup> it is reasonable to expect that a significant fraction of **21** would be associated with CA at these concentrations of protein and gA derivative. Two potential mechanisms can explain the decrease in observed channel activity upon binding of CA to **21**:<sup>6</sup> 1) CA may have associated with **21** and caused the CA-bound **21** to partition less in the membrane compared to **21** alone (i.e., binding of CA may have extracted **21** from the bilayer), or 2) CA may have associated with membrane-bound **21** and sterically blocked ions from entering or exiting the channel (Figure 4.3B). Both mechanisms would result in the observed strong reduction in channel activity and they may act in parallel. To

test whether the observed strong reduction in ion channel activity shown in Figure 4.3B was indeed due to a specific and reversible protein-ligand binding event, we added an excess of a competitive inhibitor, 4-carboxybenzenesulfonamide, to the aqueous solution to displace **21** from CA. Upon addition of the competitive inhibitor, we observed a rapid restoration (within 20 seconds) of ion channel activity (Figure 4.3C), confirming the specificity of the interaction between CA and **21**. These results illustrate the utility of gA-based building blocks **3** and **13** for constructing specific and sensitive nanoprobe for fundamental studies of protein-ligand interactions in membranes as well as for sensing applications.

## 4.6 Conclusion

In conclusion, we demonstrate a practical method to synthesize chemically-reactive gA-based building blocks from commercially available native gA. These amine- and azide-containing building blocks can be used to rapidly generate stable, C-terminally modified derivatives of gA that retain single channel conductance properties, and can, therefore, serve as an enabling tool for basic and applied studies on ion channels. For instance, these gA-based building blocks make it possible to tune the chemical and physical properties at the opening of the pore, which is useful for basic biophysical studies of ion channels on the single molecule level.<sup>24, 44, 48, 100-105</sup> These synthetic methods also make it possible to rapidly gain access to derivatives of gA for sensing applications,

where changes in the ion flux through gA derivatives in response to a specific external stimulus can be detected using ion channel conductance measurements.<sup>13-15, 81, 106</sup> Recent advances in bilayer recording technology and microfabrication<sup>52, 55, 59, 63, 64</sup> are addressing many of the non-synthetic challenges that have also previously limited studies on ion channels such as limited mechanical stability of membranes<sup>10, 49, 59, 62</sup> and poor signal to noise ratios for conductance measurements.<sup>61</sup> A convenient and general synthetic procedure to rapidly produce gA derivatives that display specific chemical functionality, along with the availability of improved and increasingly automated commercial planar lipid bilayer setups, could make such fundamental and applied studies on ion channels accessible to a broad scientific community.

## 4.7 Protocol for ion channel measurements

**Formation of Planar Lipid Bilayers.** We formed most planar lipid bilayers by the “folding technique.”<sup>82</sup> Briefly, we used a Teflon film (Eastern Scientific Inc, pore diameter 0.1-0.2 mm) that we pretreated on both sides of the pore with 2  $\mu$ L of 5% (v/v) hexadecane in pentane. This film was mounted using vacuum grease (Dow Corning, High vacuum grease) to a custom-made Teflon chamber separating two buffer compartments each with a volume capacity of 4 mL.<sup>61</sup> After addition of 1 mL of electrolyte (20 mM KCl buffered with 0.2 mM HEPES pH 7.4 or 140 mM KCl buffered with 10 mM phosphate pH 8.0) to each compartment, we spread lipids at the air-water interface of the electrolyte solution

in both compartments (specifically, we added 5  $\mu\text{L}$  from a 25  $\text{mg mL}^{-1}$  solution of 1,2-diphytanoyl-sn-glycero-3-phosphatidylcholine, DiPhyPC, in pentane). Three additional milliliters of the same electrolyte solution were added to each compartment to raise the liquid level above the aperture in the Teflon film. We formed the bilayers on the pore of the Teflon film by aspirating the electrolyte solution into a 3 mL syringe, followed by dispensing the electrolyte solution back into each compartment. This cycle of raising and lowering the liquid levels was repeated until we obtained a bilayer that had a minimum capacitance of 70 pF and that was stable (i.e., no significant current fluctuations above the baseline noise level) at 100 mV of applied potential for at least 2 minutes.

**Ion Channel Measurements.** We performed single channel recordings in “voltage clamp mode” using Ag/AgCl pellet electrodes (Warner Instruments) in each compartment of the bilayer setup. Data acquisition and storage was carried out using custom software in combination with either an EPC-7 patch clamp amplifier from Heka (set at a gain of 10  $\text{mV pA}^{-1}$  and a filter cutoff frequency of 3 kHz). The data acquisition board for the amplifier was set to a sampling frequency of 15 kHz. All current traces shown in the figures were further filtered using a digital Gaussian low-pass filter with a cutoff frequency of 4 Hz.

We performed the analysis of the single channel current traces by computing histograms of the currents from the original current versus time traces with ClampFit 9.2 software from Axon Instruments. From these histograms we extracted the main current values by fitting a Gaussian function to the peaks in

the histograms. All gramicidin molecules showed a predominant conductance and occasionally subconductance states (i.e., single channel currents that were smaller than the main current values). Single channel conductances reported in this paper always refer to the main conductance state (i.e., to the dominant peaks in the current histograms). All conductance values were obtained from the slopes of I-V curves taken at -75, -50, +50 and +75 mV.

**Monitoring a 1,3-dipolar cycloaddition (“click”) reaction *in situ* using single ion channel recordings.** We added 3  $\mu\text{L}$  (from a 100 ng mL<sup>-1</sup> solution in ethanol) of **13** (to afford a final concentration of 40 pM of **13**) to each compartment of a bilayer setup containing as electrolyte 20 mM KCl and 0.2 mM HEPES buffer. Solutions of sodium ascorbate and sodium propargylsulfonate were added to both compartments to bring the final concentration of each molecule to 2 mM. We added a solution of CuSO<sub>4</sub> • 5H<sub>2</sub>O to each compartment to a final concentration of 0.5 mM. The final pH of this solution was 6.9. In order to facilitate the analysis of single ion channel traces, we kept the concentration of **13** low (40 pM) during the reaction to minimize the possibility for multichannel events (i.e., opening of two or more channels simultaneously) and, therefore, to observe measured currents that would frequently return to baseline (i.e., current steps separated by no observed channel events). We, therefore, observed a low number of events over time, and thus analyzed the data over a window of time rather than at specific time points. Events were recorded over time windows of 4-15, 90-104 and 150-165 minutes throughout the course of the reaction. The

percent composition of **13** and **20** in the reaction mixture in each time window were estimated by manually counting the number of observed single ion channel events corresponding to the conductance of **13** or **20**. For the 4-15 minute time window, we measured 26 total channel events. For the 90-105 minute time window, we recorded 15 total channel events. For the 150-165 minute time window, we recorded 15 total channel events. Since the number of total channel events from each time window ranged from only 15-26 events, the reported percent of conversion of starting material to product should be considered as estimated values. The capacitance of the folded membranes throughout the course of these studies ranged from 70 – 88 pF. The conductivities of the buffer before and after the reaction were 323 and 336 mS cm<sup>-1</sup>, respectively.

**Detection of protein-ligand binding interactions using ion channel measurements.** We added 1  $\mu$ L (from a 100 ng mL<sup>-1</sup> solution in ethanol) of **21** (to afford a final concentration of 12 pM of **21**) to each compartment of a bilayer setup containing as electrolyte 140 mM KCl and 10 mM phosphate buffer (pH 8.0). The conductance was recorded at 100 mV. Upon addition of bovine carbonic anhydrase II (CA, EC 4.2.1.1) to the trans compartment to bring the final concentration of CA to 50  $\mu$ M, the membrane broke and was refolded. We recorded the conductance through the refolded membrane for 40 minutes to assure that the observed reduction of ion channel activity was due to the interaction of CA with **21**. We then added 4-carboxybenzenesulfonamide (to give a final concentration of 1.5 mM of inhibitor) to the trans compartment of the

bilayer setup, and again observed that the membrane broke. After refolding the membrane, we rapidly observed (within 20 seconds of re-establishing a planar lipid bilayer) the re-emergence of significant ion channel activity. The capacitance of all folded membranes throughout the course of these studies ranged from 84 – 88 pF.

## **Chapter 5**

# **A Semi-Synthetic Ion Channel Platform for Detection of Enzyme Activity**

### **5.1 Introduction**

This chapter presents an ion channel platform for detecting the activity of enzymes through their reaction with tailored substrates attached to gramicidin A (gA). This platform exploits the catalytic activity of an enzyme in combination with the amplification characteristics of ion conductance through an ion channel-forming peptide (gA) to detect picomolar concentrations of active protein in aqueous solution.

The activity of enzymes can be indicative of normal or abnormal cellular function, and can be used to diagnose diseases.<sup>107-109</sup> Here, we investigate alkaline phosphatase (AP) as a model enzyme to explore the possibility of employing an ion channel platform as a novel analytical strategy for detecting enzyme activity. Assessing AP activity in blood is a routine part of health examinations since abnormal levels can be early indicators of cancer<sup>110</sup> or liver damage.<sup>111</sup> Although colorimetric,<sup>112, 113</sup> chromatographic,<sup>114, 115</sup> electrochemical,<sup>116-118</sup> and ELISA-based<sup>119, 120</sup> methods have been developed to quantify the activity of clinically relevant enzymes, new diagnostic platforms are still needed to improve the robustness, sensitivity, selectivity, portability, and cost-effectiveness of bioanalytical assays.

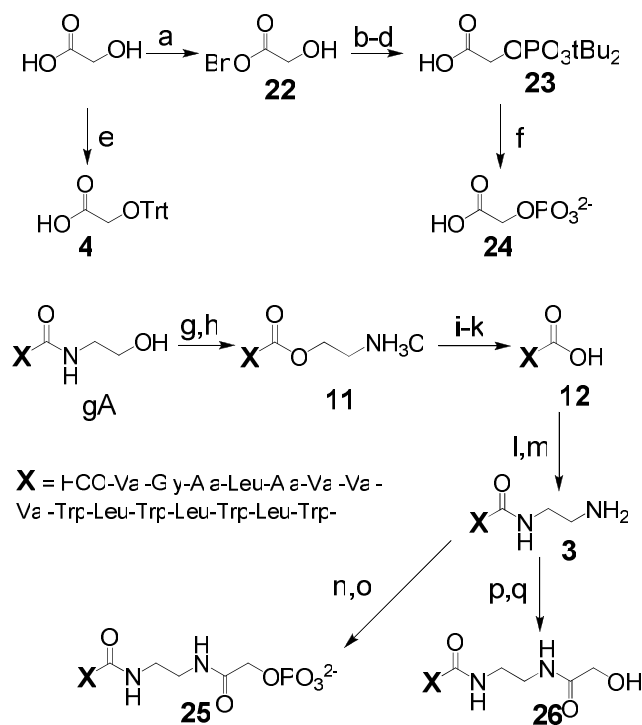
The research presented here explores an ion channel-based strategy for the detection of enzymatic activity that offers at least four complementary advantages compared to current platforms. These advantages include: (1) the method utilizes the amplification characteristics of ion flux<sup>82</sup> through a single ion channel to achieve high sensitivity; (2) the method is orthogonal to colorimetric assays and can, therefore, be advantageous for solutions that are strongly colored or contain quenchers of fluorescence or intrinsic fluorescence (e.g., blood);<sup>82</sup> (3) the method requires very small quantities ( $< 1$  picomole) of the ion channel probe (which minimizes cost); and (4) the nanoscale size of ion channels makes it possible to develop enzyme activity assays within miniaturized, cost-effective, and potentially portable devices.<sup>59, 61, 121, 122</sup> Furthermore, gA is

particularly well-suited for the development of an ion channel-based assay to detect enzyme activity because it is available in gram-scale quantities and is, therefore, conducive to synthetic derivatization while preserving its ion channel function,<sup>82</sup> it can be tailored for the detection of specific chemically or biochemically reactive analytes,<sup>14, 15, 81, 82, 123, 124</sup> and it is simple to use due to its spontaneous self-incorporation into bilayers and its discrete conductance values.

## **5.2 Detection of the catalytic activity of Alkaline Phosphatase**

Here, we explore whether charge-based sensing can be used to detect the enzyme activity of AP through its capability to catalyze the hydrolysis of negatively-charged phosphate groups on substrates attached to the C-terminus of gA. We demonstrate that enzymatic hydrolysis of a phosphate group from gA and the concomitant removal of two negative charges from the entrance of the gA pore results in a measurable change in single channel conductance. Although ion channel recordings have been investigated for detecting protein-ligand binding interactions,<sup>6, 14, 15, 39, 81, 82, 125-127</sup> this paper represents the first example of the detection of enzyme activity by monitoring changes in single ion channel conductance through an ion channel.<sup>128</sup>

In order to develop a substrate for AP that we could readily attach to the opening of a gA pore, we investigated the reactivity of AP with glycolic acid-O-



**Scheme 5.1.** Synthesis of Alkaline Phosphatase substrates **24** and **25** and their respective hydrolysis products **8** and **26**. a) benzyl bromide, acetone, triethylamine ( $\text{NEt}_3$ ),  $60^\circ\text{C}$  (51% yield); b) Di-*tert*-butyl-N,N-diethyl phosphoramidite, tetrazole, dry tetrahydrofuran (THF); c) *m*-chloro perbenzoic acid,  $-78^\circ\text{C}$  to  $0^\circ\text{C}$ ; d)  $\text{H}_2$ , Pd/C, MeOH (40% yield over 3 steps); e) trityl chloride, diisopropylethylamine (DIEA), dichloromethane (DCM) (22% yield); f) trifluoroacetic acid (TFA), ethanedithiol (EDT), dimethyl sulfide ( $\text{Me}_2\text{S}$ ), DCM (94% yield); g)  $\text{POCl}_3$ , acetonitrile (ACN); h)  $\text{H}_2\text{O}$ , ACN (96% yield over 2 steps); i) acetic anhydride, formic acid, THF (72% yield); j)  $\text{LiOH}$ ,  $\text{H}_2\text{O}$ , THF; k)  $\text{HCl}$ ,  $\text{H}_2\text{O}$  (65% yield, over 2 steps); l)  $\text{ClCO}_2\text{Et}$ ,  $\text{NEt}_3$ , DCM followed by *N-tert*-butyloxycarbonyl-ethylenediamine; m) TFA, EDT,  $\text{Me}_2\text{S}$ , DCM (74% yield over 2 steps); n) **23**, 2-ethoxy-1-ethoxycarbonyl-1,2-dihydroquinoline (EEDQ),  $\text{NEt}_3$ , DCM; o) TFA, EDT,  $\text{Me}_2\text{S}$ , DCM (58% yield over 2 steps); p) **8**, EEDQ, DIEA, THF; q) TFA, EDT,  $\text{Me}_2\text{S}$ , DCM (72% yield over 2 steps).

phosphate (Scheme 1, molecule **24**). We chose **24** as a substrate since, after attaching it to the C-terminus of gA (Scheme 1), it will present a negatively charged phosphate group very close to the opening of the pore (a feature that is important for charge-based sensing<sup>82</sup>). Since AP is a promiscuous enzyme that

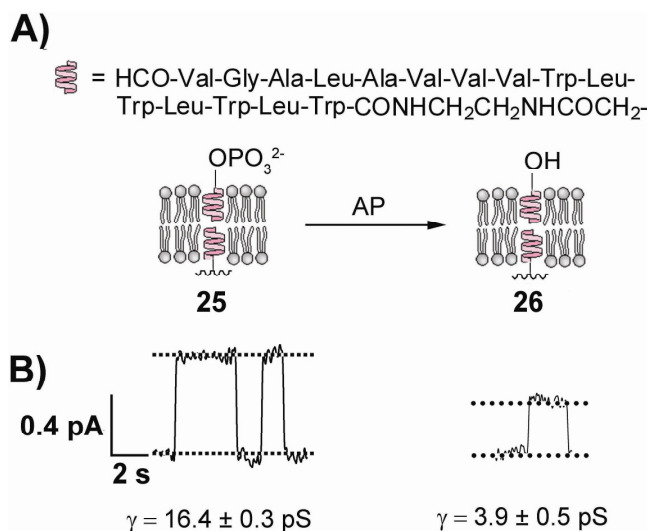


**Figure 5.1.** Cartoon of the detection of Alkaline Phosphatase (AP) using an ion channel platform. A) Conversion of a negatively-charged phosphate on gA derivative **25** to a neutral alcohol in the presence of AP. B) Representative single ion channel conductance traces of **25** and **26**. The traces were recorded using as electrolyte a buffered solution containing 50 mM CsCl, 0.5 mM K<sub>2</sub>CO<sub>3</sub> at pH 9.8.

reacts with a variety of organic phosphates,<sup>129</sup> we hypothesized that **24** would act as a substrate for AP. We confirmed by <sup>31</sup>P-NMR spectroscopy that a 14 mM solution of **24** was completely hydrolyzed by 2  $\mu$ M AP (from bovine intestinal mucosa, EC 3.1.3.1) within 50 min in a D<sub>2</sub>O buffered solution containing 100 mM KCl and 140 mM Na<sub>2</sub>CO<sub>3</sub> (pD 9.4). In a control experiment, we did not observe any hydrolysis of **24** over the course of 24 h when AP was not present in these NMR experiments.

We also measured the single channel conductance of gA phosphate (**25**) and its hydrolysis product (**26**) by incorporating them into a planar lipid bilayer setup. Figure 5.1 shows representative current-versus-time traces of **25** and **26** under an applied potential of 125 mV in buffered recording electrolyte. These traces show that **25** had a dramatically larger (by a factor of 4) conductance than

**26** in this recording electrolyte. We attribute this difference to the pre-concentration of cesium cations near the negatively charged phosphate group presented at opening of the ion channel pore in **25**.<sup>82</sup> Analysis of the current-versus-voltage (I-V) curves of **25** and **26** revealed distinct single channel

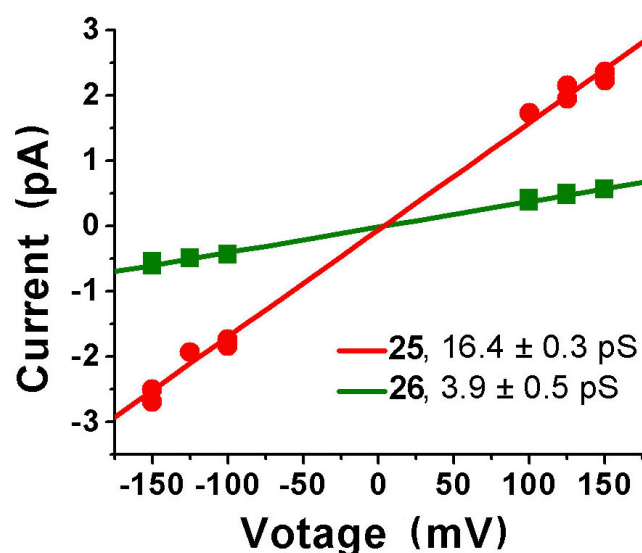


**Figure 5.2:** Single channel current versus voltage (I-V) curves of **25** and **26**. The phosphorylated derivative, **25** (red), exhibits a larger conductance than the de-phosphorylated analog, **26** (green). The linear fits of the slopes of these I-V curves provides an estimate of the conductance of **25** ( $16.4 \pm 0.3$  pS ) and **26** ( $3.9 \pm 0.5$  pS).

recording electrolyte (Figure 5.2). These results suggest that the conversion of gA derivative **25** to **26** can be used for detection of the de-phosphorylating enzyme activity of AP by employing single ion channel conductance measurements.

In order to test if the enzyme activity of AP could be detected in situ by monitoring single ion channel currents, we added **25** to a final concentration of 200 pM to both compartments of a planar lipid bilayer setup containing the

recording electrolyte. We subsequently added AP to a final concentration of 600 nM and monitored the enzymatic conversion of **25** to **26** over time. We estimated the time-dependent conversion of **25** to **26** by comparing the fraction of events from **26** to the fraction of events from **25** throughout the course of the reaction. We defined the fraction of ion channel events from **26** as the number of events originating from **26** ( $\gamma \approx 4$  pS) divided by the total number of events (from **25** and **26**) observed during a 5 or 10 min interval of recording. Similarly, we defined the fraction of ion channel events from **25** as the total number of events originating from **25** ( $\gamma \approx 16$  pS) divided by the total number of events observed during a 5 or 10 min interval of recording.

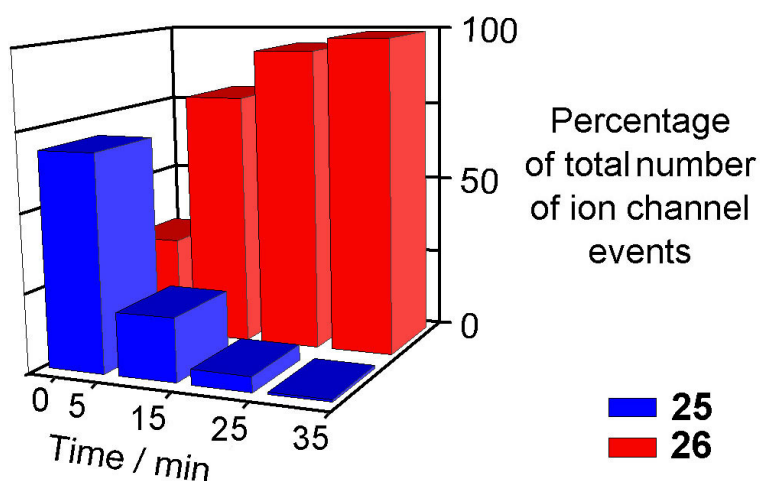


**Figure 5.3.** Time dependent enzymatic hydrolysis of the phosphate group in **25** to **26** in the presence of 600 nM AP as determined using single ion channel conductance measurements. The recording buffer contained 50 mM CsCl, 0.5 mM  $K_2CO_3$  at pH 9.8. We estimated the percentage of total ion channel events corresponding to **25** and **26** over time by counting the number of big and small events within 5 minute time windows; these time windows were separated by 10 minutes intervals.

Figure 5.3 shows that while the enzymatic reaction progressed in the bilayer chamber, the fraction of ion channel events from gA phosphate **25**

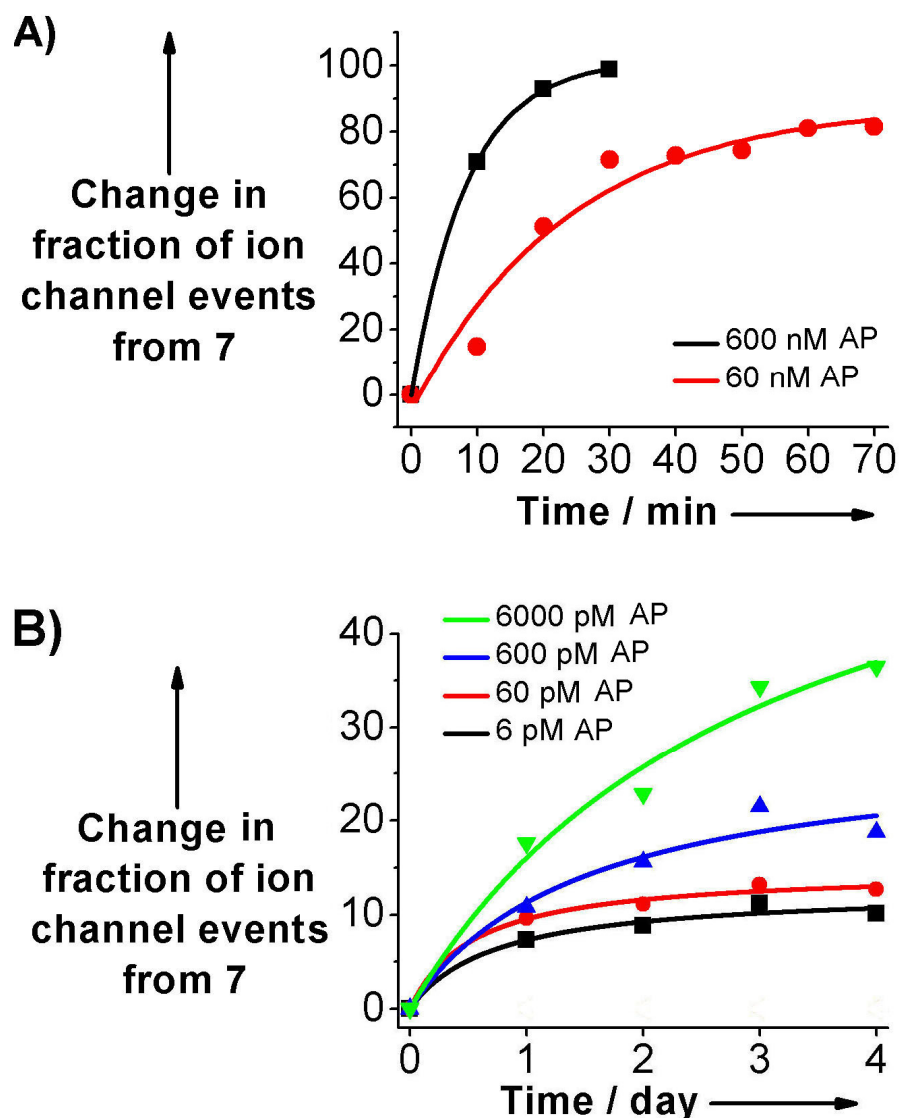


**Figure 5.4.** Monitoring the formation of **26** from enzymatic hydrolysis of **25** over time as a function of the concentration of AP using single ion channel conductance measurements. A) *In situ* detection of the hydrolysis of 200 pM **25** in the presence of 60 nM and 600 nM AP. B) *Ex situ* detection of the hydrolysis of **25** to **26** over 4 days. Solutions containing 120 pM gA derivative **25** were incubated with 6 pM - 6 nM AP in vials (outside of the bilayer chamber) at 23 °C. We analyzed the progression of these reactions in daily intervals by introducing aliquots of the reaction mixture to the planar lipid bilayer setup. Before addition of AP, ion channel recordings showed that a fraction of events (< 30%) corresponded to impurities of the hydrolysis product (**26**) in the samples of gA phosphate (**25**). For clarity, we therefore represented the data as the change in the fraction of events that we recorded from gA derivative **26** with respect to the fraction of events from **26** before addition of AP (i.e., all data points are shown relative to the background in the absence of AP).

decreased whereas the fraction of events from the hydrolysis product **26** increased. Figure 5.3 also illustrates that after 35 min almost all recorded ion channel events originated from the hydrolysis product **26**. We did not observe any hydrolysis of **25** to **26** in these ion channel experiments over the course of 1 h in the absence of AP. Figure 5.4A shows that these types of in situ measurements of ion channel events make it possible to monitor the hydrolysis of **25** to **26** by AP at enzyme concentrations as low as 60 nM. At AP concentrations lower than 60 nM, complete hydrolysis of **25** to **26** required reactions times that exceeded 1 h. Bilayer experiments can, however, be limited to ~ 1 h due to the limited stability of the bilayer membrane.<sup>6</sup> In order to afford extended reaction times that would make it possible to explore the detection limit of the assay, we incubated samples of **25** with solutions of AP at concentrations ranging from 6 pM to 6 nM in reaction vials (i.e., outside of the bilayer setup) for 4 days prior to daily analysis of single ion channel events. Figure 5.4B shows that this ex situ incubation strategy made it possible to detect picomolar concentrations of AP corresponding to femtomoles of enzyme in the bilayer chamber.<sup>130</sup>

The results shown in Figure 5.4 demonstrate that an ion channel platform based on gA can be an attractive strategy to detect the activity of an enzyme in solution. This detection modality takes advantage of two fold amplification (the catalytic turnover properties of enzymes and the amplification characteristics of ion flux through a single ion channel pore) to detect enzyme activity with high sensitivity. Although the results described here demonstrate that ion channels can be employed to detect femtomoles of AP using a conventional bilayer setup,

increasingly available automated, microfabricated<sup>52, 55, 59, 63, 64</sup> and chip-based<sup>56, 59, 121, 122</sup> bilayer platforms can improve the stability of membranes as well as reduce the volume of electrolyte solutions required for single ion channel measurements. Such technological advances may make it possible to push the detection limit of ion channel platforms to sub-femtomole quantities of active enzymes in solution. These novel, automated techniques may also render ion channel recordings accessible to a broad community by overcoming the requirement for specialized expertise.<sup>131</sup> In addition, recent advances in chemical synthesis may make it possible to extend this approach to detection of a wide range of enzymes (such as disease-specific phosphatases<sup>132</sup> and kinases<sup>133</sup>) by designing ion channels whose conductance behavior can be altered by the interaction of biologically or medically relevant enzymes with tailored ion channel pores.<sup>82</sup> Due to its nanoscale size and single molecule detection characteristics, an ion channel-based strategy is particularly well-suited for detecting enzyme activity within small volumes (such as, for instance, detecting kinase activity within individual cells).

### 5.3 Protocol for Ion channel Measurements

**Formation of Planar Lipid Bilayers.** We formed most planar lipid bilayers by the “folding technique” as described in reference 13. The recording electrolyte was 1 mM MgCl<sub>2</sub>, 50 mM CsCl buffered with 0.5 mM K<sub>2</sub>CO<sub>3</sub> at pH 9.8. A 25 mg mL<sup>-1</sup> solution of 1,2-diphytanoyl-sn-glycero-3-phosphatidylcholine lipids,

DiPhyPC, in pentane was spread at the air-water interface of the electrolyte solution in both compartments. The 4 mL of electrolyte solution in each bilayer compartment was aspirated into a 3 mL syringe, followed by dispensing the electrolyte solution back into each compartment. This cycle of raising and lowering the liquid levels was repeated until we obtained a bilayer that had a minimum capacitance of 70 pF and that was stable (i.e., no significant current fluctuations above the baseline noise level) at 100 mV of applied potential for at least 2 minutes.

**Ion Channel Measurements.** We performed single channel recordings in “voltage clamp mode” using Ag/AgCl pellet electrodes (Warner Instruments) in each compartment of the bilayer setup. Data acquisition and storage was carried out using custom software in combination with an EPC-7 patch clamp amplifier from Heka (set at a gain of 10 mV pA<sup>-1</sup> and a filter cutoff frequency of 3 kHz). The data acquisition board for the amplifier was set to a sampling frequency of 15 kHz. The current traces shown in the Figure 5.2 were further filtered using a digital Gaussian low-pass filter with a cutoff frequency of 4 Hz.

We performed the analysis of the single channel current traces by computing histograms of the currents from the original current versus time traces with ClampFit 9.2 software from Axon Instruments. From these histograms we extracted the main current values by fitting a Gaussian function to the peaks in the histograms. All gramicidin molecules showed a predominant conductance and occasionally subconductance states (i.e., single channel currents that were

smaller than the main current values). Single channel conductances reported in this paper always refer to the main conductance state (i.e., to the dominant peaks in the current histograms). All conductance values were obtained from the slopes of I-V curves taken at -150, -125, -100, -75, -60, -30, +30, +60 +75, +100, +125, and +150 mV.

**General procedure monitoring the enzymatic hydrolysis of 25 in the presence of alkaline phosphatase using single ion channel recordings.** For online measurements, we added 19  $\mu\text{L}$  (from a 100 ng mL<sup>-1</sup> solution in ethanol) of **25** (to afford a final concentration of 200 pM of **25**) to each compartment of a bilayer setup containing as electrolyte 1 mM MgCl<sub>2</sub>, 50 mM CsCl buffered with 0.5 mM K<sub>2</sub>CO<sub>3</sub>. (pH 9.8) We added a solution of alkaline phosphatase (from bovine intestinal mucosa, EC 3.1.3.1) to both compartments. Ion channel events were recorded every 10 minutes. For offline experiments, we added alkaline phosphatase (to a final concentration of 6 – 6000 pM) and **25** (to a final concentration of 120 pM ) to a solution of 50 mM CsCl, 2  $\mu\text{M}$  BSA, 1 mM MgCl<sub>2</sub> buffered with 0.5 mM K<sub>2</sub>CO<sub>3</sub> at pH 9.8. Over the course of 4-days, we placed aliquots of 4 mL of solution into each compartment of a bilayer setup and we recorded single ion channel events at an applied potential of 100 mV during a 10-minute time windows once a day (50-120 events were recorded each day). The percent composition of **26** in the reaction mixture at each time point was estimated by manually counting the number of observed single ion channel events corresponding to the conductance of **26** within 5-minute time windows.

The capacitance of the folded membranes throughout the course of these studies ranged from 79 – 81 pF.

**Monitoring the enzymatic hydrolysis of glycolic acid-O-phosphate with Alkaline Phosphatase by NMR.** Glycolic acid-O-phosphate (1.1 mg, 7.1  $\mu\text{mol}$ ) was added to a buffer containing 0.5 mL of 100 mM KCl, 140 mM  $\text{Na}_2\text{CO}_3$  buffer in 0.5 ml of  $\text{D}_2\text{O}$  at pD 9.4. Alkaline phosphate (0.5 mg, 1 nmol) was added to the solution and  $^{31}\text{P}$ -NMR spectra were taken at various time points to monitor the enzymatic hydrolysis of glycolic acid-O-phosphate to glycolic acid.  $^{31}\text{P}$ -NMR (300 MHz,  $\text{D}_2\text{O}$ ): glycolic acid-O-phosphate:  $\delta$  3.33 ppm, free inorganic phosphate: 2.54 ppm using an internal 85% phosphoric acid standard. The reaction was completed in 50 min and the pD was 9.4.

**Note about the chapter:** A lot of the work carried out in this chapter were based on the principles developed in the published reference: Steven Blake, Ricardo Capone, Michael Mayer, and Jerry Yang. Chemically Reactive Derivatives of Gramicidin A for Developing Ion Channel-Based Nanoprobes. *Bioconjugate Chem.*, 19 (8), 1614–1624, **2008**.

## Chapter 6

# Using hydrogen-bonding to tune the conductance of Gramicidin A

### 6.1 Introduction

This chapter describes that structural alterations to gA near the lumen of the ion channel lead to a measurable effect on the conductance of ions. Here, we abolished a H-bond donor in an amide moiety near the pore of a gA derivative by synthesizing a gA derivative that had an ester moiety in the place of the amide. We hypothesized that this change in the H-bonding network near the pore of the ester derivative resulted in a structural modification that perturbed the conductance of ions. In general, H-bonding plays a major role as a dipole-dipole interaction (typically, 4 - 20 kJ / mol) between an electronegative atom (H-bond acceptor) and a hydrogen atom bonded to fluorine, nitrogen, and oxygen (H-bond donors). In nature, one of H-bonding chief functions is to determine the 3D

structure of proteins. The structure of the protein that results from H-bonding dictates function of the protein and, in the case of gA, H-bonding is responsible for: (1) two gA monomers reversibly dimerizing to form a conducting channel;<sup>134</sup> (2) the interaction between the tryptophan side chains in gA and the polar head groups of lipids, allowing full ion channel activity;<sup>135</sup> and (3) stabilizing the helical structure of gA by providing attractive intramolecular forces between amino acid residues.<sup>136</sup> In this research, we wished to investigate the conductance of two derivatives of gA to probe if H-bonding can indirectly influence the conductance properties of derivatives of gA through a structural change near the pore in two derivatives of gA.

## 6.2 Effect of H-bonding on the conductance of gA

We already had derivatives **5** and **17** in hand from our studies in the previous chapters. Derivative **5** contains an ester moiety, while **17** instead contains an amide moiety at the analogous position to the ester in **5** (Figure 6.1). The ester lacks a H-bond donating N-H group. We calculated the energy-minimized structures of **5** and **17** from a conformational search based on molecular mechanics calculations using Macromodel (Figure 6.1) to determine the difference in the H-bonding network near the pore of **5** and **17**. From these calculations, the distances between N-H<sup>#</sup> and Leu10 (O=C) and between C=O<sup>#</sup> and Leu12 (N-H) in **17** (Figure 6.1A) are 2.159 Å and 2.026 Å, respectively, which are within the range of typical H-bonding.<sup>137</sup> However, in **5**,

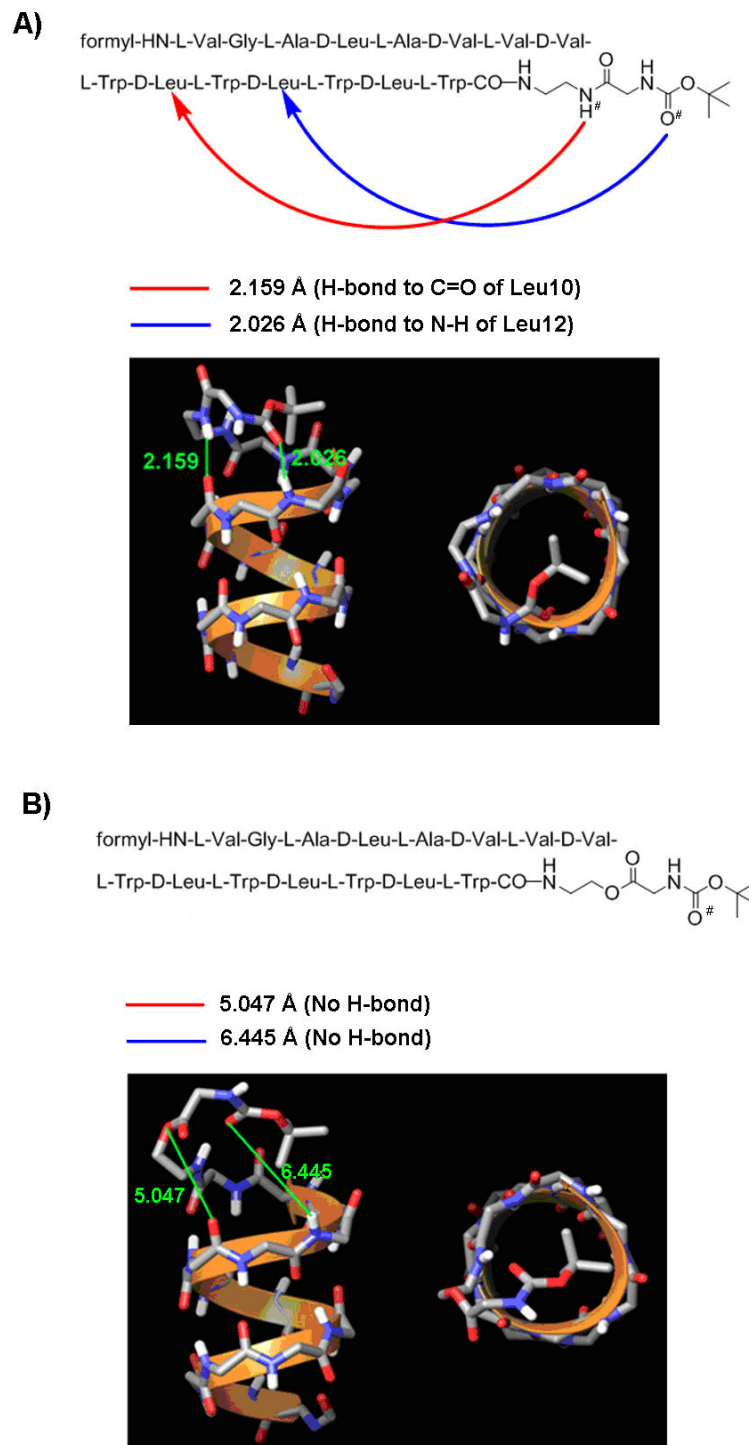


**Figure 6.1.** Illustration depicting the chemical structure and energy minimized structure (side and top view) of A) **17** and B) **5**. A) The blue and red arrows in derivative **17** indicate a H-bond donating from N-H<sup>#</sup> to the C=O in Leu10 and a H-bond donating from N-H in Leu12 to the C=O<sup>#</sup>, respectively. B) The blue and red arrows indicate no H-bonding taking place between analogous atom pairs in **5**.

the oxygen ( $sp^3$ ) of the ester moiety can not donate a H-bond to Leu10 ( $O=C$ ) and the distance (6.445 Å) between  $C=O^\#$  and Leu12 (N-H) is too long for effective H-bonding to occur (Figure 6.1B). As a result, the two H-bonds described in **17** are predicted to be absent in **5**. From these energy-minimized structures, we, subsequently, hypothesized that due to the two H-bonds in **17**, the BOC group (Figure 6.1A) would be more restricted in movement over the lumen of the channel than compared to BOC group in **5**, which isn't fixed over the pore by H-bonding (Figure 6.1B). We believe that if the BOC group in **17** is being restricted over the pore, the functional group will sterically block incoming cations (resulting in a lower conductance in **17**).

We tested the hypothesis by measuring the single-channel current of **5** and **17** to see if there would be a difference in conductance between the two derivatives. Figure 6.2 shows representative current-versus-time traces of **5** and **17** under an applied potential of 75 mV in buffered solution (20 mM KCl, 0.2 mM HEPES buffer, pH 7.2). These traces show that **5** displays a larger current compared to **17** (Figure 6.2A). Conductance measurements of the two derivatives show that **17** has a conductance of  $2.7 \pm 0.1$  pS and **5** has a conductance of  $4.2 \pm 0.1$  pS. Each derivative of gA was measured several times independently and a two sample *t*-test confirmed that the mean conductances of **5** and **17** were significantly different from each other with a significance level that is less than 0.01. The experiments, here, supported the hypothesis that **17** would display a smaller conductance. We presume that due to the H-bonding that is present in **17** and absent in **5** (Figure 6.1), **17** will show a lower conductance

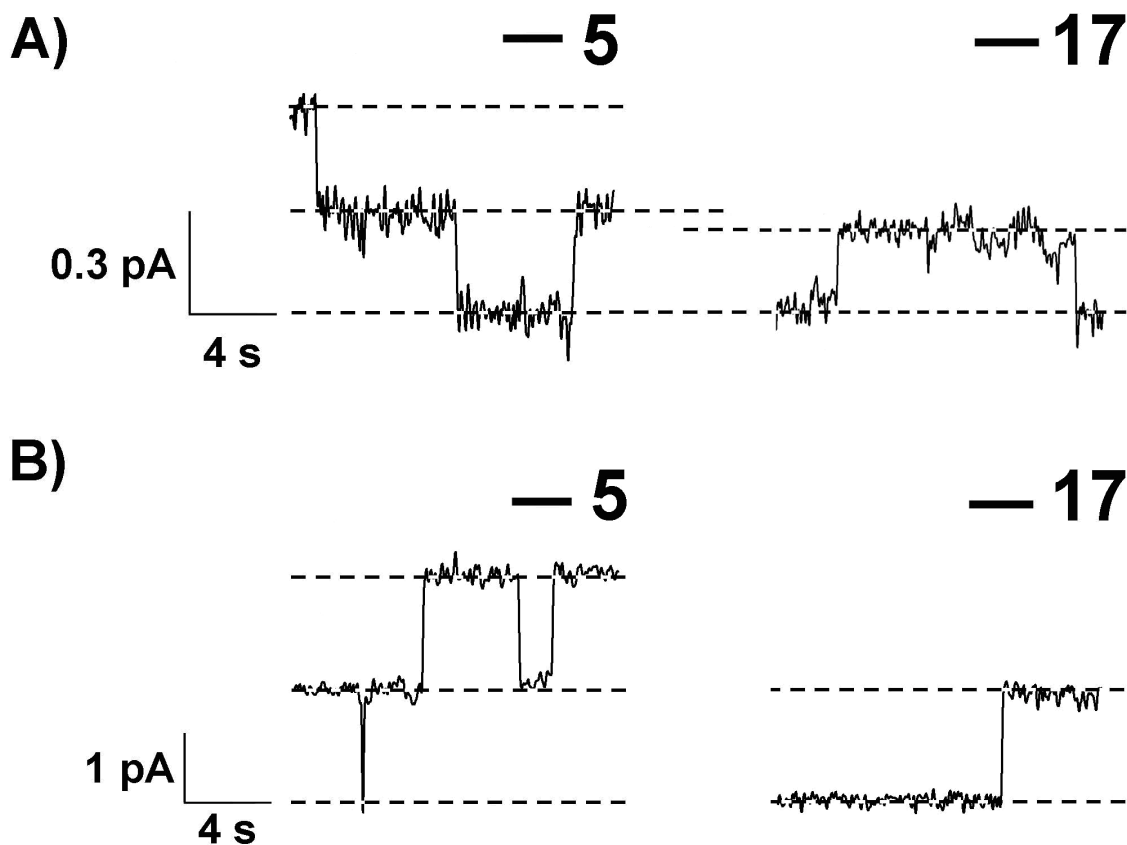


**Figure 6.2.** Single channel traces of **5** and **17** at 75 mV in A) low ionic strength and B) high ionic strength buffer. A) Derivatives **5** and **17** show different single channel current in 20 mM KCl, 0.2 mM HEPES buffer at pH 7.2. B) Derivatives **5** and **17** show equal single channel current in 1 M KCl, 10 mM HEPES buffer at pH 7.2.

compared to the **5** because of the restricted movement of the BOC group over the pore.

In order to support the claim that H-bonding in **17** was responsible for the lower conductance with respect to **5**, we also measured the two derivatives **5** and **17** in a higher ionic strength buffer. At higher ionic strength, we hypothesized that the increased concentration of ions will increase the polarity of the aqueous environment near the pore, thereby disrupting intramolecular H-bonding at the

entrance of the channel **17** (because the majority of the channel is in the membrane while it is conducting, the H-bonds that stabilize the channel are unaffected by the high ionic strength buffer), causing the BOC group to be less restricted over the pore. As a result of the removal of intramolecular H-bonding in **17**, both **5** and **17** should now display equal conductances. When single ion conductances of both derivatives were obtained in 1 M KCl, 10 mM HEPES buffer at pH 7.2, derivative **17** showed a conductance of  $19.2 \pm 0.4$  pS and **5** showed a conductance of  $17.6 \pm 1.5$  pS ( Figure 6.2B). Each derivative of gA was measured 2 - 4 times independently and a two sample *t*-test confirmed that the mean conductance of **5** and **17** were not significantly different from each other ( $p = 0.1$ ). The similarity in the conductance values for **5** and **17** in high ionic strength buffer supported our hypothesis that higher ionic strength buffer disrupted H-bonding. We presume the higher ionic strength buffer weakened the H-bonding that was responsible for difference in conductance between the two derivatives in low ionic strength buffer.

### 6.3 Conclusions

We have shown in this chapter that by introducing a small modification to the H-bonding network of a derivative of gA, a dramatic change to the steric environment near the pore can take place producing a change in the conductance of ions. In Chapter 2, we discussed parameters of which we can take advantage for charge-based sensing to increase the change in conductance

when going from R to R' (Figure 2.2). Modification of the H-bonding network of a derivative of gA near the lumen of the channel introduces another design parameter that we can exploit in sensing to produce a measurable difference in conductance in the presence of the analyte to be detected.

## 6.4 Protocol for Ion channel measurements

**Formation of Planar Lipid Bilayers.** We formed planar lipid bilayers by the “folding technique.” Briefly, we used a Teflon film (Eastern Scientific Inc, pore diameter 0.1-0.2 mm) that we pretreated on both sides of the pore with 2  $\mu\text{L}$  of 5% (v/v) hexadecane in pentane. This film was mounted using vacuum grease (Dow Corning, High vacuum grease) to a custom-made Teflon chamber separating two buffer compartments each with a volume capacity of 4 mL. After addition of 1 mL of electrolyte (20 mM KCl buffered with 0.2 mM HEPES at pH 7.2 or 1 M KCl buffered with 10 mM HEPES at pH 7.2) to each compartment, we spread lipids at the air-water interface of the electrolyte solution in both compartments (specifically, we added 5  $\mu\text{L}$  from a 25  $\text{mg mL}^{-1}$  solution of 1,2-diphytanoyl-sn-glycero-3-phosphatidylcholine, DiPhyPC, in pentane). Three additional milliliters of the same electrolyte solution were added to each compartment to raise the liquid level above the aperture in the Teflon film. We formed the bilayers on the pore of the Teflon film by aspirating the electrolyte solution into a 3 mL syringe, followed by dispensing the electrolyte solution back into each compartment. This cycle of raising and lowering the liquid levels was

repeated until we obtained a bilayer that had a minimum capacitance of 70 pF and that was stable (i.e., no significant current fluctuations above the baseline noise level) at 100 mV of applied potential for at least 2 minutes. After verifying that bilayers were stable for couple minutes (in the range of  $\pm 200$  mV applied voltage) and that the capacitance was above 80-90 pF for painted bilayers, we added **5** (0.3  $\mu\text{L}$  from 50  $\text{ng mL}^{-1}$  in ethanol) to a final concentration of 1.8 pM or derivative **17** (7  $\mu\text{L}$  from 100  $\text{ng mL}^{-1}$  in ethanol) to final concentration of 86 pM directly to the bilayer chambers containing 1 M KCl, 10 mM HEPES buffer at pH 7.2. We added **5** (5  $\mu\text{L}$  from 100  $\text{ng mL}^{-1}$  in ethanol) to a final concentration of 1.8 pM or **17** (0.8  $\mu\text{L}$  from 100  $\text{ng mL}^{-1}$  in ethanol) to final concentration of 10 pM directly to the bilayer chambers containing 20 mM KCl, 0.2 HEPES buffer at pH 7.2.

**Ion Channel Measurements.** We performed single channel recordings in “voltage clamp mode” using Ag/AgCl pellet electrodes (Warner Instruments) in each compartment of the bilayer setup. Data acquisition and storage was carried out using custom software in combination with either an EPC-7 patch clamp amplifier from Heka (set at a gain of 10  $\text{mV pA}^{-1}$  and a filter cutoff frequency of 3 kHz). The data acquisition board for the amplifier was set to a sampling frequency of 15 kHz. All current traces shown in the figures were further filtered using a digital Gaussian low-pass filter with a cutoff frequency of 4 Hz.

We performed the analysis of the single channel current traces by computing histograms of the currents from the original current versus time traces

with ClampFit 9.2 software from Axon Instruments. From these histograms we extracted the main current values by fitting a Gaussian function to the peaks in the histograms. All gramicidin molecules showed a predominant conductance and occasionally subconductance states (i.e., single channel currents that were smaller than the main current values). Single channel conductances reported in this paper always refer to the main conductance state (i.e., to the dominant peaks in the current histograms). All conductance values were obtained from the slopes of I-V curves taken at -75, -50, +50 and +75 mV.

## Chapter 7

# Experimentals for the synthesis of derivatives of Gramicidin A

### Materials

We purchased all reagents and chemicals from Sigma-Aldrich unless otherwise stated. Gramicidin A (gA) was purchased as gramicidin D from Sigma Aldrich and purified by silica chromatography using a literature procedure<sup>138</sup> (to afford a final purity of 97% of gA). Carbonic anhydrase II (CA, bovine, EC 4.2.1.1) was from Sigma-Aldrich, Inc. We purchased 1,2-diphytanoyl-*sn*-glycero-3-phosphocholine (DiPhyPC) lipids from Avanti Polar Lipids, Inc. All analyses by HPLC were performed on an Agilent Zorbax C-18 column (4.6  $\mu\text{m}$  x 25 cm) using a gradient of 60 to 92% MeOH in H<sub>2</sub>O over 45 minutes.

**Synthesis of gramicidyl taurinyl succinate (1).** We dissolved 2.6 mg (1.3  $\mu\text{mol}$ ) of gramicidyl succinic acid and 0.17  $\mu\text{L}$  (1.3  $\mu\text{mol}$ ) of tert-butyl chloroformate in 1 mL of anhydrous THF. The solution was stirred for 10 min at -20 °C. Then 0.15  $\mu\text{L}$  (1.3  $\mu\text{mol}$ ) of diisopropylethylamine was added and the flask was flushed with  $\text{N}_2$ . The reaction was stirred at 0 °C for 30 min, and 0.02 mL of an aqueous 16 mg  $\text{mL}^{-1}$  solution of taurine (2.6  $\mu\text{mol}$ ) was added to the mixture. The mixture was stirred at 0 °C for 3 h, warmed to 23 °C, and then stirred for an additional 10 h. The solution was concentrated *en vacuo* and the product was isolated in 28% yield (relative to gA) by chromatography over silica using a 9:1 mixture of DCM / MeOH as eluent. The desired product had an  $R_f$  value of 0.1 in the same eluent. ESI-MS showed a peak at  $m/z = 2090.48$  corresponding to the expected  $[\text{M}+\text{H}]^+$  of **1**.

**Synthesis of taurinyl gramicidate (2).** We dissolved 4 mg (2.2  $\mu\text{mol}$ ) of **8** in 0.3 mL of THF. We added 34.1  $\mu\text{L}$  (237.6  $\mu\text{mol}$ ) of  $\text{Et}_3\text{N}$  and flushed the flask with  $\text{N}_2$ . The reaction vessel was cooled to 0 °C and 1.2  $\mu\text{L}$  of ethyl chloroformate was added. The solution was stirred at 0 °C for 3.5 h and then a solution of 1.65 mg of taurine (dissolved in 30.0  $\mu\text{L}$  of  $\text{H}_2\text{O}$ ) was added to the solution containing desethanolamine gramicidin. The reaction was stirred for 30 min at 0 °C, warmed to 23 °C, and stirred an additional 12 h. The solution was concentrated *en vacuo* and purified by silica chromatography (9:1 DCM / MeOH) to give an overall isolated yield (over 4 steps) of 41% relative to gA. ESI-MS revealed a

major peak at  $m/z = 1944.79$  corresponding to the expected  $[M+H]^+$  of the product.

**Synthesis of gramicidamine (3).** Desethanolamine gA **12** (25 mg, 13.6  $\mu\text{mol}$ ) and triethylamine (7.6  $\mu\text{L}$ , 54.4  $\mu\text{mol}$ ) were added to 1 mL of anhydrous THF and the resulting mixture was stirred and cooled to 0 °C. After adding ethyl chloroformate (5.20  $\mu\text{L}$ , 54.4  $\mu\text{mol}$ ) to the cooled mixture, the reaction was stirred for 3.5 hours at 0 °C. Mono-*tert*-butyloxycarbonyl (BOC) ethylenediamine, (8.6  $\mu\text{L}$ , 54.4  $\mu\text{mol}$ , purchased from Alfa Aesar), was dissolved in 0.2 mL of THF and cooled to 0 °C. This solution was added to the mixture containing desethanolamine gA **12** and the resulting solution was stirred for an additional 30 minutes at 0 °C, followed by stirring at 23 °C for 8 hours. After concentrating to dryness, the BOC-protected gramicidamine was purified using preparative silica chromatography (using a 9:1 mixture of DCM:MeOH as eluent). ESI-MS ( $m/z$ ) calcd for  $\text{C}_{104}\text{H}_{149}\text{N}_{21}\text{O}_{18}$  ( $M^+$ ), 1981.14; found ( $M-H$ )<sup>-</sup>, 1979.66. A mixture containing 1 mL of DCM, 1 mL of trifluoroacetic acid (TFA), 0.1 mL of dimethylsulfide, and 0.05 mL of ethanedithiol was prepared and cooled to 0 °C. BOC-protected gramicidamine (22.4 mg, 11.3  $\mu\text{mol}$ ) was dissolved in the cooled mixture. The reaction was allowed to warm up to 23 °C and stirred for 3 hours. The reaction mixture was concentrated *en vacuo* to dryness and purified by silica chromatography. The eluent initially consisted of a mixture of DCM:MeOH (9:1) to elute the less-polar impurities. After confirming by thin layer chromatography (TLC) that the impurities had eluted, the eluent was changed to DCM:MeOH

(9:2). HR-MS ( $m/z$ ) calcd for  $C_{99}H_{141}N_{21}O_{16}$  ( $M+H$ )<sup>+</sup>, 1881.0937; found ( $M+H$ )<sup>+</sup>, 1881.0943. The retention time by HPLC was 40.5 minutes. The overall yield was 74% (19 mg) from desethanolamine gA **12**.

**Synthesis of Gramicidyl succinic acid (4).** We dissolved 6 mg of gramicidin A (gA) (3.2  $\mu$ mol) in 0.5 mL of dichloromethane (DCM). We added 2.6  $\mu$ L (32  $\mu$ mol) of pyridine and 3.2 mg (32  $\mu$ mol) of succinic anhydride to the solution of gA. To increase the solubility of succinic anhydride, a few drops of tetrahydrofuran (THF) were added. The solution was stirred for 12 h at 23 °C. After concentrating the solution *en vacuo*, the desired product was isolated by chromatography over silica using a 9:1 mixture of DCM / methanol (MeOH) as eluent. The desired product had an  $R_f$  value of 0.3 (for comparison, gA had an  $R_f$  value of 0.5) using the same eluent. The product was taken directly to the next step without further characterization.

**Synthesis of N-(*tert*-butyloxycarbonyl)glycylgramicidin (5).** Gramicidin A (24.5 mg, 0.013 mmol), (N-BOC) glycine (9.11 mg, 0.052 mmol), dicyclohexylcarbodiimide (DCC) (26.8 mg, 0.13 mmol) and dimethylaminopyridine (DMAP) (7.9 mg, 0.065 mmol) were dried separately *en vacuo*. N-BOC glycine, DCC, and DMAP were each dissolved in 2 ml freshly-distilled dichloromethane. Each solution was then added to gA in the order of (N-BOC) glycine, DCC, and DMAP. The resulting solution was stirred at room temperature for 6 hrs under  $N_2$ . The solvent was evaporated and **5** was purified

from the crude mixture on silica with dichloromethane (DCM) / Methanol (MeOH) (9:1) as eluent to give 23 mg (87% yield) of the purified compound. HPLC experiment was performed using a C-18 column (9.6  $\mu$ m x 25 cm, Biotage, Inc.) using a 90-minute gradient from 60% Methanol (MeOH) in deionized water to 100% MeOH at room temperature. The retention time of **5** on reverse-phase HPLC was 67.69 minutes. ESI-MS reveals a  $[M + 2Na]^{2+}$  fragment at 1042.34.  $^1H$ -NMR (400 MHz,  $CD_3OD$ ):  $\delta$  0.33-0.48 (m, 18H),  $\delta$  0.6 (bd, 3H, 8 Hz),  $\delta$  0.7-1.0 (m, 28H),  $\delta$  1.1-1.2 (m, 4H),  $\delta$  1.23-1.4 (m, 9H),  $\delta$  1.43 (s, 9H),  $\delta$  1.6 (bs, 2H),  $\delta$  1.95 (bs, 2H),  $\delta$  2.01-2.03 (m, 4H),  $\delta$  3.35 (s, 6H),  $\delta$  3.47-3.57 (m, 2H),  $\delta$  3.84 (s, 1H),  $\delta$  3.90 (bs, 1H),  $\delta$  3.95 (bs, 1H),  $\delta$  4.14 (bd, 2H, 12 Hz),  $\delta$  4.22 (bd, 2H, 12 Hz),  $\delta$  4.28-4.42 (m, 3H),  $\delta$  4.54-4.68 (m, 4H),  $\delta$  6.87-7.1 (m, 11H),  $\delta$  7.23-7.36 (m, 5H),  $\delta$  7.4 (d, 2H, 8 Hz),  $\delta$  7.49-7.59 (m, 4H),  $\delta$  8.12 (s, 1H).

**Synthesis of glycygramicidin (6).** A solution of 2 ml trifluoroacetic acid (TFA) / DCM (1:1, v:v) with 0.02 ml dimethylsulfide and 0.01 ml ethanedithiol is cooled to 0°C. The TFA solution is then added to dried **6** and stirred while warming to room temperature for 4 hours. After evaporated to dryness, the crude solid was dissolved in 0.75 ml of DCM / MeOH (2:1). This solution was added dropwise into a beaker containing 80 ml of deionized, stirring water at 0 °C and **6** was precipitated out and filtered to yield 20.1 mg (90.2 % yield) of pure material. ESI-MS reveals three fragments:  $[M]^+ = 1938.72$ ,  $[M + Na]^+ = 1961.86$ , and  $[M + 2Na]^{2+} = 992.39$ .  $^1H$ -NMR (400 MHz,  $CD_3OD$ ):  $\delta$  0.33-0.48 (m, 18H),  $\delta$  0.6 (bd, 3H, 8 Hz),  $\delta$  0.7-1.0 (m, 28H),  $\delta$  1.1-1.2 (m, 4H),  $\delta$  1.23-1.4 (m, 9H),  $\delta$  1.6 (bs,

2H),  $\delta$  1.95 (bs, 2H),  $\delta$  2.01-2.03 (m, 4H),  $\delta$  3.35 (s, 6H),  $\delta$  3.47-3.57 (m, 2H),  $\delta$  3.84 (s, 1H),  $\delta$  3.90 (bs, 1H),  $\delta$  3.95 (bs, 1H),  $\delta$  4.14 (bd, 2H, 12 Hz),  $\delta$  4.22 (bd, 2H, 12 Hz),  $\delta$  4.28-4.42 (m, 3H),  $\delta$  4.54-4.68 (m, 6H),  $\delta$  6.87-7.1 (m, 11H),  $\delta$  7.23-7.36 (m, 5H),  $\delta$  7.4 (d, 2H, 8 Hz),  $\delta$  7.49-7.59 (m, 4H),  $\delta$  8.12 (s, 1H).

**Gramicidyl glycolate (7).** A solution of 1 ml TFA / DCM (1:1) with 0.02 ml dimethylsulfide and 0.01 ml ethanedithiol along with separately dried 2 mg of Gramicidyl O-trityl glycolate is cooled to 0°C. The TFA solution is then added to Gramicidyl O-trityl glycolate while stirring and allowed to warm to room temperature for 2 hours. Upon purification by silica chromatography with DCM / MeOH (9:1) as eluent, 1.8 mg (98% yield) of **7** was obtained. HPLC experiment was performed using a C-18 column (9.6  $\mu$ m x 25 cm, Biotage, Inc.) using a 90-minute gradient from 60% Methanol (MeOH) in deionized water to 100% MeOH at room temperature. Reverse-phase HPLC retention time was 62.3 minutes (99% purity). ESI-MS reveals a  $[M + Na]^+$  fragment at 1962.79 and a  $[M + 2Na]^{2+}$  fragment at 992.74.  $^1H$ -NMR (400 MHz,  $CD_3OD$ ):  $\delta$  0.33-0.48 (m, 18H),  $\delta$  0.6 (bd, 3H, 8 Hz),  $\delta$  0.7-1.0 (m, 28H),  $\delta$  1.1-1.2 (m, 4H),  $\delta$  1.23-1.4 (m, 9H),  $\delta$  1.6 (bs, 2H),  $\delta$  1.95 (bs, 2H),  $\delta$  2.01-2.03 (m, 4H),  $\delta$  3.35 (s, 6H),  $\delta$  3.47-3.57 (m, 2H),  $\delta$  3.84 (s, 1H),  $\delta$  3.90 (bs, 1H),  $\delta$  3.95 (bs, 1H),  $\delta$  4.14 (bd, 2H, 12 Hz),  $\delta$  4.22 (bd, 2H, 12 Hz),  $\delta$  4.28-4.42 (m, 3H),  $\delta$  4.54-4.68 (m, 6H),  $\delta$  6.87-7.1 (m, 11H),  $\delta$  7.23-7.36 (m, 5H),  $\delta$  7.4 (d, 2H, 8 Hz),  $\delta$  7.49-7.59 (m, 4H),  $\delta$  8.12 (s, 1H).

**Synthesis of O-trityl glycolic acid (8).**<sup>139</sup> A solution of 800 mg of glycolic acid and 2.75 g of diisopropylethylamine (DIEA) was prepared in 5 ml of DCM. The resulting mixture was cooled to 0°C. Then a solution of 1.62 g of trityl chloride in DCM was added dropwise to the cooled solution of glycolic acid and DIEA. The reaction was allowed to stir for 1 hr at 0°C, then 18 hours at RT. The solution was then concentrated *en vacuo*. Reaction mixture was purified by silica chromatography using DCM as the eluent until all of the unreacted trityl chloride eluted out. The polarity of eluent was increased to 45:4 (DCM:MeOH) to elute O-trityl glycolic acid. Upon concentration *en vacuo*, a white solid (902 mg, 22% yield) of O-trityl glycolic acid was obtained. <sup>1</sup>H-NMR (400 MHz, CDCl<sub>3</sub>): δ 3.893 (s, 2H), δ 7.266 – 7.363 (m, 9H), δ 7.47 (d, 8 Hz)

**Synthesis of gramicidyl O-trityl glycolate (9).** A solution of 3.18 mg of O-trityl glycolic acid and 5.3 mg of DCC in 2 ml of dry DCM was stirred for 10 min. Then a 1 ml solution containing 5 mg of gA and a 1 ml solution containing 1.6 mg of DMAP were subsequently added in that order. The reaction was allowed to stir at RT under N<sub>2</sub> for 14 hours. Upon purification by silica chromatography with DCM / MeOH (9:1) as eluent, 3.2 mg (55% yield) of Gramicidyl O-trityl glycolate was obtained. HPLC experiment was performed using a C-18 column (9.6 μm x 25 cm, Biotage, Inc.) using a 90-minute gradient from 60% Methanol (MeOH) in deionized water to 100% MeOH at room temperature. Reverse-phase HPLC retention time was 78.8 min (99% purity). ESI-MS reveals a [M + 2Na]<sup>2+</sup> fragment at 1113.8 and a [M-H+3Na]<sup>2+</sup> fragment at 1124.91. <sup>1</sup>H-NMR (400 MHz, CD<sub>3</sub>OD):

$\delta$  0.33-0.48 (m, 18H),  $\delta$  0.6 (bd, 3H, 8 Hz),  $\delta$  0.7-1.0 (m, 28H),  $\delta$  1.1-1.2 (m, 4H),  $\delta$  1.23-1.4 (m, 9H),  $\delta$  1.6 (bs, 2H),  $\delta$  1.95 (bs, 2H),  $\delta$  2.01-2.03 (m, 4H),  $\delta$  3.35 (s, 6H),  $\delta$  3.47-3.57 (m, 2H),  $\delta$  3.84 (s, 1H),  $\delta$  3.90 (bs, 1H),  $\delta$  3.95 (bs, 1H),  $\delta$  4.14 (bd, 2H, 12 Hz),  $\delta$  4.22 (bd, 2H, 12 Hz),  $\delta$  4.28-4.42 (m, 3H),  $\delta$  4.54-4.68 (m, 4H),  $\delta$  6.87-7.1 (m, 8H),  $\delta$  7.23-7.36 (m, 17H),  $\delta$  7.49-7.59 (m, 15H),  $\delta$  8.12 (s, 1H).

**Synthesis of 2-azidoethylammonium chloride (10).**<sup>140</sup> Sodium azide (236 mg, 3.6 mmol) and 2-bromoethylammonium bromide (200 mg, 0.98 mmol) were dissolved in 1 mL of H<sub>2</sub>O. The reaction was refluxed at 95 °C for 1 hour. After cooling the solution to 23 °C, 1 M NaOH was added to the solution until the pH was 12. The 2-azidoethylammonium chloride was then co-distilled with H<sub>2</sub>O, acidified to pH 4 with 1 M HCl, and lyophilized to provide 76 mg of product as a white powder (65% yield). ESI-MS (m/z) calcd for C<sub>2</sub>H<sub>6</sub>N<sub>4</sub> (M)<sup>+</sup>, 86.06; found (M+H)<sup>+</sup>, 86.99. <sup>1</sup>H-NMR (D<sub>2</sub>O, 400 MHz):  $\delta$  3.414 (t, 2H, 5.6 Hz), 3.301 (t, 2H, 5.6 Hz).

**Synthesis of 2-aminoethyl gramicidate (11).** Gramicidin A (142 mg, 75  $\mu$ mol) was added to 10 mL of acetonitrile (ACN). Phosphorus oxychloride (287  $\mu$ L, 3 mmol) was added dropwise to the solution of gA and the reaction was stirred at 23 °C for 4 hours. The reaction mixture was concentrated to dryness and 10 mL of 8:2 mixture of ACN:H<sub>2</sub>O was added. The mixture was stirred for 20 min. The mixture was concentrated to dryness and 5 mL of a 2:1 mixture of

dichloromethane (DCM):methanol (MeOH) was added. This mixture was added dropwise to a stirred beaker containing 200 mL of H<sub>2</sub>O. The resulting precipitate was collected by filtration. The crude yield was 96% by weight. The retention time by HPLC was 34.7 min. ESI-MS (m/z) calcd for C<sub>99</sub>H<sub>140</sub>N<sub>20</sub>O<sub>17</sub> (M<sup>+</sup>), 1882.07; found (M-H)<sup>-</sup>, 1880.85.

**Synthesis of desethanolamine gA (12).** Anhydrous formic acid (0.55 mL, 14.4 mmol) was combined with acetic anhydride (1.36 mL, 14.4 mmol) and heated to 65 °C for 30 minutes. After cooling the formic acid/acetic anhydride solution to 23 °C, the mixture was added to 2-aminoethyl gramicidate **11** (139 mg, 72 μmol) that was dissolved in 20 mL of dry tetrahydrofuran (THF). The reaction was stirred for 3.5 hours followed by concentration to dryness. We dissolved the crude product in a minimal volume of a 2:1 mixture of DCM:MeOH at 23 °C (until the solution was clear) and added this solution dropwise to a stirred beaker containing 200 mL of H<sub>2</sub>O. The resulting precipitate was collected by filtration and taken to the next step without further purification. **Note:** When performing these reactions on smaller scales (< 100 mg of peptides), it is possible to isolate the product by silica chromatography using DCM:MeOH (9:1) as the eluent to afford *N*-formyl-2-aminoethyl gramicidate as a white powder in 72% isolated yield. ESI-MS (m/z) calcd for C<sub>100</sub>H<sub>140</sub>N<sub>20</sub>O<sub>18</sub> (M<sup>+</sup>), 1910.07; found (M+Na)<sup>+</sup>, 1932.97. The crude product of *N*-formyl-2-aminoethyl gramicidate (150 mg, 78 μmol) was dissolved in 25 mL of THF. In a separate flask, LiOH · H<sub>2</sub>O (327 mg, 7.8 mmol) was dissolved in 25 mL of H<sub>2</sub>O. The two mixtures were combined and

stirred at 23 °C for 3 hours, followed by slow addition of 1 M HCl until the solution had a pH of 2. The reaction mixture was concentrated *en vacuo* to dryness and redissolved in 15 mL of 2:1 DCM:MeOH. The mixture was added dropwise to 150 mL of H<sub>2</sub>O while stirring. The resulting precipitate was collected by filtration and purified by silica chromatography. The eluent initially consisted of a mixture of CHCl<sub>3</sub>:MeOH:H<sub>2</sub>O:acetic acid (750:75:10:2.5) to elute the less-polar impurities. After confirming by thin layer chromatography (TLC) that the impurities had eluted, the eluent was changed to CHCl<sub>3</sub>:MeOH:H<sub>2</sub>O:acetic acid (200:30:4:1). The fractions containing desethanolamine gA **12** were concentrated *en vacuo*, and the resulting gel was re-dissolved in 15 mL of 2:1 DCM:MeOH. The mixture was added dropwise to 150 mL of H<sub>2</sub>O while stirring. The resulting precipitate was collected by filtration to yield 93 mg of **12** (65 % yield over two steps from **11**). ESI-MS (m/z) calcd for C<sub>97</sub>H<sub>135</sub>N<sub>19</sub>O<sub>17</sub> (M)<sup>+</sup>, 1839.03; found (M+Na)<sup>+</sup>, 1861.94. The retention time by HPLC was 40.7 minutes.

**Synthesis of gramicidazide (13).** Desethanolamine gA **12** (20 mg, 10.8 μmol) and DIEA (7.6 μL, 43.4 μmol) were added to 2 mL of anhydrous THF and the resulting mixture was stirred and cooled to 0 °C. After adding ethyl chloroformate (4.6 μL, 43.4 μmol) to the cooled mixture, the reaction was stirred for 3.5 hours at 0 °C. Separately, 2-azidoethylammonium chloride (5.3 mg, 43.4 μmol) was dissolved in 0.2 mL of 1 M NaOH and cooled to 0 °C. This solution was added to the mixture containing desethanolamine gA and the resulting solution was stirred for an additional 30 minutes at 0 °C and then at 23 °C for 8 hours. After

concentrating to dryness, the product was purified using preparative silica chromatography (using a mixture of 9:1 DCM:MeOH as eluent) to give 14.2 mg of **13** (69% yield). HR-MS ( $m/z$ ) calcd for  $C_{99}H_{139}N_{23}O_{16}$  ( $M+H$ )<sup>+</sup>, 1907.0842; found ( $M+H$ )<sup>+</sup>, 1907.0782. The retention time by HPLC was 42.4 minutes.

**Synthesis of N-propargyl-4-sulfamoylbenzamide (14).**<sup>88</sup> Propargyl amine (34  $\mu$ L, 0.497 mmol) and 4-carboxybenzenesulfonamide (100 mg, 0.497 mmol) were dissolved in 2 mL of dry dimethylformamide. N-hydroxybenzotriazole (44.7 mg, 0.33 mmol), O-(benzotriazol-1-yl)-N,N,N',N'-tetramethyluronium hexafluorophosphate (188 mg, 0.497 mmol) and DIEA (79.4  $\mu$ L, 0.497 mmol) were added in this order to the stirred solution. After 4 hours, the solution was evaporated to dryness and 30 mL of ethylacetate was added. The solution was washed twice with 30 mL of H<sub>2</sub>O and with 30 mL of brine, dried over Na<sub>2</sub>SO<sub>4</sub>, filtered, and concentrated to dryness. The compound was purified by column chromatography using a 2:8 mixture of DCM:ethylacetate as eluent, affording 52 mg (44% yield) as a white solid. <sup>1</sup>H-NMR (DMSO-*d*<sub>6</sub>, 400 MHz):  $\delta$  9.148 (t, 1H, 5.6 Hz), 8.003 (d, 2H, 8.4 Hz), 7.902 (d, 2H, 8.4 Hz), 7.506 (s, 2H), 4.075 (m, 2H), 3.172 (t, 1H, 2.4 Hz).

**Synthesis of N-hydroxysuccinimidyl 4-sulfonamidobenzoate (15).**<sup>141</sup> N-hydroxysuccinimide (345 mg, 3 mmol) and 4-carboxybenzenesulfonamide (500 mg, 2.5 mmol) were dissolved in 10 mL of DMF. To this stirring solution, EDC (573 mg, 3 mmol) was added. The solution was stirred at room temperature for 8

hours and concentrated to dryness. The title compound, **15**, was isolated using silica chromatography (using a mixture of 3:7 EtOAc:DCM as eluent) to give 380 mg of the product as a white powder (51% yield).  $^1\text{H-NMR}$  (300 MHz, DMSO- $d_6$ )  $\delta$  8.256 (d, 2H, 6.3 Hz), 7.983 (d, 2H, 6.3 Hz), 7.644 (s, 2H), 2.834 (s, 4H).

**Synthesis of sodium propargyl sulfonate (16).**<sup>87</sup> Propargyl bromide (1 mL, 9 mmol), purchased from Acros Organics as a solution containing 80 wt % in toluene, and sodium sulfite (1.43 g, 11.35 mmol) were dissolved in 3.5 mL of  $\text{H}_2\text{O}$  and 3.5 mL of MeOH. The mixture was stirred for 7 hours at 65 °C. MeOH (60 mL) was added and the resulting precipitate was filtered and removed. The filtrate was diluted in acetone and the resulting precipitate was collected as white crystals (1.3 g, 81% yield). ESI-MS ( $m/z$ ) calcd for  $\text{C}_3\text{H}_3\text{O}_3\text{S}$  ( $\text{M}^+$ ), 118.98; found ( $\text{M}^+$ ), 119.04.  $^1\text{H-NMR}$  ( $\text{D}_2\text{O}$ , 400 MHz):  $\delta$  3.849 (d, 2H, 1.4 Hz), 2.714 (t, 1H, 1.4 Hz).

**Synthesis of 17.** Gramacidamine **3** (1.2 mg, 0.64  $\mu\text{mol}$ ), (N-BOC-protected) glycine N-hydroxysuccinimidyl ester (0.52 mg, 2  $\mu\text{mol}$ ), and diisopropylethylamine (DIEA, 0.32  $\mu\text{L}$ , 2  $\mu\text{mol}$ ) were dissolved in 0.4 mL of THF. The reaction was stirred for 14 hours at 23 °C. The product was purified by HPLC. The isolated yield of **17** was 76%. The retention time by HPLC was 43.3 minutes. HR-MS ( $m/z$ ) calcd for  $\text{C}_{106}\text{H}_{152}\text{N}_{22}\text{O}_{19}$  ( $\text{M}+\text{H}^+$ ), 2038.1676; found ( $\text{M}+\text{H}^+$ ), 2038.1661.

**Synthesis of 18.** A mixture containing 1 mL of DCM, 1 mL of trifluoroacetic acid (TFA), 0.1 mL of dimethylsulfide, and 0.05 mL of ethanedithiol was prepared and cooled to 0 °C. The cooled mixture was added to **17** (5.2 mg, 2.6 µmol). The reaction was allowed to warm up to 23 °C and stirred for 3 hours. The reaction mixture was concentrated *en vacuo* to dryness and purified by silica chromatography. The eluent initially consisted of a mixture of DCM:MeOH (9:1) to elute the less-polar impurities. After confirming by thin layer chromatography (TLC) that the impurities had eluted, the eluent was changed to DCM:MeOH (9:2).

**Synthesis of 19.** Gramicidamine **3** (1.2 mg, 0.64 µmol), 4-carboxybenzenesulfonamide N-hydroxysuccinimidyl ester (0.57 mg, 2 µmol), and DIEA (0.32 µL, 2 µmol) were dissolved in 0.4 mL of THF. The reaction was stirred for 14 hours at 23 °C. The product was purified by HPLC. The isolated yield of **19** was 41%. The retention time by HPLC was 37.6 minutes. HR-MS (m/z) calcd for C<sub>106</sub>H<sub>146</sub>N<sub>22</sub>O<sub>19</sub>S (M+H)<sup>+</sup>, 2064.0928; found (M+H)<sup>+</sup>, 2064.1015.

**Synthesis of 20.** Gramicidazide **13** (10 mg, 5.2 µmol) and sodium propargyl sulfonate (1.2 mg, 8.6 µmol) were dissolved in 2 mL of *tert*-butanol (t-BuOH). Sodium ascorbate (8.2 mg, 41.4 µmol) was dissolved in 0.5 mL of H<sub>2</sub>O, and CuSO<sub>4</sub>·5H<sub>2</sub>O (2.6 mg, 10.4 µmol) was dissolved separately in 0.5 mL of H<sub>2</sub>O. The solution of sodium ascorbate was added to the solution of gramicidazide **13**, followed by addition of the solution of CuSO<sub>4</sub>·5H<sub>2</sub>O. The reaction was stirred at

23 °C for 14 hours. The solution was then concentrated *en vacuo* and purified by HPLC to give 32% yield of **20**. The retention time by HPLC was 36.1 minutes. HR-MS (m/z) calcd for  $C_{102}H_{143}N_{23}O_{19}S$  (M-H)<sup>-</sup>, 2025.0578; found (M-H)<sup>-</sup>, 2025.0512.

**Synthesis of 21.** Gramicidazide **13** (1.5 mg, 0.79 μmol) and N-propargyl-4-sulfamoylbenzamide (0.30 mg, 1.26 μmol) was dissolved in 0.2 mL of t-BuOH. To the solution of **13**, a solution of sodium ascorbate (1.1 mg, 5.5 μmol) dissolved in 0.05 mL of H<sub>2</sub>O was added, followed by addition of a solution of CuSO<sub>4</sub>·5H<sub>2</sub>O (700 μg, 2.8 μmol) dissolved in 0.05 mL of H<sub>2</sub>O. The reaction was stirred for 3 days. The solution was then concentrated *en vacuo* and purified by HPLC to give an 88% yield of **21**. HR-MS (m/z) calcd for  $C_{109}H_{149}N_{25}O_{19}S$  (M+H)<sup>+</sup>, 2145.1254; found (M+H)<sup>+</sup>, 2145.1216. The retention time by HPLC was 37.6 minutes.

**Synthesis of benzyl glycolate (22).**<sup>142</sup> Glycolic acid (200 mg, 2.6 mmol) and triethylamine (401 μL, 2.86 mmol) were dissolved in 2.6 mL of acetone. After a couple minutes of stirring, benzyl bromide (279 μL, 2.34 mmol) was added to the solution. The reaction was refluxed at 60°C for 12 hours. The solution was filtered to remove precipitated triethylammonium bromide and was concentrated *en vacuo*. Purification was done by silica chromatography with DCM to remove the non-polar impurities and then 2% EtOAc in DCM to elute the desired product as

a colorless oil (200 mg, 51% yield).  $^1\text{H-NMR}$  (400 MHz,  $\text{CDCl}_3$ )  $\delta$  7.362 (5H, s)  $\delta$  5.198 (2H, s)  $\delta$  4.201 (2H, s)  $\delta$  3.366 (1H, s) ppm.

**Synthesis of glycolic acid-O-(di-*tert*-butyl) phosphate (23).**<sup>143</sup> Di-*tert*-butyl-N,N-diethyl phosphoramidite (0.62 mL, 2.5 mmol), benzyl glycolate, **22**, (265 mg, 1.6 mmol) and tetrazole (560 mg, 8 mmol) were dissolved in 46 mL of anhydrous THF. The reaction stirred at room temperature for 2 hours and then it was cooled to  $-78^\circ\text{C}$ . *m*-chloro perbenzoic acid (825 mg, 4.8 mmol) was added to the cooled solution and was allowed to stir for 20 min at  $-78^\circ\text{C}$  and then at room temperature for 10 min. The solution was concentrated *en vacuo* and was taken up in 30 mL of DCM and washed twice with 40 mL of saturated  $\text{NaHCO}_3$ , dried over  $\text{Na}_2\text{SO}_4$  and concentrated *en vacuo*. The resulting crude oil was purified by preparative silica chromatography using DCM:acetone (9:1) to afford 240 mg of material. The compound was dissolved in 1.5 mL of MeOH and subjected to hydrogenation over 240 mg Pd/C for 3 hours. Upon filtration over celite, the filtrate was concentrated *en vacuo* to yield a pure colorless liquid (180 mg, 40% yield).  $^1\text{H-NMR}$  (300 MHz,  $\text{CD}_3\text{OD}$ )  $\delta$  4.477 (2H, d,  $J = 9$  Hz),  $\delta$  1.408 (18H, s);  $^{31}\text{P-NMR}$  (300 MHz,  $\text{CD}_3\text{OD}$ )  $\delta$  -10.437 ppm using an internal 85% phosphoric acid standard.

**Synthesis of glycolic acid-O-phosphate (24).**<sup>144</sup> Glycolic acid-O-(di-*tert*-butyl) phosphate (6 mg, 22  $\mu\text{mol}$ ) was added to 1.5 mL solution of 1:1 DCM:TFA and the resulting mixture was stirred at room temperature for 3 hours. The resulting

solution was concentrated to dryness to yield a clear film that measured 3.1 mg (91% yield).  $^1\text{H-NMR}$  (300 MHz,  $\text{CD}_3\text{OD}$ )  $\delta$  4.477 (2H, d,  $J = 9$  Hz);  $^{31}\text{P-NMR}$  (300 MHz,  $\text{CD}_3\text{OD}$ )  $\delta$  3.33 ppm using an internal 85% phosphoric acid standard.

**Synthesis of 25.** O-(di-*t*-butylphosphate) glycolic acid (3.4 mg, 12.6  $\mu\text{mol}$ ) and gramicidamine (8 mg, 4.2  $\mu\text{mol}$ ) were dissolved in 2 mL of DCM. Triethylamine (0.72  $\mu\text{L}$ , 15.1  $\mu\text{mol}$ ) was added to the stirring solution. After a couple minutes of stirring, EEDQ (3.1 mg, 1.6  $\mu\text{mol}$ ) was added and stirring continued for 16 hours. The solution was concentrated down and resulting product was purified using preparative silica chromatography using DCM:MeOH (9:1) to afford 6 mg of yellow powder. A mixture of 1 mL of 1:1 DCM:TFA, 0.1 mL dimethylsulfide and 0.02 mL ethanedithiol was prepared and cooled to 0 °C. The yellow powder was dissolved in the cooled mixture. The reaction was allowed to warm up to room temperature and stirred for 3 hours. The reaction mixture was concentrated down and taken up in 2 mL of 2:1 DCM:MeOH. The mixture was added dropwise to a stirring beaker of 100 mL of water. The resulting precipitate was collected by filtration, giving a yellow solid (5.6 mg, 58% yield). For conductance measurements, the compound was further purified by analytical RP-HPLC using a Zorbax C-18 column (4.6 x 250 mm), 60% to 92% MeOH in water over 45 min. The retention time is 36.15 min. MALDI-TOF MS showed a  $[\text{M-H}]^-$  peak at 2017.21.

**Synthesis of 26.** Gramicidamine (8 mg, 4.3  $\mu\text{mol}$ ) was dissolved in 1.5 mL of THF and DIEA (3.8  $\mu\text{L}$ , 9.9  $\mu\text{mol}$ ) was added and the solution was stirred. O-trityl glycolic acid (1.7 mg, 8.6  $\mu\text{mol}$ ) and 2-ethoxy-1-ethoxycarbonyl-1,2-dihydroquinoline (2.1 mg, 8.6  $\mu\text{mol}$ ) were added to the solution in that order. The reaction was stirred for 12 hours. The trityl-protected derivative of **26** was purified by preparative silica chromatography with DCM:MeOH (9:1) and was dissolved in 1 mL of DCM and cooled to 0°C. A solution of 1 mL TFA / DCM (1:1) with 0.02 mL of dimethylsulfide and 0.01 mL of ethanedithiol is cooled to 0°C. The TFA solution is then added to the solution containing the trityl-protected derivative of **26**. The reaction was stirred at RT for 4 hours. Upon purification by silica chromatography with DCM / MeOH (9:1) as eluent, 6 mg (72% yield) of **26** was obtained. ESI-MS shows a  $[\text{M}+\text{Na}]^+$  fragment at 1962.01 and a  $[\text{M}+2\text{Na}]^{2+}$ .

## References

1. Apell, H. J.; Bamberg, E.; Alpes, H. *J. Mem. Biol.* **1979**, *50*, (3-4), 271-285.
2. Apell, H. J.; Bamberg, E.; Lauger, P. *Biochim. Biophys. Acta.* **1979**, *552*, (3), 369-378.
3. Bamberg, E.; Apell, H. J.; Alpes, H.; Gross, E.; Morell, J. L.; Harbaugh, J. F.; Janko, K.; Lauger, P. *Fed. Proc.* **1978**, *37*, (12), 2633-2638.
4. Gross, E.; Morell, J. L.; Bamberg, E.; Lauger, P. *Fed. Proc.* **1977**, *36*, (3), 864.
5. K. Janko, R. R., E. Bamberg, H.-J. Apell, H. Alpes, P. Lauger, *Peptides: Structure and Function*. Pierce Chemical Company: Rockford, 1983; Vol. 8.
6. Mayer, M.; Semetey, V.; Gitlin, I.; Yang, J.; Whitesides, G. M. *J. Am. Chem. Soc.* **2008**, *130*, (4), 1453-1465.
7. Gitlin, I.; Mayer, M.; Whitesides, G. M. *J. Phys. Chem. B* **2003**, *107*, (6), 1466-1472.
8. Aidley, D. J. S., P. R., *Ion Channels: Molecules in Action*. 1st ed.; Cambridge University Press: Cambridge, UK, 1996.
9. Bayley, H. *Curr. Opin. Chem. Biol.* **2006**, *10*, (6), 628-637.
10. Bayley, H.; Cremer, P. S. *Nature* **2001**, *413*, 226-230.

11. Gu, L. Q.; Braha, O.; Conlan, S.; Cheley, S.; Bayley, H. *Nature* **1999**, *398*, (6729), 686.
12. Gu, L. Q.; Cheley, S.; Bayley, H. *Biophys. J.* **2005**, *88*, (1), 657A-657A.
13. Bali, D.; King, L.; Kim, S. *Austr. J. Chem.* **2003**, *56*, (4), 293-300.
14. Cornell, B. A.; Braach-Maksvytis, V. L. B.; King, L. G.; Osman, P. D. J.; Raguse, B.; Wieczorek, L.; Pace, R. J. *Nature* **1997**, *387*, (6633), 580-583.
15. Futaki, S.; Zhang, Y. J.; Kiwada, T.; Nakase, I.; Yagami, T.; Oiki, S.; Sugiura, Y. *Bioorg. Med. Chem.* **2004**, *12*, (6), 1343-1350.
16. Loughheed, T.; Borisenko, V.; Hand, C. E.; Woolley, G. A. *Bioconjug. Chem.* **2001**, *12*, (4), 594-602.
17. Borisenko, V.; Zhang, Z. H.; Woolley, G. A. *Biochim. Biophys. Acta. - Biomembranes* **2002**, *1558*, (1), 26-33.
18. Terrettaz, S.; Ulrich, W. P.; Guerrini, R.; Verdini, A.; Vogel, H. *Angewandte Chemie International Edition* **2001**, *40*, (9), 1740-1743.
19. Gokel, G. W.; Schlesinger, P. H.; Djedovic, N. K.; Ferdani, R.; Harder, E. C.; Hu, J. X.; Leevy, W. M.; Pajewska, J.; Pajewski, R.; Weber, M. E. *Bioorg. Med. Chem.* **2004**, *12*, (6), 1291-1304.
20. Matile, S.; Sakai, N.; Mareda, J.; Kumaki, J.; Yashima, E. *J. Recept. Signal Transduction* **2006**, *26*, (5-6), 461-472.
21. Banghart, M.; Borges, K.; Isacoff, E.; Trauner, D.; Kramer, R. H. *Nature Neuroscience* **2004**, *7*, 1381-1386.
22. Andersen, O. S. *Annual Reviews in Physiology* **1984**, *46*, (1), 531-548.
23. Chadwick, D. J.; Cardew, G., *Gramicidin and related ion channel-forming peptides*. Chichester; New York: John Wiley & Sons: 1999.
24. Wang, Z.; Fried, J. R. *Soft Matter* **2007**, *3*, (8), 1041-1052.
25. Eisenman, G.; Horn, R. *Journal of Membrane Biology* **1983**, *76*, (3), 197-225.
26. Myers, V. B.; Haydon, D. A. *Biochim Biophys Acta* **1972**, *274*, (2), 313-22.

27. Levitt, D. G. *Curr. Top. Membr. Transp* **1984**, 21, 181-197.
28. Levitt, D. G. *Biophysical Journal* **1982**, 37, (3), 575.
29. Urban, B. W.; Hladky, S. B.; Haydon, D. A. *Biochim Biophys Acta* **1980**, 602, (2), 331-54.
30. Bamberg, E.; Läuger, P. *Journal of Membrane Biology* **1977**, 35, (1), 351-375.
31. Antonenko, Y. N.; Rokitskaya, T. I.; Kotova, E. A.; Reznik, G. O.; Sano, T.; Cantor, C. R. *Biochemistry* **2004**, 43, (15), 4575-4582.
32. Apell, H. J.; Bamberg, E.; Alpes, H.; Lauger, P. *J. Mem. Biol.* **1977**, 31, (1-2), 171-188.
33. Borisenko, V.; Loughheed, T.; Hesse, J.; Fertig, N.; Behrends, J. C.; Woolley, A.; Schuetz, G. J. *Biophys. J.* **2002**, 82, (1), 46A-46A.
34. Jin, X. Z.; Durrant, J. D.; Duffin, R.; Busath, D. D. *Biophys. J.* **2004**, 86, (1), 206A-206A.
35. Diociaiuti, M.; Molinari, A.; Ruspantini, I.; Gaudiano, M. C.; Ippoliti, R.; Lendaro, E.; Bordi, F.; Chistolini, P.; Arancia, G. *Biochim. Biophys. Acta. - Biomembranes* **2002**, 1559, (1), 21-31.
36. Miller, C., *Ion Channel Reconstitution*. 1st ed.; Plenum Press: New York, 1986.
37. Ohlsson, P. A.; Tjarnhage, T.; Herbai, E.; Lofas, S.; Puu, G. *Bioelectrochem. Bioenerg.* **1995**, 38, (1), 137-148.
38. Pizzolato, F.; Morelis, R. M.; Coulet, P. R. *Quim. Anal.* **2000**, 19, 32-37.
39. Hirano, A.; Wakabayashi, M.; Matsuno, Y.; Sugawara, M. *Biosens Bioelectron* **2003**, 18, (8), 973-83.
40. Antonenko, Y. N.; Stoilova, T. B.; Kovalchuk, S. I.; Egorova, N. S.; Pashkovskaya, A. A.; Sobko, A. A.; Kotova, E. A.; Surovoy, A. Y. *BBA-Biomembranes* **2006**, 1758, (4), 493-498.
41. Nikolelis, D. P.; Siontorou, C. G.; Krull, U. J.; Katrivanos, P. L. *Anal. Chem* **1996**, 68, (10), 1735-1741.

42. Banghart, M. R.; Volgraf, M.; Trauner, D. *Biochemistry* **2006**, *45*, (51), 15129-15141.
43. Stankovic, C. J.; Heinemann, S. H.; Schreiber, S. L. *Biochim Biophys Acta* **1991**, *1061*, (2), 163-70.
44. Bamberg, E.; Alpes, H.; Apell, H. J.; Bradley, R.; Harter, B.; Quelle, M. J.; Urry, D. W. *J. Mem. Biol.* **1979**, *50*, (3-4), 257-270.
45. Roeske, R. W.; Hrinyopavlina, T. P.; Pottorf, R. S.; Bridal, T.; Jin, X. Z.; Busath, D. *Biochim. Biophys. Acta* **1989**, *982*, (2), 223-227.
46. Hamann, C. H. H., A.; Wolf, V., *Electrochemistry*. 1st ed.; Wiley-VCH: Weinheim, Germany, 1998.
47. To rationalize our interpretation of non-linear I-V curves at low ionic strength, we approximated the mass transport limited maximum current through a gA pore (diameter  $\sim 4 \text{ \AA}$ ) as the diffusion limited current that can be measured by a disk-shaped nanoelectrode (with a radius  $r = 2 \times 10^{-10} \text{ m}$ ) due to the reduction or oxidation of an electroactive species (with one transferred electron per reaction,  $n = 1$ ). In analogy to the electroactive species reacting instantaneously at the nanoelectrode surface, we assumed that  $\text{K}^+$  ions that reach the opening of gA pore are instantaneously driven through the pore by the applied electric field. Using a concentration of  $c = 20 \text{ mol m}^{-3}$  (20 mM)  $\text{K}^+$  ions that have a diffusion constant of  $D = 1.96 \times 10^{-9} \text{ m}^2 \text{ s}^{-1}$ . and the equation that describes the steady state limiting current ( $i$ ) of a nanodisk electrode:  $i = 4nFDcr$  where  $F = 96,485 \text{ C}$  is the Faraday constant (From Bard, A.J. and Faulkner, L.R. *Electrochemical Methods, Fundamentals and Applications*, John Wiley & Sons, 2nd Ed., 2001, p. 171), we predict that the maximum achievable mass transport limited current through a gA pore in 20 mM  $\text{K}^+$  ions is  $\sim 3 \text{ pA}$ . Since this maximum current will be approached asymptotically with increasing potentials, it is reasonable that the measured currents will deviate from ohmic behavior (current = applied potential  $\times$  conductance) as the measured current approaches this mass transport limited current of 3 pA (for instance, at 200 mV applied potential (Figure 4), the current through **2-2** was  $\sim 30\%$  of the mass transport limited current).
48. Rostovtseva, T. K.; Aguilera, V. M.; Vodyanoy, I.; Bezrukov, S. M.; Parsegian, V. A. *Biophys. J.* **1998**, *75*, (4), 1783-1792.
49. Terrettaz, S.; Mayer, M.; Vogel, H. *Langmuir* **2003**, *19*, (14), 5567-5569.
50. Chen, C.; Folch, A. *Lab on a Chip* **2006**, *6*, (10), 1338-1345.

51. Craighead, H. *Nature* **2006**, 442, (7101), 387-93.
52. Fertig, N.; Blick, R. H.; Behrends, J. C. *Biophysical Journal* **2002**, 82, (6), 3056-3062.
53. Funakoshi, K.; Suzuki, H.; Takeuchi, S. *Anal. Chem* **2006**, 78, (24), 8169-8174.
54. Klemic, K. G.; Klemic, J. F.; Sigworth, F. J. *Pflügers Archiv European Journal of Physiology* **2005**, 449, (6), 564-572.
55. Malmstadt, N.; Nash, M. A.; Purnell, R. F.; Schmidt, J. J. *Nano Lett* **2006**, 6, (9), 1961-1965.
56. Mayer, M. T., S.; Giovanngrandi, L.; Vogel, H., *Biosensors: A practical approach*. 2nd ed.; Oxford University Press: Oxford, 2003.
57. Pantoja, R.; Sigg, D.; Blunck, R.; Bezanilla, F.; Heath, J. R. *Biophysical Journal* **2001**, 81, (4), 2389-2394.
58. Romer, W.; Lam, Y. H.; Fischer, D.; Watts, A.; Fischer, W. B.; Goring, P.; Wehrspohn, R. B.; Gosele, U.; Steinem, C. *J Am Chem Soc* **2004**, 126, (49), 16267-74.
59. Schmidt, C.; Mayer, M.; Vogel, H. *Angew. Chem. Int. Ed.* **2000**, 39, (17), 3137-3140.
60. Suzuki, H.; Tabata, K. V.; Noji, H.; Takeuchi, S. *Langmuir* **2006**, 22, (4), 1937-1942.
61. Mayer, M.; Kriebel, J. K.; Tosteson, M. T.; Whitesides, G. M. *Biophys. J.* **2003**, 85, 2684-2695.
62. Peterman, M. C.; Ziebarth, J. M.; Braha, O.; Bayley, H.; Fishman, H. A.; Bloom, D. M. *Biomedical Microdevices* **2002**, 4, (3), 231-236.
63. Jeon, T. J.; Malmstadt, N.; Schmidt, J. J. *J. Am. Chem. Soc* **2006**, 128, (1), 42-43.
64. Shim, J. W.; Gu, L. Q. *Anal. Chem* **2007**, 79, (6), 2207-2213.
65. Montal, M.; Mueller, P. *Proceedings of the National Academy of Sciences of the United States of America* **1972**, 69, (12), 3561.

66. Lundt, B. F.; Johansen, N. L.; Volund, A.; Markussen, J. *Int J Pept Protein Res* **1978**, *12*, (5), 258-68.
67. T. W. Greene, P. G. M. W., *Protective Groups in Organic Synthesis*. 3rd ed.; Wiley Interscience: New York, 1999.
68. Kirmse, W. *Angew Chem* **1976**, *88*, 273-283.
69. Lavigne, J. J.; Anslyn, E. V. *Angew. Chem. Int. Ed* **2001**, *40*, 3118-3130.
70. Lee, K.; Dzubeck, V.; Latshaw, L.; Schneider, J. P. *J Am Chem Soc* **2004**, *126*, (42), 13616-7.
71. McFarland, S. A.; Finney, N. S. *J. Am. Chem. Soc* **2002**, *124*, (7), 1178-1179.
72. Mello, J. V.; Finney, N. S. *J Am Chem Soc* **2005**, *127*, (29), 10124-5.
73. Moreira, R.; Havranek, M.; Sames, D. *J. Am. Chem. Soc* **2001**, *123*, (17), 3927-3931.
74. Rurack, K.; Resch-Genger, U. *Chemical Society Reviews* **2002**, *31*, (2), 116-127.
75. Tremblay, M. S.; Zhu, Q.; Martí, A. A.; Dyer, J.; Halim, M.; Jockusch, S.; Turro, N. J.; Sames, D. *Org. Lett* **2006**, *8*, (13), 2723-2726.
76. Mahal, L. K.; Yarema, K. J.; Bertozzi, C. R. *Science* **1997**, *276*, (5315), 1125.
77. Bamberg, E.; Lauger, P. *J. Mem. Biol.* **1973**, *11*, (2), 177-194.
78. Fields, C. G.; Fields, G. B.; Noble, R. L.; Cross, T. A. *Int J Pept Protein Res* **1989**, *33*, (4), 298-303.
79. Fields, G. B.; Fields, C. G.; Petefish, J.; Van Wart, H. E.; Cross, T. A. *Proc Natl Acad Sci U S A* **1988**, *85*, (5), 1384-8.
80. Rizzolo, F.; Sabatino, G.; Chelli, M.; Rovero, P.; Papini, A. M. *Biopolymers* **2007**, *88*, (4), 620-620.
81. Suarez, E.; De, E.; Molle, G.; Lazaro, R.; Viallefont, P. *J. Pept. Sci.* **1998**, *4*, (6), 371-377.
82. Blake, S.; Capone, R.; Mayer, M.; Yang, J. *Bioconjug Chem* **2008**.

83. Kolb, H. C.; Finn, M. G.; Sharpless, K. B. *Angew. Chem. Int. Ed.* **2001**, *40*, (11), 2004-2021.
84. Nefkens, G. H.; Tesser, G. I. *J. Am. Chem. Soc.* **1961**, *83*, (5), 1263-1263.
85. Rambhav, S.; Ramachan.Lk. *Indian J. Biochem. Biophys.* **1972**, *9*, (3), 225-229.
86. Gee, K. R.; Archer, E. A.; Kang, H. C. *Tetrahedron Lett.* **1999**, *40*, (8), 1471-1474.
87. Ryu, E. H.; Zhao, Y. *Org. Lett.* **2005**, *7*, (6), 1035-1037.
88. Wilkinson, B. L.; Bornaghi, L. F.; Houston, T. A.; Innocenti, A.; Supuran, C. T.; Poulsen, S. A. *J. Med. Chem.* **2006**, *49*, (22), 6539-6548.
89. Rostovtsev, V. V.; Green, L. G.; Fokin, V. V.; Sharpless, K. B. *Angew. Chem. Int. Ed.* **2002**, *41*, (14), 2596-2599.
90. Wu, P.; Hilgraf, R.; Fokin, V. V. *Adv. Synth. Catal.* **2006**, *348*, (9), 1079-1085.
91. Culf, A. S.; Gerig, J. T.; Williams, P. G. *J. Biomol. NMR* **1997**, *10*, (3), 293-299.
92. Mahmood Ul, H.; Chohan, Z. H.; Scozzafava, A.; Supuran, C. T. *J. Enzyme. Inhib. Med. Chem.* **2004**, *19*, (3), 263-267.
93. Menziani, M. C.; Debenedetti, P. G.; Gago, F.; Richards, W. G. *J. Med. Chem.* **1989**, *32*, (5), 951-956.
94. Merz, K. M.; Murcko, M. A.; Kollman, P. A. *J. Am. Chem. Soc.* **1991**, *113*, (12), 4484-4490.
95. Saczewski, F.; Innocenti, A.; Brzozowski, Z.; Slawinski, J.; Pomarnacka, E.; Kornicka, A.; Scozzafava, A.; Supuran, C. T. *J. Enzyme. Inhib. Med. Chem.* **2006**, *21*, (5), 563-568.
96. Santos, M. A.; Marques, S.; Vullo, D.; Innocenti, A.; Scozzafava, A.; Supuran, C. T. *Bioorg. Med. Chem. Lett.* **2007**, *17*, (6), 1538-1543.
97. Supuran, C. T.; Scozzafava, A. *J. Enzyme. Inhib.* **2000**, *15*, (6), 597-610.
98. Rokitskaya, T. I.; Kotova, E. A.; Antonenko, Y. N. *The Journal of General Physiology* **2003**, *121*, (5), 463-476.

99. Lahiri, J.; Isaacs, L.; Grzybowski, B.; Carbeck, J. D.; Whitesides, G. M. *Langmuir* **1999**, *15*, (21), 7186-7198.
100. Antonenko, Y. N.; Borisenko, V.; Melik-Nubarov, N. S.; Kotova, E. A.; Woolley, G. A. *Biophys. J.* **2002**, *82*, (3), 1308-1318.
101. Bastug, T.; Gray-Weale, A.; Patra, S. M.; Kuyucak, S. *Biophys. J.* **2006**, *90*, (7), 2285-2296.
102. Biswas, S. C.; Rananavare, S. B.; Hall, S. B. *Biochim. Biophys. Acta. - Biomembranes* **2005**, *1717*, (1), 41-49.
103. Broniatowski, M.; Obidowicz, K.; Vila Romeu, N.; Broniatowska, E.; Dynarowicz-Latka, P. *Journal of Colloid and Interface Science* **2007**, *313*, (2), 600-607.
104. Durrant, J. D.; Caywood, D.; Busath, D. D. *Biophys. J.* **2006**, *91*, (9), 3230-3241.
105. Portella, G.; Pohl, P.; de Groot, B. L. *Biophys. J.* **2007**, *92*, (11), 3930-3937.
106. Anastasiadis, A.; Morton, C. J.; Talbo, G. H.; Koeppe, R. E., II; Separovic, F. *International Journal of Peptide Research and Therapeutics* **2006**, *12*, (3), 243-252.
107. Katus, H. A.; Remppis, A.; Looser, S.; Hallermeier, K.; Scheffold, T.; Kubler, W. *J Mol Cell Cardiol* **1989**, *21*, 1349-53.
108. Makler, M. T.; Hinrichs, D. J. *The American Journal of Tropical Medicine and Hygiene* **1993**, *48*, (2), 205.
109. Puleo, P. R.; Meyer, D.; Wathen, C.; Tawa, C. B.; Wheeler, S.; Hamburg, R. J.; Ali, N.; Obermueller, S. D.; Triana, F. J.; Zimmerman, J. L. *New England Journal of Medicine* **1994**, *331*, (9), 561.
110. Keshaviah, A.; Dellapasqua, S.; Rotmensz, N.; Lindtner, J.; Crivellari, D.; Collins, J.; Colleoni, M.; Thurlimann, B.; Mendiola, C.; Aebi, S. *Annals of Oncology* **2007**, *18*, (4), 701.
111. Garba, I. H.; Gregory, U. *The Internet Journal of Infectious Diseases* **2005**, *4*, (2), 18-40.

112. Johansson, A.; Stanley, C. J.; Self, C. H. *Clin Chim Acta* **1985**, *148*, (2), 119-24.
113. Sinha, A. K. *Analytical Biochemistry* **1972**, *47*, (2), 389-394.
114. Chui, W. K.; Wainer, I. W. *Analytical Biochemistry* **1992**, *201*, (2), 237-245.
115. Rosenberg, D. W.; Roque, H.; Kappas, A. *Analytical Biochemistry* **1990**, *191*, (2), 354-358.
116. Audebert, P.; Demaille, C.; Sanchez, C. *Chemistry of Materials* **1993**, *5*, (7), 911-913.
117. Ito, S.; Yamazaki, S.; Kano, K.; Ikeda, T. *Analytica Chimica Acta* **2000**, *424*, (1), 57-63.
118. Ruan, C.; Li, Y. *Talanta* **2001**, *54*, (6), 1095-1103.
119. Hocchi, K.; Ohashi, T.; Miura, T.; Sasagawa, K.; Sato, Y.; Nomura, F.; Tomonaga, T.; Sunaga, M.; Kojima, R.; Katayama, K.; Kato, T.; Sato, T.; Komoda, T.; Oda, K. *Journal of Clinical Laboratory Analysis* **2007**, *21*, (5), 322-329.
120. Vega-Warner, A. V.; Gandhi, H.; Smith, D. M.; Ustunol, Z. *Journal of Agricultural and Food Chemistry* **2000**, *48*, (6), 2087-2091.
121. Laiwalla, F.; Klemic, K. G.; Sigworth, F. J.; Culurciello, E. *Circuits and Systems I: Regular Papers, IEEE Transactions on [Circuits and Systems I: Fundamental Theory and Applications, IEEE Transactions on]* **2006**, *53*, (11), 2364-2370.
122. Sondermann, M.; George, M.; Fertig, N.; Behrends, J. C. *BBA-Biomembranes* **2006**, *1758*, (4), 545-551.
123. Antonenko, Y. N.; Rokitskaya, T. I.; Kotova, E. A.; Agapov, II; Tonevitsky, A. G. *Biochemistry (Moscow)* **2004**, *69*, (2), 220-227.
124. Rokitskaya, T. I.; Antonenko, Y. N.; Kotova, E. A.; Anastasiadis, A.; Separovic, F. *Biochemistry* **2000**, *39*, (42), 13053-13058.
125. Das, G.; Talukdar, P.; Matile, S. *Science* **2002**, *298*, (5598), 1600-1602.
126. Talukdar, P.; Bollot, G.; Mareda, J.; Sakai, N.; Matile, S. *Chem.-Eur. J.* **2005**, *11*, (22), 6525-6532.

127. Xie, H.; Braha, O.; Gu, L. Q.; Cheley, S.; Bayley, H. *Chemistry & Biology* **2005**, *12*, (1), 109-120.
128. In related work, Matile and coworkers reported a fluorimetric method to detect enzyme activity using synthetic pores embedded in large unilamellar vesicles where the conversion of a substrate in the presence of enzymes affected the leakage of a dye from the vesicles; see ref. 125. In addition, Walker and Bayley showed by assays based on changes in optical density that a pore-forming protein can be activated in the presence of a protease trigger; see B. Walker, H. Bayley *Protein Eng.* **1994**, *7*, 91-97.
129. Millan, J. L., *Mammalian Alkaline Phosphatases: From Biology to Applications in Medicine and Biotechnology*. Wiley-VCH: 2006; p 337.
130. In all ex situ recording experiments using AP, we added bovine serum albumin to maintain a constant concentration of 2  $\mu$ M total protein in solution in order to prevent denaturation of AP.
131. Kreir, M.; Farre, C.; Beckler, M.; George, M.; Fertig, N. *Lab on a Chip* **2008**, *8*, (4), 587-595.
132. Boutros, R.; Lobjois, V.; Ducommun, B. *NATURE REVIEWS CANCER* **2007**, *7*, (7), 495.
133. Yu, Q.; Sicinska, E.; Geng, Y.; Ahnström, M.; Zagozdzon, A.; Kong, Y.; Gardner, H.; Kiyokawa, H.; Harris, L. N.; Stll, O. *Cancer Cell* **2006**, *9*, (1), 23-32.
134. Burkhart, B. M.; Li, N.; Langs, D. A.; Pangborn, W. A.; Duax, W. L. *Proceedings of the National Academy of Sciences of the United States of America* **1998**, *95*, (22), 12950.
135. Hu, W.; Cross, T. A. *Biochemistry* **1995**, *34*, (43), 14147-14155.
136. Wallace, B. A. *Annual Reviews in Biophysics and Biophysical Chemistry* **1990**, *19*, (1), 127-157.
137. Taylor, R.; Kennard, O.; Versichel, W. *J. Am. Chem. Soc.* **1983**, *105*, (18), 5761-5766.
138. Stankovic, C. J.; Delfino, J. M.; Schreiber, S. L. *Anal. Biochem.* **1990**, *184*, (1), 100-103.

139. Rijkers, D. T. S.; Höppener, J. W. M.; Posthuma, G.; Lips, C. J. M.; Liskamp, R. M. J. *Chemistry--A European Journal* **2002**, *8*, (18), 4285-4291.
140. Forster, M. O.; Newman, S. H. *J. Chem. Soc.* **1911**, *99*, 244-250.
141. Woon-Seok Yeo, D.-H. M. R. W. H. G. L. G. M. M. *Angewandte Chemie International Edition* **2005**, *44*, (34), 5480-5483.
142. Barrish, J. C.; Lee, H. L.; Mitt, T.; Pizzolato, G.; Baggiolini, E. G.; Uskokovic, M. R. *J. Org. Chem.* **1988**, *53*, (18), 4282-4295.
143. Thaisrivongs, S.; Pals, D. T.; DuCharme, D. W.; Turner, S. R.; DeGraaf, G. L.; Lawson, J. A.; Couch, S. J.; Williams, M. V. *J. Med. Chem.* **1991**, *34*, (2), 633-642.
144. Chen, B.; Zhou, X.; Taghizadeh, K.; Chen, J.; Stubbe, J.; Dedon, P. C. *Chem. Res. Toxicol.* **2007**, *20*, (11), 1701-1708.